

Department of Mechanical Engineering

**Study and Development of Novel Composite Materials for the
Application of Car Brake Rotor**

Kimberly Fu Ping Rong

**This thesis is presented for the Degree of
Master of Philosophy
of
Curtin University**

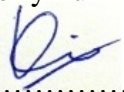
March 2014

Declaration

To the best of my knowledge and belief this thesis contains no material previously published by any other person except where due acknowledgement has been made.

This thesis contains no material which has been accepted for the award of any other degree or diploma in any university.

Name: Kimberly Fu Ping Rong

Signature: 

Date: 10th September 2014

Abstract

Gray cast iron is a widely used brake rotor material with high density that increases fuel consumption. It also generates heat easily during braking which affects its mechanical properties (tensile strength, yield strength and Young's modulus). In this research, aluminium alloy reinforced with silicon carbide and aluminium alloy reinforced with alumina Metal Matrix Composite (MMC) are investigated. MMC acquired density almost three times lower than that of gray cast iron. Both aluminium alloy reinforced with SiC and aluminium alloy reinforced with Al₂O₃ MMC have attained a higher wear rate compared to gray cast iron. This is due to the larger-sized and higher number of particles which contributed to the increase of real contact area. The wear of brake pins sliding against MMC is higher than that of brake pad pins sliding against gray cast iron. Friction coefficient for MMC is observed to be within range typical for automotive vehicles. For estimations, it is expected that both aluminium alloy reinforced with Al₂O₃ and aluminium alloy reinforced with SiC acquire higher specific heat capacity, coefficient of thermal expansion and thermal conductivity compared to gray cast iron. Alumina and aluminium titanate based ceramics Functionally Graded Material (FGM) has lower density than that of gray cast iron. The estimated thermal properties of FGM samples show that FGM possesses higher specific heat capacity compared to gray cast iron. It is estimated that FGM acquires lower thermal conductivity values compared to that of gray cast iron. From the results of this experimental study, properties including density, tensile strength, Young's modulus, fracture toughness, estimated values for thermal conductivity and specific heat capacity for MMC, density and estimated values for specific heat capacity for FGM, show promising results for the use of these materials for car brake rotor.

Acknowledgement

I would like to express my heartfelt gratitude and appreciation to my supervisor, Associate Professor Sujana Debnath, my co-supervisor, Dr Zeya Oo and my adjunct supervisor, Professor Alexander Gorin for their guidance, motivation and insightful discussions on this research project.

A special thanks to University Malaysia Sabah and Associate Professor Dr Willey Liew for providing technical support and facilities used in this research. In addition, I would like to thank all the laboratory technicians and officers in both Curtin University Sarawak Campus and University Malaysia Sabah for their technical support on the use of equipments.

I would also like to thank Grace Puang, Faith Foo and her husband for sacrificing their convenience to accommodate me in Kota Kinabalu, Sabah. At the same time, I would like to thank Ming Ming, Bridgid, Zhenyue, Siaw Khur, new friends which I have made in Sabah and also my office CE205 colleagues for their friendship and help in various ways.

Furthermore I would like to thank my parents for their unconditional love and support for allowing me to embark on this research project.

Last but not least, all the glory I give unto God for making all things possible for me to finish this journey.

Publications

P. R. K. Fu., A. Gorin., D. Sujana. & Z. Oo. 2012. On the problem of novel composite materials development for car brake rotor. International Journal of Engineering and Physical Sciences, Vol. 6, pp 333-336

P. R. K. Fu, Z. Oo. & D. Sujana. 2013. Microstructure analysis, physical and thermal properties of $\text{Al}_2\text{O}_3\text{-Al}_2\text{TiO}_5$ functionally graded ceramics for the application of car brake rotor. Journal of Science & Technology, Vol. 23 (1).

P. R. K. Fu., D. Sujana., Z. Oo., A. Gorin. & W. Y. H. Liew. Wear behavior of Al-SiC and Al- Al_2O_3 matrix composites sliding against automobile friction material. 7th Global Conference on Power Control and Optimization, Yangon, Myanmar (2 – 3 December 2013).

Nomenclature

Notation	Description
ASTM	American Society for Testing and Materials
°C	Celcius
C	Specific heat capacity
C/C	Carbon/Carbon
C/C-SiC	Carbon/Carbon-Silicon Carbide
C/SiC	Carbon/Silicon Carbide
cm	centimetre
CMC	Ceramic Matrix Composite
CVI	Chemical Vapour Infiltration
DTV	Disc Thickness Variation
f	Volume fraction
FGM	Functionally Graded Material
g	gram
HV	Vickers Pyramid Number
J	Joule
K	Kelvin
k	kilo
kg	Kilogramme
kgf	Kilogramme-force
LSI	Liquid Silicon Infiltration

ml	millilitre
m	metre
M	Mega
MMC	Metal Matrix Composite
N	Newton
n	Total number of layers
ρ	density
Pa	Pascal
PIP	Polymer Impregnation Pyrolysis
PMC	Polymer Matrix Composite
RMI	Reactive Melt Infiltration
s	Second
SAE	Society of Automotive Engineers
SEM	Scanning electron microscope
W	Watt
WCISR	Warm Compaction and In Situ Reaction

Table of Contents

DECLARATION	i
ABSTRACT	ii
ACKNOWLEDGEMENT	iii
PUBLICATIONS	iv
NOMENCLATURE.....	v
TABLE OF CONTENTS	vii
LIST OF FIGURES	ix
LIST OF TABLES	xiv
CHAPTER 1 INTRODUCTION	1
CHAPTER 2 LITERATURE REVIEW.....	5
2.1 BACKGROUND OF THE CAR BRAKE ROTOR	5
2.2 GRAY CAST IRON DISC BRAKES	8
2.2.1 Classes of Gray Cast Iron Disc Brakes	9
2.2.2 Problems Arising from Gray Cast Iron Disc Brakes.....	11
2.2.3 Thermal Behaviour of a Disc Brake.....	12
2.2.4 Other Vital Properties of a Disc Brake	13
2.3 MATERIALS FOR DISC BRAKES IN THE MARKET	15
2.4 INTRODUCTION TO METAL MATRIX COMPOSITE.....	18
2.4.1 Materials Selection for Metal Matrix Composite.....	18
2.4.2 Properties of Aluminium-based Metal Matrix Composites	21
2.5 INTRODUCTION TO FUNCTIONALLY GRADED MATERIAL (FGM) 34	
2.5.1 Materials Selection for Functionally Graded Material.....	34
2.5.2 Properties of Functionally Graded Material.....	36
2.6 Summary	38
CHAPTER 3 EXPERIMENTAL METHODOLOGY.....	40
3.1 BACKGROUND	40
3.2 MATERIALS' PREPARATION.....	40
3.3 FABRICATION METHODS	41
3.4 MICROSTRUCTURAL CHARACTERIZATION.....	44
3.5 PROPERTIES' TESTING	45

3.5.1	Density Measurement.....	45
3.5.2	Tensile Test.....	46
3.5.3	Compression Test.....	46
3.5.4	Hardness Test.....	47
3.5.5	Estimation of Thermal Properties of MMC and FGM.....	47
3.6	FRAC TOGRAPHY	48
3.7	WEAR TEST FOR GRAY CAST IRON AND MMC.....	48
CHAPTER 4 RESULTS AND DISCUSSION		52
4.1	MICROSTRUCTURAL CHARACTERIZATION.....	52
4.1.1	Metal Matrix Composite (MMC).....	52
4.1.2	Functionally Graded Material (FGM).....	53
4.2	DENSITY AND POROSITY	54
4.3	HARDNESS.....	58
4.4	TENSILE STRENGTH, YIELD STRENGTH AND YOUNG’S MODULUS	59
4.4.1	Fracture Analysis	63
4.5	FRACTURE TOUGHNESS	68
4.5.1	Fracture Analysis	69
4.6	COMPRESSIVE STRENGTH RESULTS	71
4.6.1	Fracture Analysis	73
4.7	WEAR PROPERTIES	76
4.7.1	Disc Wear Rate	76
4.7.2	Coefficient of Friction (COF)	81
4.7.3	Pin Wear Rate	86
4.7.4	Wear Analysis	91
4.8	THERMAL PROPERTIES	100
4.9	SUMMARY	104
CHAPTER 5 CONCLUSIONS AND RECOMMENDATIONS		108
5.1	CONCLUSIONS.....	108
5.2	RECOMMENDATIONS	112
REFERENCES.....		114

List of Figures

Figure 2.1 Automotive disc brake configuration	6
Figure 2.2 Cross section of the automotive disc brake.....	7
Figure 2.3 Variation of ventilated/vented disc brakes in the market (a) blank rotors (b) slotted rotors (c) drilled rotors	8
Figure 2.4 Schematic of the chase machine	29
Figure 2.5 Brake drum test rig	30
Figure 3.1 Stir casting equipment with bottom pouring method for casting	42
Figure 3.2 Cross section of A1 batch.....	44
Figure 3.3 Cross section of A2 batch.....	44
Figure 3.4 Cross section of A3 batch.....	44
Figure 3.5 Disc specimen.....	49
Figure 3.6 Ducom TR-20EV-M3 wear and friction monitor assembly.....	49
Figure 3.7 Schematic diagram wear and friction monitor.....	49
Figure 3.8 Brake pad pin.....	50
Figure 4.1 Optical microscopy images of the cross section of aluminium alloy MMC with 5wt% of reinforced silicon carbide (SiC).....	52
Figure 4.2 Optical microscopy images of the cross section aluminium alloy MMC with 20 wt% of reinforced alumina (Al ₂ O ₃).....	53
Figure 4.3 Optical microscopy images of the cross section of different batches of FGM (a) A1 batch (b) A2 batch (c) A3 batch, (d) Scanning electron image of cross section of A1 batch.....	54
Figure 4.4 Stress versus strain curves for aluminium alloy MMC (reinforced with different weight percentage of SiC).....	62
Figure 4.5 Stress versus strain curves for aluminium alloy MMC (reinforced with different weight percentage of Al ₂ O ₃).....	62
Figure 4.6 Scanning electron images microstructure of tensile fracture surface of gray cast iron.....	64

Figure 4.7 Scanning electron images (at 100 μ m) microstructure of tensile fracture surface of aluminium alloy MMC with different weight percentage of reinforced silicon carbide (SiC) (a) 5 wt% SiC (b) 10 wt% SiC (c) 15 wt% SiC (d) 20 wt% SiC.....	65
Figure 4.8 Scanning electron images (at 100 μ m) microstructure of tensile fracture surface of aluminium alloy MMC with different weight percentage of reinforced alumina (Al ₂ O ₃) (a) 5 wt% Al ₂ O ₃ (b) 10 wt% Al ₂ O ₃ (c) 15 wt% Al ₂ O ₃ (d) 20 wt% Al ₂ O ₃	66
Figure 4.9 Scanning electron images (at 10 μ m) microstructure of tensile fracture surface of aluminium alloy MMC with different weight percentage of reinforced silicon carbide (SiC) (a) 5 wt% SiC (b) 10 wt% SiC (c) 15 wt% SiC (d) 20 wt% SiC.....	67
Figure 4.10 Scanning electron images (at 10 μ m) microstructure of tensile fracture surface of aluminium alloy MMC with different weight percentage of reinforced alumina (Al ₂ O ₃) (a) 5 wt% Al ₂ O ₃ (b) 10 wt% Al ₂ O ₃ (c) 15 wt% Al ₂ O ₃ (d) 20 wt% Al ₂ O ₃	68
Figure 4.11 Scanning electron images microstructure of fracture toughness' fracture surface of aluminium alloy MMC with different weight percentage of reinforced silicon carbide (SiC) (a) 5 wt% SiC (b) 10 wt% SiC (c) 15 wt% SiC (d) 20 wt% SiC.....	70
Figure 4.12 Scanning electron images microstructure of fracture toughness' fracture surface of aluminium alloy MMC with different weight percentage of reinforced alumina (Al ₂ O ₃) (a) 5 wt% Al ₂ O ₃ (b) 10 wt% Al ₂ O ₃ (c) 15 wt% Al ₂ O ₃ (d) 20 wt% Al ₂ O ₃	71
Figure 4.13 Scanning electron images microstructure of compressive fracture surface of gray cast iron.....	73
Figure 4.14 Scanning electron images microstructure of compressive fracture surface of aluminium alloy MMC with different weight percentage of reinforced silicon carbide (SiC) (a) 5 wt% SiC (b) 10 wt% SiC (c) 15 wt% SiC (d) 20 wt% SiC.....	74
Figure 4.15 Scanning electron images microstructure of compressive fracture surface of aluminium alloy MMC with different weight percentage of reinforced alumina (Al ₂ O ₃) (a) 5 wt% Al ₂ O ₃ (b) 10 wt% Al ₂ O ₃ (c) 15 wt% Al ₂ O ₃ (d) 20 wt% Al ₂ O ₃	75

Figure 4.16 Scanning electron images microstructure of compressive fracture surface of FGM (a) A1 batch (b) A2 batch (c) A3 batch (d) Cross section of A1.....	76
Figure 4.17 Variation of wear rate ($\times 10^{-3} \text{mm}^3/\text{m}$) for gray cast iron samples.....	77
Figure 4.18 Variation of wear rate ($\times 10^{-3} \text{mm}^3/\text{m}$) with different weight percentage of SiC for aluminium alloy reinforced with SiC MMC samples under 1m/s sliding speed.....	79
Figure 4.19 Variation of wear rate ($\times 10^{-3} \text{mm}^3/\text{m}$) with different weight percentage of SiC for aluminium alloy reinforced with SiC MMC samples under 0.42m/s sliding speed.....	79
Figure 4.20 Variation of wear rate ($\times 10^{-3} \text{mm}^3/\text{m}$) with different weight percentage of Al_2O_3 for aluminium alloy reinforced with Al_2O_3 MMC samples under 1m/s sliding speed.....	80
Figure 4.21 Variation of wear rate ($\times 10^{-3} \text{mm}^3/\text{m}$) with different weight percentage of Al_2O_3 for aluminium alloy reinforced with Al_2O_3 MMC samples under 0.42m/s sliding speed.....	80
Figure 4.22 Variation of coefficient of friction for gray cast iron samples.....	81
Figure 4.23 Variation of coefficient of friction with different weight percentage of SiC for aluminium alloy reinforced with SiC MMC samples under 1m/s sliding speed.....	83
Figure 4.24 Variation of coefficient of friction with different weight percentage of SiC for aluminium alloy reinforced with SiC MMC samples under 0.42m/s sliding speed.....	83
Figure 4.25 Variation of coefficient of friction with different weight percentage of Al_2O_3 for aluminium alloy reinforced with Al_2O_3 MMC samples under 1m/s sliding speed.....	85
Figure 4.26 Variation of coefficient of friction with different weight percentage of Al_2O_3 for aluminium alloy reinforced with Al_2O_3 MMC samples under 0.42m/s sliding speed.....	86
Figure 4.27 Variation of pin wear rate ($\times 10^{-3} \text{mm}^3/\text{m}$) for gray cast iron samples....	87
Figure 4.28 Variation of pin wear rate ($\times 10^{-3} \text{mm}^3/\text{m}$) with different weight percentage of SiC for aluminium alloy reinforced with SiC MMC samples under 1m/s sliding speed.....	87

Figure 4.29 Variation of pin wear rate ($\times 10^{-3}\text{mm}^3/\text{m}$) with different weight percentage of SiC for aluminium alloy reinforced with SiC MMC samples under 0.42m/s sliding speed.....	88
Figure 4.30 Variation of pin wear rate ($\times 10^{-3}\text{mm}^3/\text{m}$) with different weight percentage of Al_2O_3 for aluminium alloy reinforced with Al_2O_3 MMC samples under 1m/s sliding speed.....	90
Figure 4.31 Variation of pin wear rate ($\times 10^{-3}\text{mm}^3/\text{m}$) with different weight percentage of Al_2O_3 for aluminium alloy reinforced with Al_2O_3 MMC samples under 0.42m/s sliding speed.....	90
Figure 4.32 Scanning electron images microstructure of worn surface of gray cast iron samples (a) 0.2MPa, 1m/s (b) 0.1MPa, 1m/s (c) 0.2MPa, 0.42m/s (d) 0.1MPa, 0.42m/s.....	91
Figure 4.33 Scanning electron images microstructure of worn surface of aluminium alloy MMC with different weight percentage of reinforced silicon carbide (SiC) (a) 5 wt% SiC (b) 10 wt% SiC (c) 15 wt% SiC.....	93
Figure 4.34 Scanning electron images microstructure of worn surface of aluminium alloy MMC with different weight percentage of reinforced silicon carbide (SiC) (a) 5 wt% SiC (b) 10 wt% SiC (c) 15 wt% SiC.....	94
Figure 4.35 Scanning electron images microstructure of worn surface of aluminium alloy MMC with different weight percentage of reinforced silicon carbide (SiC) (a) 5 wt% SiC (b) 10 wt% SiC (c) 15 wt% SiC.....	95
Figure 4.36 Scanning electron images microstructure of worn surface of aluminium alloy MMC with different weight percentage of reinforced silicon carbide (SiC) (a) 5 wt% SiC (b) 10 wt% SiC (c) 15 wt% SiC.....	96
Figure 4.37 Scanning electron images microstructure of compressive fracture surface of aluminium alloy MMC with different weight percentage of reinforced alumina (Al_2O_3) (a) 5 wt% Al_2O_3 (b) 10 wt% Al_2O_3 (c) 15 wt% Al_2O_3	97
Figure 4.38 Scanning electron images microstructure of compressive fracture surface of aluminium alloy MMC with different weight percentage of reinforced alumina (Al_2O_3) (a) 5 wt% Al_2O_3 (b) 10 wt% Al_2O_3 (c) 15 wt% Al_2O_3	98
Figure 4.39 Scanning electron images microstructure of compressive fracture surface of aluminium alloy MMC with different weight percentage of reinforced alumina (Al_2O_3) (a) 5 wt% Al_2O_3 (b) 10 wt% Al_2O_3 (c) 15 wt% Al_2O_3	99

Figure 4.40 Scanning electron images microstructure of compressive fracture surface of aluminium alloy MMC with different weight percentage of reinforced alumina (Al_2O_3) (a) 5 wt% Al_2O_3 (b) 10 wt% Al_2O_3 (c) 15 wt% Al_2O_3	100
Figure 5-1 Modified stir casting equipment.....	112

List of Tables

Table 2.1 Properties of gray cast iron.....	8
Table 2.2 Mechanical properties of ASTM A48 classes of gray cast iron.....	9
Table 2.3 Properties of ASTM A48 classes of gray cast iron.....	9
Table 2.4 Summary of Requirements.....	14
Table 2.5 Properties of Silicon carbide and alumina particle.....	20
Table 2.6 Selected cast composite components with proven applications.....	20
Table 2.7 Summary of measured density of available composites.....	21
Table 2.8 Summary of measured thermal conductivity of available composites.....	22
Table 2.9 Summary of measured specific heat capacity of available composites.....	22
Table 2.10 Summary of measured coefficient of thermal expansion (CTE) of available composites.....	23
Table 2.11 Summary of measured tensile strength of available composites.....	25
Table 2.12 Summary of measured Young's modulus of available composites.....	25
Table 2.13 Summary of wear tests done on MMC by various researchers.....	33
Table 2.14 Alumina's properties.....	35
Table 2.15 Aluminium titanate's properties.....	36
Table 3.1 Summary of MMC specimens fabricated in this study.....	43
Table 3.2 Summary of density.....	45
Table 4.1 Weight and volume percentage of reinforcements for MMC.....	54
Table 4.2 Results of theoretical and experimental density for gray cast iron.....	55
Table 4.3 Results of porosity measurements for gray cast iron.....	55
Table 4.4 Results of theoretical and experimental density for aluminium alloy reinforced with SiC.....	55
Table 4.5 Results of porosity measurements for aluminium alloy reinforced with SiC.....	56
Table 4.6 Results of theoretical and experimental density for aluminium alloy reinforced with Al ₂ O ₃	56
Table 4.7 Results of porosity measurements for aluminium alloy reinforced with Al ₂ O ₃	57
Table 4.8 Results of theoretical and experimental density for FGM.....	57

Table 4.9 Results of porosity measurements for FGM.....	58
Table 4.10 Density of available composite materials in the market.....	58
Table 4.11 Results of hardness tests carried out for gray cast iron.....	59
Table 4.12 Results of hardness tests carried out for aluminium alloy reinforced with SiC.....	59
Table 4.13 Results of hardness tests carried out for aluminium alloy reinforced with Al ₂ O ₃	59
Table 4.14 Results of tensile properties for gray cast iron and MMC.....	59
Table 4.15 Tensile strength of MMC by different researchers.....	60
Table 4.16 Young's modulus comparison of available materials with MMC.....	63
Table 4.17 Tensile strength of available materials in the market.....	63
Table 4.18 Results of fracture toughness for aluminium alloy reinforced with SiC.....	69
Table 4.19 Results of fracture toughness for aluminium alloy reinforced with Al ₂ O ₃	69
Table 4.20 Results of compression test for gray cast iron.....	72
Table 4.21 Results for compression test for aluminium alloy MMC (with different weight percentage of SiC).....	72
Table 4.22 Results for compression test for aluminium alloy MMC (with different weight percentage of Al ₂ O ₃).....	72
Table 4.23 Results for compressive tests of gray cast iron and FGM samples.....	73
Table 4.24 Summary of disc wear rate of various studies.....	78
Table 4.25 Summary of range of COF of various studies.....	84
Table 4.26 Summary of brake pad pin wear rate of various studies.....	89
Table 4.27 Thermal properties of gray cast iron.....	101
Table 4.28 Typical thermal properties of aluminium, silicon carbide and alumina based ceramic.....	101
Table 4.29 Estimated thermal properties of aluminium alloy reinforced with SiC.....	101
Table 4.30 Estimated thermal properties of aluminium alloy reinforced with Al ₂ O ₃	102
Table 4.31 Typical data for thermal properties of alumina and aluminium titanate based ceramics.....	102
Table 4.32 Theoretical data for thermal properties of FGM samples.....	103

Chapter 1 Introduction

The development of automobile brakes has come a long way since the crude brakes of horse drawn vehicles to the automobile brakes. Gotlieb Daimler and Carl Benz's first prototypes of internal combustion automobiles in 1886 gave rise to the development of several automobile components and more notably, the brake system. The first material used in brake lining was invented in 1897. The material was made of cotton combined with a bitumen solution and was used in both railway car wheels and the first automobiles. Herbert Froad's invention led to the modern-day production of brake materials (Maluf et al., 2007).

As drum brakes evolved into hydraulic drum brakes, the Federal Motor Vehicle Safety Standards 105 made front drum brakes a general rule in the 1970s (Limpert, 1999; Owen, 2004). At present time, it was noted that larger, heavier or lower-priced vehicles were built to have drum brakes on the rear wheels. One of the major drawbacks of drum brakes is that it is sensitive to high temperatures (not exceeding 500 – 600°C) due to the way it operates. Another drawback is its effect on its coefficient of friction. It expands at high temperatures, resulting in longer pedal travel and unstable contact between the drum and shoes.

Comparatively, disc brakes provide better heat dissipation. This is because of its larger exposed surface areas and a better cooling geometry. The disc brake system, in terms of its geometry design, has higher wear resistance and easier maintenance compared to the drum brake system. Due to its cooling characteristics, contamination and other design issues, the front brakes are usually of the disc type and the rear brakes are of the drum type (Kapoor et al., 2001).

Gray cast iron is the most commonly used material in automobile brake rotors (Cueva et al., 2003; Eriksson et al., 2001). Most disc brake rotors in use today are made of gray cast iron, typically containing 3.25% to 3.70% dissolved carbon within its matrix and various additives (Cueva et al., 2003). Due to its low cost and relatively ease of manufacture in high volumes, gray cast iron is a more specialized

material for almost all the automotive disc brakes. As braking system efficiency improved, cars could go faster hence causing the disc operating temperatures to increase as well. Due to the temperature gradients generated from braking, the friction surface of the disc brake undergoes compressive yield followed by plastic deformation. When the disc brake subsequently cools down, it suffers from residual tensile stress generated in these spots (Yamabe et al., 2003). In addition, repetitions of such actions will cause cracks to appear on the friction surface. This may also lead to a variety of performance related problems such as distortion and heat cracking.

There are other advanced materials which have been in the commercial market for a few decades. These materials were developed to overcome the problems caused by gray cast iron. These advanced materials are carbon/carbon composite (C/C), carbon/silicon carbide (C/SiC) composite and carbon/carbon-silicon carbide (C/C-SiC) composite. However, these materials still have their own shortcomings. Carbon/carbon (C/C) composite disc brakes exhibit a low coefficient of friction (0.25) below 450°C while a high wear rate is noted for the brake pads (Chen et al., 1996; Stadler et al., 2008; Wang et al., 2007). The time consuming processes to fabricate carbon/silicon carbide (C/SiC) composites not only pose a high risk of toxicity to the handlers, the preforms involved are also expensive (Xiao et al., 2010; Xu et al., 1999). Carbon/carbon-silicon carbide (C/C-SiC) composite and carbon/silicon carbide (C/SiC) composite share similar fabrication methods; hence, they share the same problems that arise during the process. As a result, these expensive composite disc brakes are only available for high-end performance and luxury vehicles.

Therefore, it is of great interest to the researcher to explore other composite materials which are inexpensive but yet possess attractive properties which have the potential to be integrated into commercial vehicles. This study investigates materials representing two classes of the composites. For the first one, aluminium alloy 6082 is selected to be reinforced with two different ceramic particulates, namely silicon carbide and alumina. The resultant material is metal matrix composite (MMC), a wear resistant and lightweight material which also demonstrate improved tensile strength and good thermal capacity. The second class of studied materials represents functionally graded materials (FGM). FGM is comparatively a new material which is

of great interest in the automobile applications such as car brake rotor. Alumina and aluminium titanate based ceramics are selected due to their high specific heat capacity and low thermal expansion coefficient. The benefit of this is the combination of the attractive properties of alumina and aluminium titanate based ceramics, which will produce potentially favourable and lightweight functionally graded material (FGM).

There are a number of properties which require further exploration. Low density is preferred for a disc brake, hence the density property will be investigated; ultimate tensile strength is a vital mechanical property because disc brakes are designed with a minimum tensile strength requirement of 150MPa (Macnaughtan and Krosnar, 1998). In addition, it is recommended that materials should have higher yielding strengths when being considered for disc brake applications (Chan, 2007; Mackin et al., 2002). Furthermore, Young's modulus property helps to promote uniform contact between the disc brake and the brake pads (Jacobsson, 2003). Its compressive strength is of importance as well because it allows to observe how the material fails under compressive load. Compressive strength is important for the development of friction materials (Blau, 2001; Lim et al., 2008; Martin and Bowron, 2000). It is noted that fracture toughness is a vital material property because the disc brake needs to operate properly without fracture (Ashby, 2005). In general, an automobile disc brake system needs to maintain a steady friction coefficient. The typical coefficient of friction for automotive vehicle, range from 0.3 - 0.6 (Blau, 2001). These mentioned properties will be studied for MMC and gray cast iron.

The key objective of this research is to study the above properties for MMC prepared from aluminium alloy 6082 reinforced with different ceramic particulates. Comparison will be made with measured in parallel properties of gray cast iron commonly used for car brake rotor.

Secondly, the compressive strength for alumina and aluminium based ceramics FGM will be studied and the density will be measured. It is desirable to observe how the material fails under compressive load because this property (compressive strength) is important for the development of a new material for friction materials (Blau, 2001; Lim et al., 2008; Martin and Bowron, 2000).

This thesis is organized into five chapters as outlined below:

- Chapter 1 defines the scope, general objectives and structure of this thesis;
- Chapter 2 is a review of the literature thus far that investigates gray cast iron as a commonly used material in disc brakes and other developed materials, thus proposing MMC and FGM as potential materials for disc brakes;
- Chapter 3 discusses the experimental setup for fabricating MMC and FGM and the mechanical and wear testing;
- Chapter 4 presents the results of the experimental investigation of the mechanical properties of tensile strength, yield strength, Young's Modulus, compressive strength; and the fracture toughness of MMC, density and compressive strength of FGM; and wear testing of MMC in relation to gray cast iron and;
- Chapter 5 draws conclusions from this study with recommendations for future research.

Chapter 2 Literature Review

2.1 BACKGROUND OF THE CAR BRAKE ROTOR

The history of automobiles began in 1700 when Nicholas Cugnot persuaded the King of France (Louis XIV) to finance his design of a 10-ton vehicle to drag cannons used then. The vehicle was powered by a steam boiler, reaching up to the speed of 10km/h. In 1886, Gottlieb Daimler and Carl Benz created the first prototypes of internal combustion automobiles (Maluf et al., 2007). In addition, Froad's invention has led to the production of brake materials until today (Nicholson, 1995).

There are two basic functions a braking system must provide: (1) deceleration of a vehicle (including stopping) and (2) maintain vehicle speed during downhill manoeuvre (Limpert, 1999). Deceleration enables the change of kinetic and potential energy of a vehicle into thermal energy while maintaining vehicle speed on a hill causes the transfer of potential energy into thermal energy.

There are currently two types of brakes in use: drum brakes and disc brakes. Drum brakes utilize brake shoes which are pushed out in a radial direction against a brake drum (Limpert, 1999). Drum brakes are still used at present on the rear wheels of many cars and light trucks. It is noted that larger, heavier or lower-priced vehicles are likely to have drum brakes on the rear wheels. One of the major drawbacks of drum brake is that it is sensitive to high temperatures (not exceeding 500 – 600°C) due to its geometry design and effects on its coefficient of friction. In a drum brake, the brake shoe applies normal force on 50-70% of the drum circumferential area. The drum brake and brake shoe are made of high-friction, low-wear materials and the frictional loss at the interface provides dissipation of energy with the necessary braking as well. Consequently, the brake shoe is the sacrificial component and wears faster than the drum. As the brake shoe wears, adjustment to the drum brake needs to be made to ensure proper contact between the shoe and the drum brake.

English engineer, Frederick William Lanchester is credited for creating one of the first known equipments for braking with disc (Harper, 1998; Kinkaid et al., 2003;

Maluf et al., 2007; Newcomb and Spurr, 1989). The disc brake is described as a leaf-shaped metal disc, rigidly connected to each of the back wheels of the vehicle. A variation of prototypes of what would be the present drum brakes was introduced in 1903. The spot-type disc brake evolution of automobiles can be traced back to the development of Dunlop, Girdling and Lockheed Corporation, whose disc is similar to those used in automobiles today (Harper, 1998).

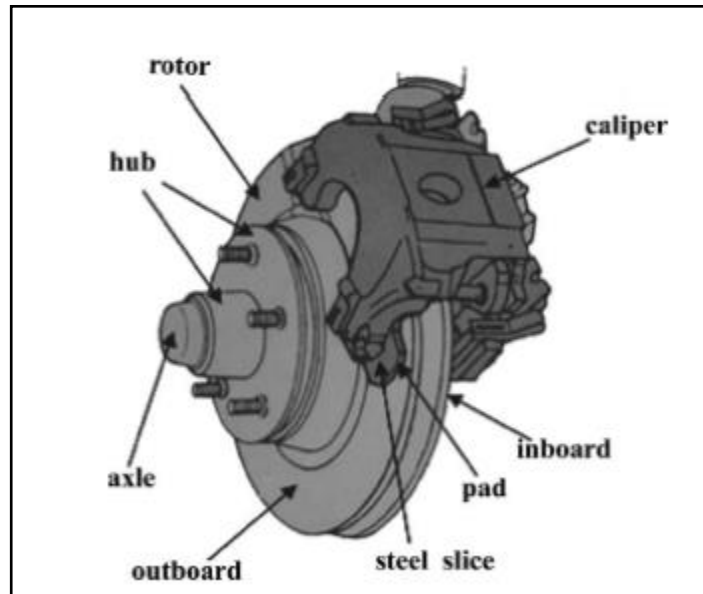


Figure 2.1 Automotive disc brake configuration (Gao et al., 2007)

A disc brake consists of a disc bolted to the wheel hub and a stationary housing called a calliper. The calliper is connected to a stationary part of the vehicle such as the axle casing or the stub axle (Figure 2.1) as is casted in two parts with each part containing a piston as seen in Figure 2.2 (Chan, 2007).

In between each piston and the disc, there is a brake pad positioned by retaining pins and spring plates. Each cylinder holds a rubber-sealing ring between the cylinder and piston. In a disc brake, the brake pads are applied on 7-25% of the disc rubbing surface. Disc brakes provide relatively better heat dissipation as compared to drum brakes. This is because of its larger exposed surface areas and a better cooling geometry. The disc brake system also has a comparatively higher wear resistance and easier maintenance. However, the exposed surface area makes them susceptible to unwanted contamination. Due to cooling characteristics, contamination and other design issues, the front brakes are usually of the disc type and the rear brakes are of

the drum type (Kapoor et al., 2001).

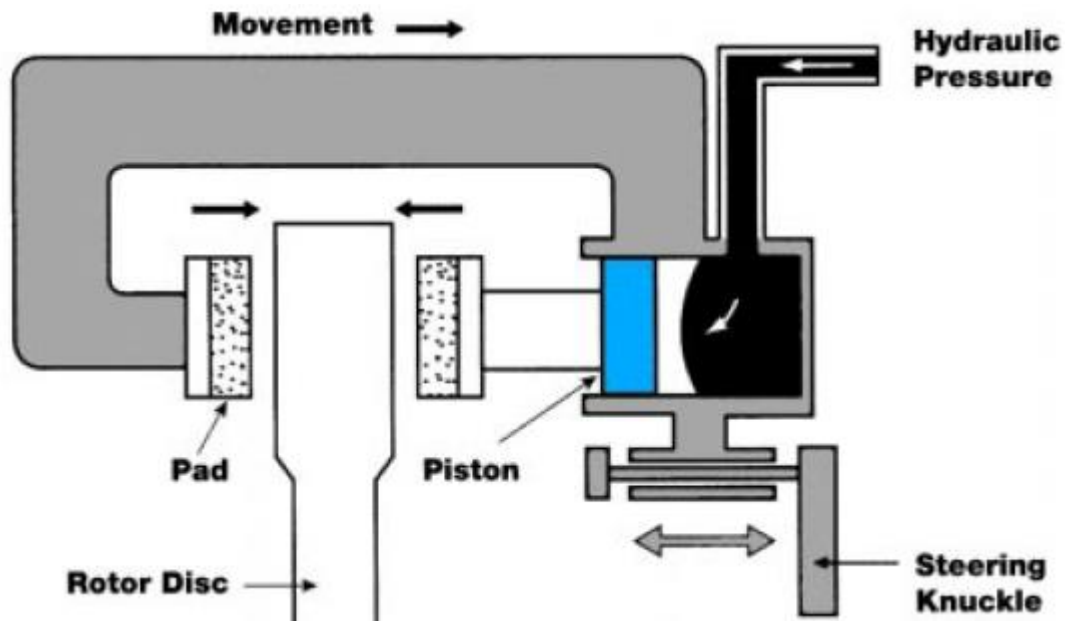


Figure 2.2 Cross section of the automotive disc brake (Lexus technical training, 2013)

There are two types of disc brakes used today: the solid disc and the ventilated or vented disc. The solid disc brake is a solid piece of metal with friction surfaces on each side. This type of disc brake is simple, cheap and easy to manufacture. It is cooled by air passing over the outside surfaces of the rotor. It is also smaller than the ventilated/vented disc brake, hence it is mostly used on lighter vehicles. A ventilated/vented disc brake consists of many various opening profiles (holes, grooves, vanes and etc) as seen in Figure 2.3 (a), Figure 2.3 (b) and Figure 2.3 (c). These opening profiles provide better cooling performance, where internal cooling is achieved by air flowing through radial passages or vanes in the disc. These discs are also more aesthetic in appearance. Thus, a ventilated/vented disc brake is more favoured by users as compared to solid disc brakes. This type of disc brake is generally used in larger cars and light trucks and in many smaller vehicles (Owen, 2004).

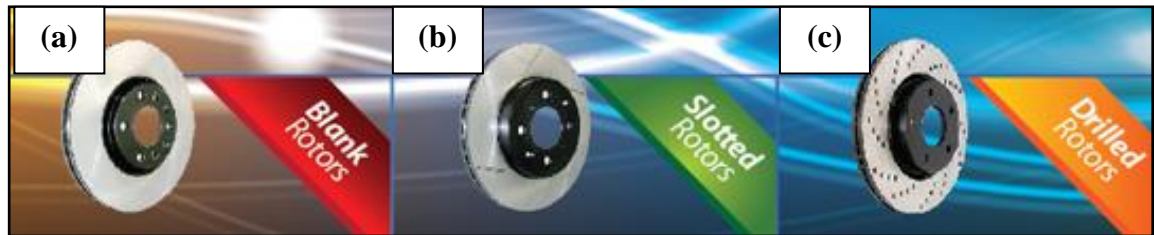


Figure 2.3 Variation of ventilated/vented disc brakes in the market (Ebay, 2013) (a) blank rotors (b) slotted rotors (c) drilled rotors

2.2 GRAY CAST IRON DISC BRAKES

Gray cast iron (containing more than 95% of pearlite) is the most commonly used in automobile brake rotors (Cueva et al., 2003; Eriksson et al., 2001). Most disc brake rotors in use today are made from gray cast iron, typically containing 3.25% to 3.70% dissolved carbon within its matrix and various additives as well (Cueva et al., 2003). Due to its low cost and relatively ease of manufacture in high volumes, gray cast iron is a more specialized material for almost all the automotive disc brakes. Table 2.1 shows some of the properties of gray cast iron (Jang et al., 2004).

Table 2.1 Properties of gray cast iron (Jang et al., 2004)

Property	Gray Cast Iron
Density (kg/m^3)	7200
Yield Strength (MPa)	214 - 269
Young's Modulus (GPa)	200 – 211
Thermal conductivity (W/m.K)	47.3
Specific heat capacity (J/kg.K)	498
Thermal expansion coefficient ($\times 10^{-6}$ 1/K)	12.6

There are two basic material principles used in the current automotive industry. The first principle is used for family sized vehicles which operate on smaller diameter and high strength discs with adequate inherent strength to resist any propensity towards the formation of thermal cracking and deformation at high operating temperatures. Though these discs have adequate strength properties, they have low thermal conductivity. The second principle, which is used for larger high-powered vehicles where space constraints are not so significant, operates on larger diameter, low strength discs with high thermal conductivity. For example, the Jaguar XJ 220

super-car utilises a modern racing disc design in a high performance application. Both front and rear discs for this vehicle utilize a high carbon, low strength material with a higher thermal conductivity of 50.5W/m.K. However, for a standard family saloon car which has approximately one third of the performance of the Jaguar, it is fitted with a low/medium carbon high strength disc with a lower thermal conductivity of 48.1w/m.K (Macnaughtan et al., 2006).

2.2.1 Classes of Gray Cast Iron Disc Brakes

There are three classes of material for the gray cast iron disc brakes, which are currently utilized by the automotive industry. Table 2.2 and Table 2.3 summarize some of its available properties (Dunaevsky, 1997; Ihm, 2013).

Table 2.2 Mechanical properties of ASTM A48 classes of gray cast iron (Dunaevsky, 1997; Ihm, 2013)

SAE J431 Casting Grade		ASTM A48 Class	Minimum Tensile Strength (MPa)	Compressive Strength (MPa)	Young's Modulus (GPa)
Current	Previous				
G7	G1800	20	124	228	69
G10	G3000	30	207	752	97
G12	G4000	40	276	965	124

Table 2.3 Properties of ASTM A48 classes of gray cast iron (Dunaevsky, 1997; Ihm, 2013)

SAE J431 Casting Grade		ASTM A48 Class	Density (kg/m ³)	Typical Carbon Content (%)
Current	Previous			
G7	G1800	20	7150	3.50 – 3.70
G10	G3000	30	7200	3.35 – 3.60
G12	G4000	40	7250	3.25 – 3.5

Low and Medium Carbon High Strength Irons

The mass of discs used currently are cast in either low or medium carbon irons. These materials are found in either alloyed or non-alloyed form and have good resistance to distortion and cracking. Non-alloyed discs are fitted to the majority of standard passenger vehicle applications while the alloyed variants are only employed where brake system requirements state that resistance to cracking and associated thermal problems are not so significant. Such discs will usually be found on 'hot hatch' types of standard vehicles, which refer to the three or five door hatchback automobile derived from a high performance car body style. Low and medium carbon high strength discs are generally small in size and are used where space considerations are of dominant importance (Macnaughtan and Krosnar, 1998).

High Carbon Low Strength Irons

These materials are developed for racing applications but have also been introduced to a range of similar materials for the large and luxury saloon/sports car market. These vehicles tend to be large in size and high in power output (Macnaughtan and Krosnar, 1998). Therefore the high carbon low strength irons have optimal thermal conductivity where the discs are large enough to prevent on-set of thermal cracking. Despite their high carbon content, the hardness levels of high carbon irons are low. Thus, its wear properties are slightly worse.

Other Alloyed Irons

Tensile strength and resistance to the on-set of thermal cracking is improved by addition of alloys (molybdenum, chromium, copper and nickel) to all grades of cast iron. However, the addition of molybdenum and chromium affects the cooling characteristics of gray cast iron to an extent that production rates generally have to be reduced in order to avoid the formation of bainitic structures (Macnaughtan and Krosnar, 1998). Problems with structural integrity are affected and machinability is reduced. If dimensional stability is to be preserved, the discs may require stress relieving before machining.

Alternatively, additions of up to 1% of copper can easily be made to maintain satisfactory strength at high carbon levels (Macnaughtan et al., 2006). Tensile strength is maintained without increasing its hardness. Nickel falls into the category

of benign additives but is extremely expensive. It should be noted that most alloy elements, except for copper and molybdenum, reduce thermal conductivity.

2.2.2 Problems Arising from Gray Cast Iron Disc Brakes

When overheating occurs in a brake system, braking may deteriorate and in extreme conditions fail completely. There are three common problems arising from gray cast iron disc brakes; brake fade, excessive component wear and judder.

Brake Fade

During braking, an amount of heat is generated when kinetic and potential energy is converted to thermal energy on a disc's surface. For a vehicle that weighs 1812kg, one emergency stop from 26.82m/s can increase the temperature of the brake pads by 71°C. The temperature will continue to rise by equal amounts if this emergency stop repeats a few times. The generated heat builds up and lowers the coefficient of friction between the brake pads and disc brake. This causes the disc brake to fade. Brake fade is a temporary loss of braking that occurs due to overheating. More pedal pressure is required to bring the vehicle to a stop as the disc brake begins to fade. After a while, even though there is pressure being applied to the brake pedal, the effect on the brakes will be very minor. In order to avoid this from happening, a built-in fade point is designed into the brake pad material (Jacobsson, 2003). It allows for most extreme braking situations. However, the importance of efficient heat removal should be of main concern.

Excessive Component Wear

Repetitive overheating from braking will lead to uneven braking, accelerated wear and possible premature replacement of the disc brake and brake pads. Day and Newcomb (1994) found that the wear of friction material is directly proportional to contact pressure but exponentially correlated to temperature. Consequently at elevated temperatures, rapid wear will occur.

Judder

While operating a vehicle, the driver may experience judder, where the steering wheel or the body shakes when force is being applied onto the pedal. In certain situations, an audible buzz is heard. There are two types of judder: hot judder and

cold judder. Hot judder is caused by thermal deformation (coning and waving of a disc), uneven thermal expansion and phase transformation of disc material. 'Hot spots' can also occur on the disc surface. Uneven wear of the disc brake owing to a 'hard' pad or harsh operating environment or heat induced thickness variation will cause disc thickness variation (DTV) (Jacobsson, 2003) on the disc brake. Phase transformation of material occurs when thermal disc thickness variation develops into a permanent state due to the phase change of pearlite in the gray cast iron to undesirable martensite when it is rapidly cooled (Kao et al., 2000). Uneven friction films sometimes occur when hot brakes are applied on a stationary vehicle, causing the brake pad to stick to the disc. At 500°C, the friction material is 'burnt' into the disc. On the other hand, cold judder is caused by geometrical irregularities of a disc brake from manufacturing error.

2.2.3 Thermal Behaviour of a Disc Brake

The thermal stability of a disc brake is greatly influenced by the behaviour of the material used and also the design of the disc brake. There are three main thermal properties are discussed in this section: thermal capacitance, thermal conductivity and thermal expansion coefficient.

Thermal capacitance (specific heat capacity) is the ability to store heat. Initially a considerable amount of frictional heat is stored during braking. During short (less than a few minutes) and high speed stops, thermal capacity is an important thermal property (Jacobsson, 2003). However, during long braking times (between 2 to 3 minutes), heat dissipation becomes an important factor. Thermal convection amounts to more than 90% of all heat dissipation for most braking conditions.

Thermal conductivity is the potential to redistribute thermal energy. The peak temperature depends mainly on the disc material's conductivity during long and low intensity brakings. However, during short brakings, this property has little effect. Thermal expansion characterizes the ability of a material to change in volume in response to a change in temperature. Thermal expansion coefficient is related to the localization of friction contact due to the thermal deformation. This property influences the propensity of hot spots and thermal DTV generation. Temperature gradients cause temporary DTV to occur due to uneven thermal expansion of the

material (Jacobsson, 2003).

Ventilated disc brakes are widely used by the automotive industry due to its cooling ability. However, if an uneven temperature field is induced around the disc, this may increase judder problems. It is noted that a higher mass solid disc runs cooler than the vented design (which has a lower mass compared to the solid disc) (Grieve et al., 1996; Kao et al., 1984). In mountain descent braking, the disc brake temperatures may increase considerably when a ventilated disc brake is utilized.

2.2.4 Other Vital Properties of a Disc Brake

In addition to thermal behaviour, the following properties are reported to be important in disc brakes: density, porosity, tensile strength, flexural strength, compressive strength and tribological behaviour (Blau, 2001). However, for the purpose of this study, only the following vital properties are studied. They are density, tensile strength, yield strength, Young's Modulus, compressive strength, fracture toughness and tribological behaviour.

Tensile Strength, Yield Strength and Young's Modulus

Disc brakes are normally designed with a minimum tensile strength requirement of 150MPa (Macnaughtan and Krosnar, 1998). This requirement applies to standard passenger vehicles and racing cars. Ultimate tensile strength is a vital mechanical property to investigate when considering materials for braking applications. During braking process, it is common for the maximum stress on the working surface of the disc brake to exceed the yield strength of the brake disc material (Gao et al., 2007). Plastic deformation in the disc brake is induced by this high stress. After cooling, plastic flow and residual tensile stresses are developed around the center of the hot spots. Plastic flow is evident on dominant hot spots. Due to this plastic yielding, it is recommended to have higher yielding strengths for materials when considering disc brake applications (Chan, 2007; Mackin et al., 2002). Furthermore, a low Young's modulus property should help to promote uniform contact and reduce thermal DTV and hot spots (Jacobsson, 2003).

Compression Strength and Fracture Toughness

It is important to study the compressive behaviour of disc brakes as it is useful to observe how the material fails under compressive load. This property is important for the development of friction materials (Blau, 2001; Lim et al., 2008; Martin and Bowron, 2000). Fracture is generally caused by thermal cracks and stress triggering the fracture which is produced by abnormal brake heating or overheating. Cracking may occur from the corner of the slot area of a disc (Wang et al., 2007). It is noted that fracture toughness is a vital material property to investigate for the design of disc brake. It is important that the disc brake operates properly without fracture. In general, designers apply the rule of thumb of having limits of fracture toughness, $K_{IC} > 15\text{MPa.m}^{1/2}$ in order to ensure adequate tolerance to stress concentrations (Ashby, 2005). This requirement applies to standard passenger vehicles.

Tribological Behaviour

In general, an automobile disc brake system consists of a brake disc and a pair of brake pads in order to maintain a steady friction coefficient. Brake wear is defined in terms of the distance travelled or the usage time (Anderson, 1992). Jang et al. (2004) stated that noise and vibration are related to the variations in the friction coefficient. Typical coefficient of friction for all automotive vehicles (standard passenger cars, racing cars and trucks), range from 0.3 - 0.6 (Blau, 2001).

Table 2.4 summarises the mentioned requirements for different types of automotive vehicles. In this study, MMC samples will be studied to observe if they meet these requirements.

Table 2.4 Summary of Requirements

Vital Properties	Ultimate tensile strength (MPa)	Fracture toughness (MPa.m^{1/2})	Coefficient of friction
	150 (Macnaughtan and Krosnar, 1998)	15 (Ashby, 2005)	0.3 – 0.6 (Blau, 2001)
Applicability	Standard vehicles and racing cars	Standard vehicles and racing cars	All automotive vehicles

2.3 MATERIALS FOR DISC BRAKES IN THE MARKET

Carbon/Carbon Composite (C/C)

There are other advanced materials for disc brake which have been in the commercial market for a few decades. The second principle used for gray cast iron disc brake requires a larger diameter of disc brake to fulfil the challenging requirement for modern luxury and sports cars' brake performance. An increase in the size of gray cast iron discs is also accompanied by an increased mass in the wheel suspension (Lim et al., 2008). This has an impact on the weight of the car as this increases inertial forces. Weight efficiency is vital in Formula 1 race cars. The race car teams spend much time trying to have components of the absolute minimum weight because this allows them to redistribute weight around the car. Therefore there is an incentive to use weight-efficient materials wherever possible (Savage, 2008).

Carbon fibre was first used in Formula 1 in 1980 where McLaren's Technical Director John Barnard designed the first carbon fibre chassis. By 1984, the entire industry for Formula 1 had started to incorporate carbon fibre in the chassis of their racing cars. In the early 1990s, these composites made their way into being fabricated as suspension components, push rods, wishbones and other components in Formula 1 race cars. This led to the advancement of carbon/carbon (C/C) composites for the racing cars and luxury cars (Reinhart, 1987), which were initially developed for the US Air Force space plane projects, US Space shuttle projects and eventually as brake pads for the military aircrafts. These composites are considered successful in the variation of high-end applications which has led them to be used in heavy-duty surface transport systems, high-speed rail system and almost all commercial aircrafts (Manocha, 2013). The key intention of these composites is to exploit on the attractive properties of graphite and combine them with carbon fibre. Thus, these composites have high specific strength and stiffness at elevated temperatures.

C/C composites have excellent resistance to high temperature, high strength and also excellent wear resistance. Despite their attractive properties, these composites exhibit a low coefficient of friction (0.25) below 450°C and also high wear rate for the brake pads (Wang et al., 2007). The inadequate stability of coefficient of friction is thought to be caused by humidity and temperature (Chen et al., 1996). Stadler et al. (2008) found that when high temperatures are generated on the disc surface of a motorcycle

during braking, a high rate of wear for the brake pads occurs. Other brake pad materials have also been studied as friction materials in order to match it tribologically with the composites disc brake for motorcycles. If C/C composites disc brake is to be used, the brake calliper needs to be redesigned as well, in order to protect it from the high temperatures generated on the disc surface during braking.

The application of this material in commercial vehicles so far is severely limited due to its long manufacturing duration and also the high cost of the fabrication method (isothermal chemical vapour infiltration or liquid-phase impregnation process) (Deng et al., 2010). These materials still suffer from insufficient stability of low coefficient of friction. For this reason, C/SiC was further developed as brake discs to be used in sports cars and high speed trains (Heine and Gruber, 2000). Wang et al. (2007) have investigated a low cost carbon/carbon composite (C/C) based on tensile testing and compact tension testing. Its tensile strength registered at 240MPa with the specimen fracturing before it yielded. This method also produces porosity of about 20% which may induce precrack.

Carbon/Silicon Carbide Composite (C/SiC)

C/SiC brake was first developed by British engineers working in the railway industry in 1988. The advantages of C/SiC composites are similar to that of C/C composites, which include low density, good high-temperature resistance, high strength and low wear rate. Its thermal properties and mechanical properties are specifically tailored. Its mechanical behaviour also varies with the processing methods used for fabrication (Heidenreich, 2013). These composites disc brakes are able to reduce judder due to its low coefficient of thermal expansion and low wear. The low Young's modulus is thought to help promote uniform contact and reduces thermal DTV and hot spots (Jacobsson, 2003). C/SiC composites overcome the disadvantage of C/C composites which was an unstable coefficient of friction. In the early 1990s, Krenkel et al. (2003) at the German Aerospace Center in Stuttgart started researching on the development of C/SiC composites for high performance automobile applications. As of now, C/SiC brakes have been successfully embedded in Porsche, Ferrari, Daimler Chrysler and other high-end performance cars (Krenkel and Berndt, 2005). C/SiC disc brakes have a stable average coefficient of friction of 0.34 (Fan et al., 2007). However, there are still limitations to this material being used in

commercial vehicles. The high cost and risk of toxicity of the chemical vapour infiltration method are the major drawbacks for this material to be integrated into commercial automobile cars (Manocha, 2013).

Carbon/Carbon-Silicon Carbide Composite (C/C-SiC)

Since the early 2000s, C/C-SiC composite has been gradually developed as advanced promising braking materials. Research at Stuttgart University and German Aerospace Center have developed C/C-SiC brake lining for 911 Turbo of Porsche . Other than that, it has been developed for clutch facings. This composite consists of a carbon/carbon-core material with a thin surface layer of SiC. In comparison with gray cast iron or carbon/carbon composite, this composite acquires better coefficient of friction (0.38) (Zhuan et al., 2008). In addition, it also exhibits low wear rate.

Currently, the main preparation methods of C/C-SiC composite involves: (1) a gas route, which is also referred to as chemical vapour infiltration (CVI); (2) a liquid phase route, involving polymer impregnation/pyrolysis (PIP) and liquid silicon infiltration (LSI), also called reactive melt infiltration (RMI); (3) a ceramic route, which is a method to combine the impregnation of the reinforcement with a slurry and sintered at high temperature and high pressure. The CVI method is known to be expensive, toxic and has low deposition rates (Xiao et al., 2010; Xu et al., 1999). The high cost is also a drawback for the RMI process. The carbon fibers of this composite are sensitive to the high pressure sintering process. Hence the preparation method has become an obstruction on the development of C/C-SiC braking composites. In order to overcome this, warm compaction and in situ reaction process (WCISR) have been developed (Xiao et al., 2005). As a result, C/C-SiC composites (fabricated by WCISR) have been effectively integrated into magnetic levitation vehicles, high-speed trains and high-end performance cars. At present, investigation on the processing methods of this composite is still ongoing and is not widely available.

Despite the fact that these available composite disc brakes are able to operate at substantially higher temperatures, this also leads to a need for heat shielding around the brakes. Metzler (1990) suggested the use of higher temperature bearing materials and a re-design of the entire brake assembly.

2.4 INTRODUCTION TO METAL MATRIX COMPOSITE (MMC)

A composite material is a material consisting of two or more physically and/or chemically distinct phases (Chawla, 1999). The reinforcing component is distributed in the continuous or matrix component. Composites is classified into three categories depending on the matrix material, namely polymer matrix composites (PMCs), ceramic matrix composites (CMCs) and metal matrix composites (MMCs). MMCs have different property combinations and processing procedures as compared to either PMCs or CMCs. MMC remains a vastly used material for aerospace, automotive, medical, sports equipment and other engineering fields due to its several advantages.

They have a combination of superior properties to an unreinforced matrix such as increased strength, increased hardness, higher Young's modulus, improved wear resistance, high thermal conductivity, wear resistance, resistance to corrosion, processing flexibility and lower cost (Miracle, 2005).

2.4.1 Materials Selection for Metal Matrix Composite (MMC)

Matrix Material (Aluminium Alloy)

The matrix of the composites is to be designed to (a) bind and support the reinforcing phase and; (b) fulfil the properties based on the intended application of the composites. Careful consideration must be given to its chemical compatibility with the reinforcement, its ability to wet the reinforcement and its processing behaviour (Kainer, 2006; Lloyd, 1994; Miracle, 2005). In addition, other considerations such as cost and availability of the matrix should be made. The matrix can generally be Al, Ti, Mg, Ni, Cu, Pb, Fe, Ag, Zn, Sn and Si. The requirements of low density and reasonably high thermal conductivity have made magnesium and aluminium alloys the most commonly used matrix materials (Lindroos et al., 2004).

Aluminium alloy (density of 2700kg/m^3) is lightweight and has a Young's modulus of 70GPa. Its melting temperature is at 660 °C. The ready availability, low costs and relatively low processing temperatures have made aluminium popular among researchers. Aluminium and its alloys have attractive properties: lightweight, high stiffness and high thermal conductivity. Besides that, aluminium possess the ease of processing, hence making them the ideal choices of materials due to its combined

properties with other metals or ceramics, for manufacturing pistons, cylinders, engine blocks, power transfer system elements, construction materials, electronics industry, packaging industry, aerospace applications and so on (Kwok and Lim, 1999; Surappa, 2003).

Reinforcement Material (Particulates)

Reinforcement in composites plays an essential role in most engineering applications as its physical and mechanical properties are improved by the addition of these reinforcements. They tend to have good thermal stability, higher Young's modulus, higher compression and tensile strength, good processability and economic efficiency when compared to matrix alloys. Selection criterion for the ceramic reinforcement includes Young's modulus, density, thermal stability, coefficient of thermal expansion, size and shape, compatibility with matrix material and cost. Choosing the appropriate reinforcements is vital because the reinforcements will improve the resultant mechanical properties (such as an increase in strength) for the matrix materials (Rack, 1987).

Particulates have an advantage as their applied production technologies and reinforcement components are cost effective and the production of units in large item numbers is possible. Particulate reinforcements are often spherical or at least have dimensions of similar order in all directions. Examples are concrete, filled polymers, metal and ceramic particles in metal matrices. Common ceramic particulate reinforcements are silicon carbide (SiC), alumina (Al_2O_3), boron nitride (BN), boron carbide (B_4C) and so on. The properties of silicon carbide and alumina are shown in Table 2.5. These are commonly used particulates due to its high hardness, raw materials' availability and low cost (Lindroos et al., 2004).

Table 2.5 Properties of Silicon carbide and alumina particle (Kainer, 1997)

Reinforcement	SiC particle	Al ₂ O ₃ particle
Crystal structure	Hexagonal	Hexagonal
Density (kg/m ³)	3200	3900
Diameter	Varies	Varies
Mohs hardness	9.7	9.0
Young's Modulus (GPa)	200-300	380

The automobile industry has successfully incorporated aluminium based particulate composites, namely Al/SiC and Al/Al₂O₃ in pistons, engine blocks, callipers, connecting rods, drive shafts, snow tired studs and other parts (Prasad and Asthana, 2004). Table 2.6 shows the examples of these components. Al/SiC shows promising materials as disc brakes as it has been used in bogies.

Table 2.6 Selected cast composite components with proven applications

Manufacturer	Component and composite
Duralcan, Martin Marietta, Lanxide	Pistons, Al/SiC _p
Duralcan	Propeller shaft, Al/SiC _p
Nissan	Connecting rod, Al/SiC _w
Lanxide	PCB heat sinks, Al/SiC _p
3M	Missile fins, aircraft electrical access door, Al/Nextel _f
Honda	Engine blocks, Al/Al ₂ O ₃ – C _f
Knorr-Bremse; Kobenhavn	Brake disc on ICE bogies, SiC/Al
Alcoa Innometalx	Multichip electronic module, Al/SiC _p
Toyota	Piston rings, Al/Al ₂ O ₃ and Al/Boria _w

(p – particulate; w – whisker; f – fiber)

Titanium Alloys and their Composites

Titanium alloys and their composites offer relatively high strength and excellent corrosion resistance (Blau et al., 2007; Qu et al., 2009). However, it has lower thermal conductivity and specific heat capacity compared to gray cast iron. In addition, the coefficient of friction was lower than the desirable range for automotive

vehicle, particularly at contact pressure of 1MPa and low speed of 2m/s. This may be due to the composites' inability to create a transfer film during sliding. Currently, there is little available research on this composite.

2.4.2 Properties of Aluminium-based Metal Matrix Composites

Density

Table 2.7 summarizes the density comparison of available composite materials in the market with MMC. Gray cast iron acquires the highest density out of all the materials stated. Consequently, other materials such as carbon/carbon composite, C/SiC composite, C/C-SiC composite are developed to fulfil the challenging demand for modern luxury and sports cars' brake performance. A356 30 vol%-SiC MMC acquires lower density compared to gray cast iron. This shows that A356 30 vol%-SiC MMC is a promising material due to its low density.

Table 2.7 Summary of measured density of available composites

Materials	Density (kg/m ³)
A356 30vol%-SiC MMC	2850 (Jang et al., 2004)
Gray Cast Iron	7200 (Jang et al., 2004)
Carbon/carbon composite	1760 (Luo and Li, 2003)
C/SiC composite	2100 (Fan et al., 2007)
C/C-SiC composite	1900 - 2000 (Heidenreich, 2013)

Thermal Properties

Table 2.8 shows the thermal conductivity of available composite materials in the market with aluminium alloy 356 reinforced with 30 vol% of silicon carbide. Carbon/carbon composite acquires the highest thermal conductivity out of all the materials stated. It is apparent that A356 30 vol%-SiC MMC acquires higher thermal conductivity than gray cast iron, C/SiC composite and C/C-SiC composite.

Table 2.8 Summary of measured thermal conductivity of available composites

Materials	Thermal Conductivity (W/m.K)
A356 30vol%-SiC MMC	148.1 (Jang et al., 2004)
Gray Cast Iron	47.3 (Jang et al., 2004)
Carbon/carbon composite	250 – 350 (Manocha, 2013)
C/SiC composite	40 (Fan et al., 2007)
C/C-SiC composite	7.5 – 22.6 (Heidenreich, 2013)

Table 2.9 shows the specific heat capacity of available composite materials in the market with aluminium alloy 356 reinforced with 30 vol% of silicon carbide. Gray cast iron acquires the lowest specific heat capacity out of all the composite materials stated. However, carbon/carbon composite acquires the highest specific heat capacity. C/C-SiC composite's specific heat capacity is within the range of 690 to 1550. Both C/SiC composite and A356 30 vol%-SiC MMC's specific heat capacity is two times of gray cast iron. During short (less than a few minutes) and high speed stops, specific heat capacity is an important thermal property (Jacobsson, 2003). Hence higher specific heat capacity is very much desirable.

Table 2.9 Summary of measured specific heat capacity of available composites

Materials	Specific Heat Capacity (J/kg.K)
A356 30vol%-SiC MMC	1027 (Jang et al., 2004)
Gray Cast Iron	498 (Jang et al., 2004)
Carbon/carbon composite	1420 (Devi and Rao, 1993)
C/SiC composite	800 (Fan et al., 2007)
C/C-SiC composite	690 – 1550 (Heidenreich, 2013)

Table 2.10 shows the coefficient of thermal expansion (CTE) of available composite materials in the market with aluminium alloy 356 reinforced with 30 vol% of silicon carbide. A356 30 vol%-SiC MMC and gray cast iron acquire high thermal expansion coefficient. Carbon/carbon composite, C/SiC composite and C/C-SiC composite acquire low CTE. Coefficient of thermal expansion influences the propensity of hot spots and thermal DTV generation (Jacobsson, 2003). A low CTE is desirable in order to minimize the tendency of hot spots and thermal DTV generation.

Table 2.10 Summary of measured coefficient of thermal expansion (CTE) of available composites

Materials	CTE ($\times 10^{-6}$ 1/K)
A356 30vol%-SiC MMC	17.4 (Jang et al., 2004)
Gray Cast Iron	12.6 (Jang et al., 2004)
Carbon/carbon composite	0.8 (Luo and Li, 2003)
C/SiC composite	2.3 – 5.7 (Fan et al., 2007)
C/C-SiC composite	0.1 – 7 (Heidenreich, 2013)

A356 30 vol%-SiC MMC exhibits a slightly higher thermal expansion coefficient compared to gray cast iron but is significantly higher than other available composite materials (C/C composite, C/SiC composite and C/C-SiC composite). However A356 30 vol%-SiC MMC acquires higher thermal conductivity and specific heat capacity compared to gray cast iron, C/SiC composite and C/C-SiC composite. These few beneficial properties of MMC will help to relieve the heat generated and also to avoid overheating in a disc brake.

Tensile Properties

Veeresh Kumar et al. (2012) concluded that composites of Al6061 containing 2 to 6wt% of SiC (prepared using stir casting route) have increased Brinell hardness (70 - 100) and tensile strength (120 - 170MPa). Compared to matrix materials, these composites exhibited approximately 50% increase in strength property. Ezatpour et al. (2013) found that Al-MMC reinforced with 7wt% of Al₂O₃ particles showed an increase in tensile strength (145MPa) when compared to matrix material (70MPa).

Hong et al. (2003) reported that aluminium alloy 2024 reinforced with 3 to 10 vol% of silicon carbide shows improved yield strength (175 - 210MPa) and tensile strength (264 - 308MPa). Alaneme and Aluko (2012) studied the tensile strength of aluminium alloy 6063 reinforced with 3 to 12 vol% of silicon carbide with a two step stir casting method. It is found that the highest vol% of reinforced silicon carbide gives the highest tensile strength, 158.5MPa. Hashim (2001) found that aluminium alloy 359 reinforced with 10 vol% of silicon carbide (with an average particle size of 29.2 μ m) fabricated by stir casting method, demonstrated improved tensile strength of 150MPa when compared to the unreinforced A359 which only registered at

103.73MPa. McDaniels (1985) stated that aluminium alloy reinforced with silicon carbide more than 30 to 40 volume fraction experienced a decrease in strength. This happens when the reinforcement particles cluster thus causing the matrix material and reinforcement particles to not bond well. It is noted that an increase in the volume fraction/weight fraction of silicon carbide particles provides an increase in tensile strength. When these materials are subjected to strain, the embedded hard particles in the aluminium alloy are able to resist plastic flow of composites. The hard particle increases the dislocation density. In addition, decreased interparticle spacing, which is caused by the increasing volume percent of silicon carbide reinforcements, creates increased resistance to dislocation motion. Hence this improves the tensile properties, compression strength and hardness. Chan (2007) recommended higher yielding strengths for materials when considering for disc brake applications due to plastic deformation induced by high stress. Nevertheless, while not all information is available from the composites (C/C composite, C/SiC composite, C/C-SiC composite and titanium alloy composite) for comparison, it is noted that the yield strength of MMC is quite close to that of gray cast iron.

Table 2.11 shows the tensile strength comparison of available composite materials in the market with MMC. C/C-SiC composite, titanium alloy composite and Al-SiC MMC acquire reasonable required tensile strength. The tensile strength and Young's modulus of carbon/carbon composite are not available for comparison. It is noted that the tensile strength and Young's modulus of carbon/carbon composite, C/SiC composite and C/C-SiC composite are dependent on the type of carbon fibre used and also their manufacturing methods (Manocha, 2013; Xiao et al., 2010). C/SiC composite acquires a slightly lower tensile strength compared to the required tensile strength for standard vehicles and racing cars.

Table 2.12 shows the Young's modulus comparison of available composite materials in the market with MMC. Gray cast iron's tensile strength and Young's modulus is dependent on its carbon content. Titanium alloy composite acquires highest tensile strength and Young's modulus. The Young's modulus of Al-SiC MMC is not available for comparison. C/SiC composite and C/C-SiC composite acquire lower Young's modulus. A low Young's modulus property is said to promote uniform contact and reduces thermal DTV and hot spots (Jacobsson, 2003).

Table 2.11 Summary of measured tensile strength of available composites

Materials	Tensile Strength (MPa)
Al-SiC MMC	120 – 170 (Veeresh Kumar et al., 2012)
Gray Cast Iron	124 – 276 (Dunaevsky, 1997; Ihm, 2013)
Carbon/carbon composite	-
C/SiC composite	145 (Fan et al., 2007)
C/C-SiC composite	80 – 190 (Heidenreich, 2013)

Table 2.12 Summary of measured Young's modulus of available composites

Materials	Young's Modulus (GPa)
Al-SiC MMC	-
Gray Cast Iron	69 – 124 (Dunaevsky, 1997; Ihm, 2013)
Carbon/carbon composite	-
C/SiC composite	65 (Fan et al., 2007)
C/C-SiC composite	50 - 70 (Heidenreich, 2013)

Despite the less impressive tensile strength of MMC in comparison to that of gray cast iron and other available composite materials, the minimum requirement for tensile strength for the design of disc brake is met (Macnaughtan and Krosnar, 1998). MMC's Young modulus is not available. The tensile strength, yield strength and Young's modulus of aluminium alloy reinforced with two different ceramic particulates (silicon carbide and alumina) at different weight percentage (5 wt%, 10wt% and 15 wt%) are investigated in this study.

Fracture Toughness and Compressive Behaviour

There are only a few studies done on both the fracture toughness and compressive behaviour of aluminium alloy reinforced with silicon carbide and alumina particulates. Fracture toughness is defined as a measure of the composites resistance to crack propagation. Alaneme and Aluko (2012) studied the fracture toughness behaviour of aluminium alloy 6063 reinforced with 3 to 12 vol% of silicon carbide with a two step stir casting method. The fracture toughness is noted to improve by 10% when compared to unreinforced matrix material. Downes and King (1992) investigated aluminium alloy reinforced with 20 wt% of silicon carbide with 3, 6 and

23 μ m in diameter. It is well noted that the fracture toughness values are almost independent of their reinforcement size. As stated in the section “Tensile Behaviour of MMC”, due to the hard particles (silicon carbide and alumina) in the aluminium alloy that resist plastic flow of composites, the compressive strength is improved as well. Vukcevic and Delijic (2002) investigated that aluminium based MMC with increasing (2wt % to 15 wt%) silicon carbide particles displayed a high compressive strength (200 - 225MPa) which is slightly lower than that of gray cast iron ASTM A48 class 20 (228MPa). Majority of the available composites’ compressive strengths registered in the range of 200 – 300MPa.

Tribological Behaviour

There are a number of literatures regarding the tribological behaviour of aluminium alloy reinforced with silicon carbide particulates composites. However, different investigators have utilized different experimental parameters, namely hardness of counterface, sliding speed, contact pressure, test environment, thus making it difficult to characterize the wear behaviour of these composites. Tribological behaviour of materials depends on many factors such as properties of material combination, experimental conditions and type of contact configuration of the wear testing equipment.

The hardness of the embedded particles involved in abrasion has an important influence on the rate of wear. Barmouz et al. (2010) found that the reduction in wear rate is attributed to the following reasons: (1) enhanced hardness of the composite reinforced by SiC particles. It is well established that improvement in hardness enhances the wear resistance of materials and; (2) Proper bonding between the aluminium alloy and SiC particles. The quality of bond between the matrix and the particles plays an important role in wear resistance.

Natarajan et al. (2006) investigated comparison of aluminium alloy 356 reinforced with 25-vol% of silicon carbide and cast iron sliding under diff contact pressures of 2.5MPa, 3.7MPa, 5MPa and 6.3MPa and different sliding speeds of 2.5m/s, 3.7m/s, 5m/s and 6.3m/s. A pin on disc tribotester was utilized for their study. It is noted that the wear of cast iron is increased with applied contact pressure and sliding speed. The wear of composite materials is lower than cast iron. The contact pressure and

sliding speed seems to have less impact on the wear of composite materials but the friction material's wear is very high due to the presence of hard silicon particles in the disc. In this case, the wear of friction material sliding against cast iron is better than that of friction material sliding against composite materials. As the sliding speed increase, the friction coefficient increases as well. The friction coefficient is noted to be more than 0.6 at all contact pressures for 6.3m/s sliding speed. At all sliding speeds and lowest contact pressure of 0.25MPa, the same trend is observed for friction coefficient. The friction coefficient of MMC is found to be 20% higher than that of cast iron. Overall, for all conditions the friction coefficient of MMC is found to be in the range of 0.5 to 0.7 whereas the friction coefficient of cast iron is noted to be from 0.25 to 0.45.

Research showed that the wear resistance of the MMC is attributed to the strength and hardness of the SiC particles and the Si phase (Daoud and Abou El-khair, 2010). Given that the SiC particles remain well bonded to the matrix during the sliding wear process, the aluminium matrix surrounding them will be worn away and all contacts will be between the friction material and SiC particles in the composite. In addition, as the size of the particle increases, large particle are likely to remain embedded longer than smaller particles until the matrix can no longer support them. Thus they are able to resist the deformation because the large particles protruding from the surface of the composite bear most of the wear load.

Daoud and Abou El-khair (2010) studied the comparison of wear and friction behaviour of commercially cast iron disc brake and A359 alloy reinforced with 20 vol% silicon carbide, under different contact pressures of 0.3MPa, 0.5MPa and 1MPa and sliding speeds of 3m/s, 6m/s, 9m/s and 12m/s. Abou El-khair (2010) utilized pin on disc tribotester for their studies. The findings show that the wear rate of A359 20-vol% silicon carbide composite is higher than that of cast iron. This is in contrast with the findings of Natarajan et al. (2006), where A356 alloy reinforced with 25-vol% silicon carbide exhibited lower wear rate than that of cast iron under sliding speeds of 2.5 – 6.3m/s with contact pressures of 0.25MPa, 0.51MPa, 0.76MPa, 1.02MPa and 1.27MPa. This is attributed to the larger silicon carbide particle size (43 μ m) that they used, whereas Daoud and Abou El-khair (2010) utilized a smaller silicon carbide particle size (5 μ m) instead. Jokinen et al. (1990) have also established

that in order to lower the wear rate of MMC, particle size beyond 13 μ m should be utilized. When the contact pressure reaches 1MPa, the silicon carbide particles lose their abilities to support the load, hence causing severe plastic deformation of the composite disc. In this case, the high hardness and wear resistance of silicon carbide particles are not fully employed. The wear rate of friction material sliding against the composite disc is marginally higher than that of the friction material sliding against cast iron. This is again in contrast with what Natarajan et al. (2006) have found where the wear rate of friction material sliding against A356 25-vol% SiC composite is much higher than that of the friction material sliding against cast iron. This too is attributed to the particle size used in the composites. Both Day and Newcomb (1994) and Natarajan et al. (2006) have found that the wear of friction material is directly proportional to contact pressure. The friction material is protected (from abrasion) by the compacted transfer layer. The transfer layer is mostly the constituents of the friction material. As the speed increases, the composite disc exhibits a lower rate which is attributed to domination of build-up of transfer layer. Both Howell et al. (1995) and Shorowordi et al. (2004) have found that the formation of a compact transfer layer consists of constituents of phenolic pad material. In comparison to cast iron, A359 20-vol% silicon carbide disc shows higher friction coefficient (but it still falls within the industry standard range for automotive brake system) at all test conditions. As the contact pressure is increased, both cast iron and A359 20-vol% silicon carbide show decrease in friction coefficient.

It has been reported that as the contact pressure increases, the real area of contact at the sliding interface increases. The softening of lubricating agents from the friction material pin may have contributed to the lower coefficient of friction at high loads (Rohatgi et al., 1992; Lasa and Rodriguez, 2003).

Zhang and Wang (2007) investigated aluminium alloy reinforced with 25 vol % of silicon carbide (3.5 μ m and 34 μ m). A chase machine test rig is developed for their study (Figure 2.4).

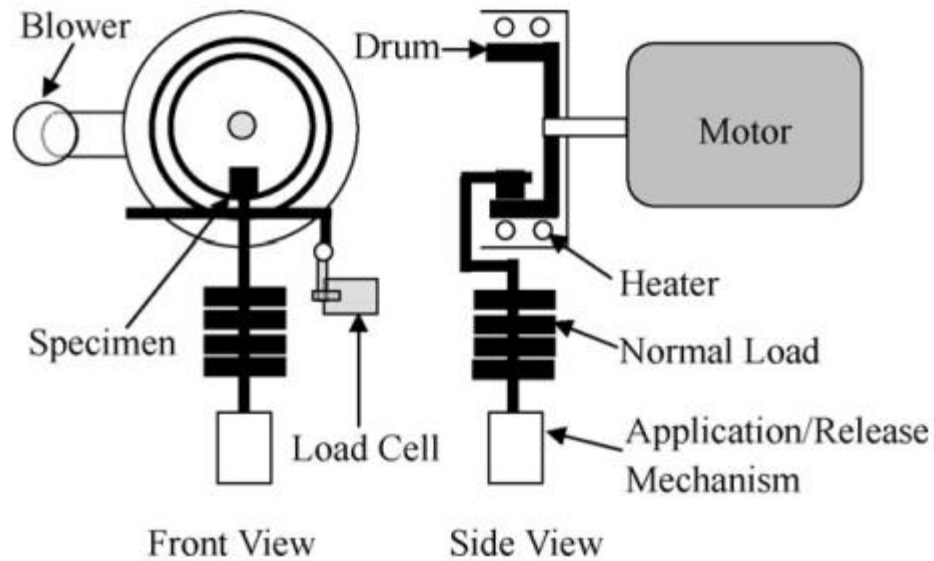


Figure 2.4 Schematic of the chase machine (Zhang and Wang, 2007)

Their study includes sliding speed of 6m/s, 9m/s, 12m/s and 15m/s with contact pressure of 1.04MPa and temperature of room temperature to 343°C. It is established that the friction performances and wear resistance for brake material sliding against drum brake with large-size silicon carbide particles (34 μ m) are better than those against the drum brakes with small-size silicon carbide particles (3.5 μ m). This is in agreement with what Natarajan et al. (2006) has found. It is noted that the friction performances strongly depend on the size of silicon carbides. The friction coefficient continuously decreases with the increase of contact pressure and sliding speed but gradually converges at two temperatures of 177°C and 316°C. It is found that the friction coefficient is more sensitive to contact pressure than sliding speed. When there is an increase in contact pressure and sliding speed, the composites' wear rate shares similar trend as the friction coefficient. However, the wear rate increases with temperature. It is also noted that the friction and wear performances of the friction materials deteriorated at high temperatures.

Anoop et al. (2009) studied aluminium alloy reinforced with 15 wt% of silicon carbide, sliding under 0.5m/s, 1m/s and 1.5m/s with applied load from 0.2MPa, 0.31MPa and 0.41MPa and temperatures ranging from 25°C to 175°C. The average silicon carbide particle size ranges from 30 to 70 μ m. The wear rate is calculated by dividing the mass loss of the disc with the disc's total area of sliding. Design of

experiments based on response surface method is utilized for their study. The wear rate of the composite disc is noted to increase steadily at higher temperatures. This is attributed to the formation of transfer layers which transforms into wear particles by the action of subsequent asperities. At higher contact pressure, the wear rate is increased. The interaction of temperature and velocity is confirmed, where at room temperature, the effect of velocity is negligible but at higher temperatures, as the velocity is increased, wear rate is increased as well. The friction coefficient is seen to be varying from 0.2 to 0.5 for most of the conditions, which is claimed to be suitable for braking applications.

Rehman et al. (2012) studied friction coefficient of aluminium alloy reinforced with 10 wt% and 15 wt% of silicon carbide (with a size range of 40 - 80 μ m) and comparison is done with cast iron drum brake. A brake drum dynamometer test rig is developed for their study (Figure 2.5).

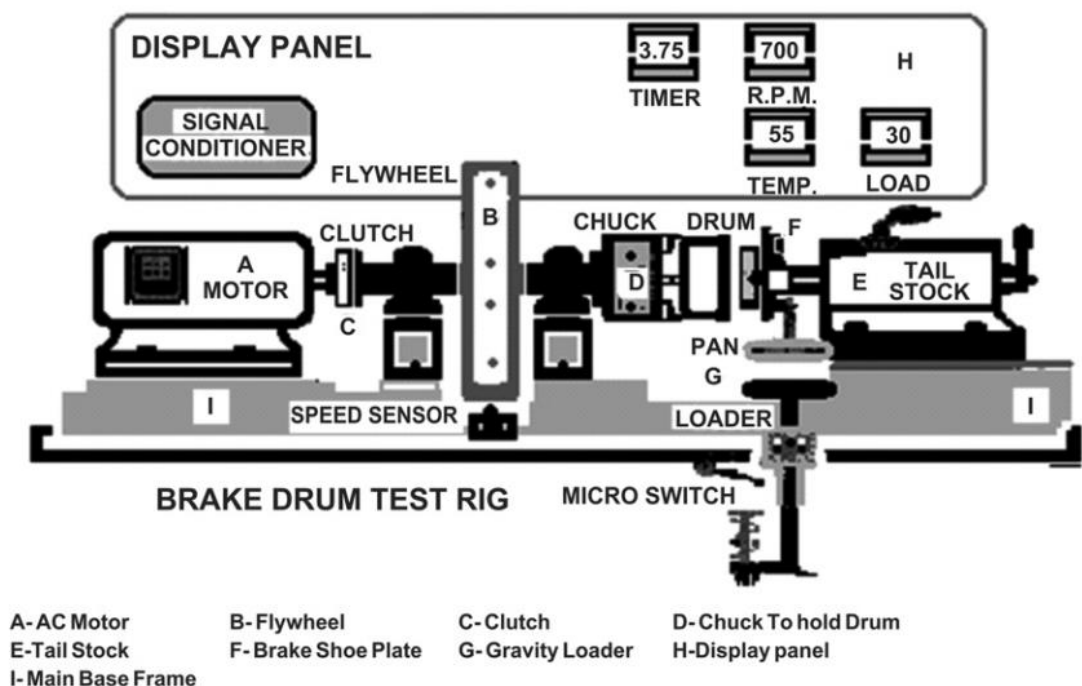


Figure 2.5 Brake drum test rig (Rehman et al., 2012)

Their study includes sliding speed of 11.11 – 22.22m/s and 6 different loads; 180N, 360N, 540N, 720N, 900N and 1080N. It is clearly noted that the friction coefficient of composite material is higher (compared to cast iron) and this is due to the presence of hard silicon carbide particles in the aluminium alloy. These particles penetrate

deeply into the friction material leading to formation of microchips from the friction material. Consequently, a higher amount of frictional force is required for the composite material to slide over the friction material. It is noted that as the silicon carbide content increases, the number of silicon carbide particles penetrating into the friction material increases as well. This increases the friction coefficient in composites when silicon carbide particles increase. It is stated that the friction coefficient of the composite materials lowers to within the limits of automobile applications if the structure and composition of lining material are correctly tailored. Salin et al. (1998) recommended that the components of friction materials to be binder, reinforcing elements, fibers, abrasive elements (SiO_2 , Al_2O_3), filling charges (BaSO_4 , CaCO_3 , Al_2O_3), lubricants (MoS_3 , Sb_2S_3 , as well as sulphides of Cu, Sn, Sb and brass), fire proofing substances and aluminium hydroxides to protect the pad from fire. These components will have properties such as low compressibility, good resistance to severe temperatures and good resistance to abrasion. While brake drum material with higher friction is not suitable for automobile brake applications, the use of higher friction coefficient has been extended to clutches used in various machines. Blanco et al. (1997) stated that the wear and frictional behaviour of the material pairs is complicated due to the contact asperities, wear debris, surface contact percentage of drum and liner rubbing surface.

Uyyuru et al. (2007) studied aluminium alloy reinforced with 15 vol% of silicon carbide ($13\mu\text{m}$) and 20 vol% of silicon carbide ($13\mu\text{m}$). Pin on disc tribotester is utilized. Their study includes sliding speed of 1.5m/s, 3m/s, 3m/s and 4m/s with applied stress of 1MPa, 2MPa, 3MPa and 4MPa. It is noted that the higher the volume fraction of silicon carbide particles, the higher was the coefficient of friction. As the contact pressure increases, the wear rate of the composite disc increases. However, the wear rate of the composite disc decreases with increasing sliding speed. In addition, the friction coefficient decreases with the increasing of contact pressure and sliding speed. The friction coefficient is higher as well but it is still within the acceptable limits for automotive brake applications. It is also noted that wear rates is said to be higher for composite discs with wider size range of silicon carbide particles. This is in contrast to the findings of Natarajan et al. (2006) and Zhang and Wang (2007). Uyyuru et al. (2007) have found that this could be due to

the higher number of silicon carbide particles which contributed to the increase of real contact area.

Shivamurthy and Surappa (2011) investigated aluminium alloy 356 reinforced with 10 and 20 vol% of silicon carbide; load of 3MPa with sliding speeds of 1m/s, 2m/s, 3m/s, 4m/s and 5m/s. The silicon carbide particles' particle size is 40 μ m. At all test conditions, aluminium alloy 356 reinforced with 20 vol% of silicon carbide exhibited at least 16-30% lower wear rates compared to aluminium alloy 356 reinforced with 10 vol% of silicon carbide. These results revealed the effect of vol% of reinforcement particles on wear rates. With the increase in reinforcing particles, more compact tribolayers have formed to reduce the wear rate of the composite materials. In addition, both composite materials show low wear rate and acquire negative wear rates from 3m/s to 5m/s. The wear rate of the friction materials however increase with the increasing sliding speed. It is also noted that the friction coefficient decreases (0.3 – 0.4) with sliding speed but are still within the limits of automobile brake applications.

Contact pressure, velocities and temperatures should be comparable to those in the real application. It is desirable to provide relative velocities of more than 10m/s which are common for automotive applications. However, these conditions are typically too high for most conventional tribological testers. In addition, the actual contact pressure is much lower (< 1MPa) for brake applications (Kermc et al., 2005). Moreover, the contact area should be larger than the typically used pin on disc tribotesters. The properties of brake materials are usually investigated on a full scale sample brake testing machines (Bergman et al., 1999; Eriksson and Jacobson, 2000).

Table 2.13 shows the summary of wear tests done by various researchers. Several authors (Uyyuru et al., 2007; Zhang and Wang, 2007) have agreed that the contact pressure is a dominant parameter affecting the wear performance. Influence of sliding speed on the wear rate is said to be less prominent when compared to contact pressure.

Table 2.13 Summary of wear tests done on MMC by various researchers

Authors	Materials		Contact pressure (MPa)	Sliding speed (m/s)	Evident Trend
	Disc	Pin			
Natarajan et al. (2006)	Aluminium alloy A356 with 25 vol%-SiC MMC and cast iron	Brake shoe lining of a commercial passenger car	0.25, 0.51, 0.76, 1.02, 1.27	2.5, 3.7, 5, 6.3	The wear of cast iron is increased with applied load and sliding speed. The wear of MMC is lower than cast iron.
Daoud and Abou El-khair (2010)	Aluminium alloy A359 with 20 vol%-SiC MMC and cast iron	Commercial automotive brake material	0.3, 0.5, 1	3, 6, 9, 12	The wear rate of MMC is higher than that of cast iron.
Zhang and Wang (2007)	Aluminium alloy with 25 vol%-SiC MMC	Disc brake pads	1.04	6, 9, 12, 15	The wear of MMC is decreased with the increase of applied load and sliding speed.
Shorowordi et al. (2004)	Aluminium with 13 vol%-SiC MMC	Commercial phenolic brake pad	0.75	1.62, 4.17	The wear of MMC is decreased with the increase of sliding speed.

Uyyuru et al. (2007)	Aluminium MMC with 15 vol%- SiC and 20 vol%-SiC	Brake pad material	1, 2, 3, 4	1.5, 2, 3, 4	The wear of MMC is increased with the increase of applied load.
Shivamurthy and Surappa (2011)	Aluminium alloy A356 with 10 vol%-SiC and 20 vol%-SiC MMC	Commercial polymer based brake pad	3	1, 2, 3, 4, 5	The wear rate of MMC is decreased with the increase of sliding speed.

2.5 INTRODUCTION TO FUNCTIONALLY GRADED MATERIAL (FGM)

Functionally graded materials (FGM) are defined as those materials in which the volume fraction of two or more constituents varies smoothly and continuously as a function of position along certain dimension(s) of the structure (Ruys et al., 2001). FGM is a composite material with microscopic inhomogeneous character. The continuous changes in their microstructure result in gradients in the properties of FGM.

Functionally Graded Materials (FGMs) have demonstrated advantages beyond mechanical applications extending to electronic, optical, nuclear, biomedical, and other fields. Ceramic materials are excellent materials due to their high hardness, corrosion resistance and ability to operate under extreme conditions as high temperatures. The unique idea of an FGM is suitable combination of layers with different compositions will yield improved mechanical response with respect to that exhibited by each individual layer (Bueno et al., 2011). FGM, comparatively a new material is a great research interest in the car brake rotor applications.

2.5.1 Materials Selection for Functionally Graded Material (FGM)

Alumina

Alumina (Corundum), Al_2O_3 has relatively good strength, corrosion resistance, high hardness and good wear resistance. Other than that, its thermal and electrical

insulation characteristics have also made it attractive for engineering applications. Stoichiometric Al_2O_3 has a molecular weight of 101.96 and exists in various crystallographic forms such as α , β , δ and γ (Wefers and Misra, 1987). The most stable form is the α - Al_2O_3 which occurs as the corundum crystal structure. The lattice of corundum consists of hexagonally close-packed oxygen ions forming layers parallel to the (0001) plane. Two-thirds of the octahedral interstices are occupied by aluminium ions. The structure may be described as consisting of alternating layers of aluminium and oxygen ions. Table 2.14 shows some of alumina's properties. Alumina is widely considered to be excellent candidates for wear resistant components due to their high hardness and thermal properties. However, its potential is hindered by its inherent brittleness.

Table 2.14 Alumina's properties (Auerkari, 1996)

Density (kg/m^3)	3530
Young's Modulus (GPa)	250 – 400
Compressive strength (MPa)	2000
Hardness (HV 1.0)	1800 – 2000
Thermal conductivity (W/m.K)	35.6
Specific heat capacity (J/kg.K)	750 – 785
Thermal expansion coefficient ($\times 10^{-6}$ 1/K)	4.5 – 5.4

Aluminium Titanate

Aluminium titanate ceramics have potential for many applications. Some of aluminium titanate's properties are shown in Table 2.15. Aluminium titanate (Al_2TiO_5) has a high melting point (1800°C), low thermal conductivity (1.5W/m.K), low thermal expansion (1×10^{-6} 1/K) (Azom, 2014) and excellent thermal shock resistance, making them potential materials for the application fields of refractory and engine components. However, Al_2TiO_5 materials have relatively low mechanical strength as a result of the micro cracks that are induced by the high anisotropy of the thermal expansion coefficients, which are -1.4, 9.8 and 20.6×10^{-6} /K for its three crystallographic axes respectively (Chen and Awaji, 2007).

Table 2.15 Aluminium titanate's properties (Azom, 2014)

Density (kg/m³)	3600
Young's Modulus (GPa)	17 – 20
Specific heat capacity (J/kg.K)	800
Thermal conductivity (W/m.K)	1.5
Thermal expansion coefficient ($\times 10^{-6}$ 1/K)	1

Aluminium titanate is formed by the solid-state reaction between Al_2O_3 and TiO_2 (rutile) above the eutectoid temperature 1280°C (Jayasankar et al., 2010). This is because aluminium titanate decomposes into alumina and rutile in the temperature range of 800 to 1300°C while cooling below the equilibrium temperature of 1280°C (Buscagli and Nanni, 1998). As a result of the decomposition, the material no longer exhibits either a low thermal expansion coefficient or favourable thermal shock behaviour. The thermal stability of Al_2TiO_5 is improved by the addition of Fe_2O_3 , MgO or TiO_2 (Korim, 2008; Low et al., 2006). Al_2TiO_5 can also be mechanically stabilized by limiting its grain growth with additives such as SiO_2 , ZrO_2 , ZrTiO_4 or mullite, most of which do not form a solid solution with Al_2TiO_5 but relatively restrain the tendency of Al_2TiO_5 toward decomposition (Nayiroh and Pratapa, 2010; Perera et al., 2011).

2.5.2 Properties of FGM

Low (1998) found that layered graded materials (LGM) formed by a homogeneous Al_2O_3 layer and a graded heterogeneous $\text{Al}_2\text{TiO}_5/\text{Al}_2\text{O}_3$ layer exhibited a relatively 'soft' surface that encased a hard core. The presence of the 'soft' surface regions is due to the high concentration of Al_2TiO_5 , which displays a low hardness value. Bueno et al. (2005) suggested that further studies be conducted to establish the effect of different stacking orders and layer thickness on the mechanical behaviour of the laminates. The method they have used in manufacturing the layered composites was slip casting. They investigated that in the system of AA10 where the external and central layers of Al_2O_3 with high strength were combined with intermediate layers of Al_2O_3 with 10vol% of Al_2TiO_5 , showed bend strength of approximately 230MPa. As for A10A40 which had intermediate layers of Al_2O_3 with 40 vol% of Al_2TiO_5 and external layers of Al_2O_3 with 10 vol% of Al_2TiO_5 , it registered bend strength of

147MPa. In addition, they discovered that laminated layer $\text{Al}_2\text{O}_3\text{-Al}_2\text{TiO}_5$ composite's thermal conductivity was similar to that of alumina (35.6W/m.K). As for the laminated layer $\text{Al}_2\text{O}_3\text{-Al}_2\text{TiO}_5$ composite with 40 vol% of Al_2TiO_5 , its thermal expansion coefficient was similar to that of alumina (4.5×10^{-6} 1/K). Nonetheless, the mechanical behaviours of FGM depend significantly on the combination and design of the individual composite layered structures. In their later research, Bueno et al. (2011) determined the Young's modulus of the laminate from the resonance frequency of bars tested in flexure. They found that the laminate acquired 391GPa.

There have not been many studies conducted on the wear properties of FGM (alumina/aluminium titanate). In situ alumina/aluminium titanate ceramic composites (prepared with spark plasma sintering) sliding against Si_3N_4 balls under normal load of 4N registered an average coefficient of friction of 0.57 (Wang et al., 2009). Further studies need to be conducted to observe the effect of wear behaviour on FGM (alumina/aluminium titanate) at this stage.

2.6 SUMMARY

Currently, gray cast iron is the most standard material for the majority of mass produced family vehicles, especially on the front brake system. As braking system efficiency improved, cars went faster hence causing the disc operating temperatures to increase as well. Due to the temperature gradients generated from the braking, the friction surface of the disc brake undergoes compressive yield accompanied by plastic deformation. The friction surface of the disc brake will also suffer from residual tensile stress generated in these spots (Yamabe et al., 2003).

Other advanced materials for disc brake namely carbon/carbon composite, carbon/silicon carbide composite, carbon/carbon-silicon carbide composite have been developed to overcome those problems. Nonetheless, these materials still have drawbacks. Carbon/carbon (C/C) composite disc brakes exhibit a low coefficient of friction (0.25) below 450°C, and also a high wear rate for the brake pads. There is a high risk of toxicity to the handlers of the production of carbon/silicon carbide (C/SiC) composites. The preforms involved are also expensive. Carbon/carbon-silicon carbide (C/C-SiC) composite disc brakes share similar fabrication method with carbon/silicon carbide (C/SiC). Therefore, both composite materials have the same problems in its fabrication method. These composite disc brakes are only available for high-end performance vehicles and luxury vehicles.

Given the fact that the braking system is a crucial safety component of the ground-based transportation systems, a disc brake should possess combination of properties such as adequate tensile strength, stable friction coefficient, good thermal capacity and wear resistant (Maleque et al., 2010). Lightweight disc brakes are also desirable as the reduction in weight also minimizes inertial forces, providing an additional benefit in fuel economy (Adebisi et al., 2011).

In the current investigation, aluminium alloy 6082 is selected to be reinforced with two different ceramic particulates, namely silicon carbide and alumina. The resultant material will acquire improved tensile strength, good thermal capacity, wear resistant and lightweight. As for FGM, alumina and aluminium titanate are selected for this study due to their high specific heat capacity and low thermal expansion coefficient. The benefit of this is the combination of the attractive properties of alumina and

aluminium titanate, which will produce FGM with potentially favourable thermal properties. As not many studies have been conducted on the different stacking orders and combination of alumina/aluminium titanate based FGM, it will be worthwhile to study the mechanical behaviour of this material at this stage.

In the following chapters we will:

- Discuss the fabrication methods for aluminium alloy reinforced with silicon carbide MMC, aluminium alloy reinforced with alumina MMC and ceramics based alumina/aluminium titanate FGM and;
- Study its mechanical properties:
 - density, tensile strength, yield strength, Young's modulus, compressive strength and fracture toughness of MMC and;
 - density and compressive strength of FGM.

in comparison to measured in parallel properties of gray cast iron commonly used in car brake rotor.

Chapter 3 Experimental Methodology

3.1 BACKGROUND

Chapter 2 has summarised the literature indicating the problems associated with gray cast iron disc brakes. Common problems are heat related problems such as brake fade, excessive component wear and judder. Thus, other advanced materials such as carbon/carbon composite, carbon/silicon carbide composite, carbon/carbon-silicon carbide composite were developed. However, these composite materials still possess drawbacks of their own. Consequently, this limits them to be used only in high end performance vehicles and luxury vehicles. It is of great interest to explore other composite materials which are inexpensive but yet offer attractive properties for the automobile brake applications.

In this study, aluminium alloy 6082 is reinforced with two different ceramic particulates, namely silicon carbide and alumina. Ceramic particulates of a range of weights are reinforced into aluminium alloy to observe its optimum mechanical and wear behaviour. Different stacking orders and combinations of alumina/aluminium titanate based FGM are explored to study its mechanical behaviour. At the end of this chapter, the results derived from this study will be analyzed and compared with gray cast iron.

3.2 MATERIALS' PREPARATION

Gray Cast Iron (GCI)

Gray cast iron, automobile grade ASTM A48 Grade 20/SAE J431 automotive gray cast iron, SAE grade G1800 is obtained and used as test specimens.

Metal Matrix Composite (MMC)

Aluminium alloy 6082 is used as the matrix material in this current investigation. Aluminium alloy 6082 rods are cut using the 9" x 16" horizontal band saw machine. As recommended by Jokinen et al (1990) and Zang and Wang (2007), a larger size of reinforcement particulates of silicon carbide (105 μ m) and alumina (120 μ m) are utilized. Hashim et al. (2001) suggested 1 wt% of magnesium powder to be used for

obtaining the best distribution and maximum mechanical properties. The presence of oxide films on a melt surface leads to non-wetting by molten alloys of reinforcement particles. This oxide layer creates a resistance to reinforcement particle penetration of a molten matrix, particularly when the particles are added from the top of a cast. This is because Magnesium reacts with the oxygen present on the surface of particles and this thins the gas layer. Thus this improves wetting and reducing the clustering tendency.

Functionally Graded Material (FGM)

The fabrication of the Functional Graded Materials ceramics composites involves two different processes; (a) Reaction-synthesis of Al_2O_3 and Al_2TiO_5 with graded interfaces and (b) heat-treatment of reaction synthesised Al_2O_3 and Al_2TiO_5 . Commercial rutile (TiO_2) and alumina (Al_2O_3) are used as base materials. Al_2TiO_5 is created by properly synthesizing the rutile and alumina ($\text{Al}_2\text{O}_3 + \text{TiO}_2 \rightarrow \text{Al}_2\text{TiO}_5$). MgO is added in as an additive for improving the thermal stability of Al_2TiO_5 , whereas SiO_2 is added in to stabilize its mechanical properties for Al_2TiO_5 .

3.3 FABRICATION METHODS

Stir Casting (for Metal Matrix Composite)

The stir casting technique, also called the vortex method, is the most commercial while relatively low cost liquid processing method to fabricate MMCs. This method is simple, flexible and attractive as it also allows very large size components to be fabricated and is also applicable to large quantity production. This method is generally used for producing composite casts, with pure matrix metal and alloys matrices. This processing technique also ensures the attainment of undamaged reinforcement materials.

The stir casting equipment setup is shown in Figure 3-2. 0.5kg of aluminium alloy and 1 wt% of magnesium is placed in the crucible at temperature of 750°C for 1 hour.



Figure 3.1 Stir casting equipment with bottom pouring method for casting

The reinforced particles (silicon carbide and alumina) are preheated beforehand at 500°C for 1 hour in the furnace to remove all the moisture on the particles' surface for better binding results. Research established that preheated SiC removes surface impurities, desorption of gases and alters the surface composition due to the formation of an oxide layer on the surface (Aqida et al., 2004; Rao and Das, 2011).

The molten metal matrix is stirred for the first two minutes to create a vortex before adding in the preheated particulates. Hashim (2001) recommended the vortex method in order to distribute the particles among the metal matrix more evenly. As recommended by Naher et al. (2007), stirring is done for 3 minutes at 200rpm in order to avoid air bubbles and impurities on the surface which could lead to porosity. These agitation speeds allow particle dispersion without introducing turbulent flow or gas entrapment. The temperature inside the furnace is controlled below 700°C in order to minimize the chemical reaction between substances.

Subsequently the composite is poured (by bottom pouring casting) into a mould made of cast iron. Bottom pouring casting is significant in obtaining a minimum level of porosity as to prevent the casting of gas entrapment and oxides formed on the melt surface (Aqida et al., 2004). The final casted MMC product is then made into specific specimen sizes. The compositions of reinforcement particles are: 5 wt%, 10 wt% and 15 wt%. The above experimental procedures are then repeated with alumina as the reinforced particles.

Table 3.1 Summary of MMC specimens fabricated in this study

Sample No.	Sample's Compositions
1	Aluminium alloy with 5% Silicon Carbide (SiC)
2	Aluminium alloy with 10% Silicon Carbide (SiC)
3	Aluminium alloy with 15% Silicon Carbide (SiC)
4	Aluminium alloy with 5% Alumina (Al ₂ O ₃)
5	Aluminium alloy with 10% Alumina (Al ₂ O ₃)
6	Aluminium alloy with 15% Alumina (Al ₂ O ₃)

Powder Stacking (for Functionally Graded Material)

Two or more different powders are mixed at the desired compositional ratio. The mixture is gradually changed through a die. After that, pressure is applied to the mixture to obtain FGM. While this process has the disadvantages of a limited number of layers and a limited size of the final product due to the limitation of compaction forces, it is effective for laboratory studies for FGM (Gooch et al., 1999; Rabin et al., 1993; Watanabe et al., 1993; Zhu et al., 1994).

Three different batches of FGM are fabricated in this study. A few layers of mixed compositions are stacked together in a cylindrical steel die; the 3cm diameter steel die is used for density measurements and the 1.15cm diameter steel die is used for compression test samples. They are uniaxially pressed by a universal testing machine (Shimadzu UH-I; accuracy of 2%) at 150MPa for approximately 20 seconds. After that, the batches of materials are sintered at temperature of 1400°C for 3 hours. They are left to be cooled in the furnace for 14 hours.

The first batch (namely A1) will include three graded layers, comprising of a 75% Al₂O₃/25% Al₂TiO₅ grade located next to the 100% Al₂O₃ outer layer, followed by a 50% Al₂O₃/50% Al₂TiO₅ grade then a 25% Al₂O₃/75% Al₂TiO₅ grade which is located next to the 100% Al₂O₃ inner layer. 6mm of 100% Al₂O₃ is placed first into the die before a layer of 25% Al₂O₃/75% Al₂TiO₅ is placed on top, followed by 50% Al₂O₃/50% Al₂TiO₅, 75% Al₂O₃/25% Al₂TiO₅ and finally 6mm of 100% Al₂O₃. The graded layers are 0.1mm in thickness. Figure 3.2 shows the schematic diagram of the first batch.

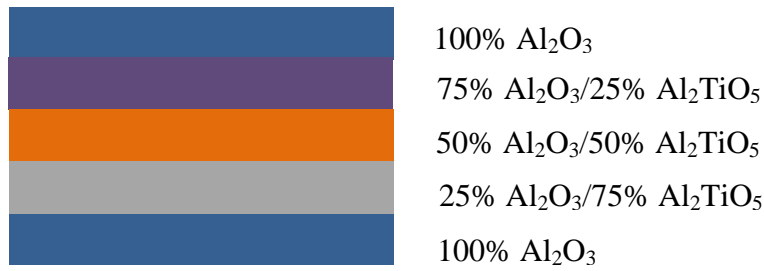


Figure 3.2 Cross section of A1 batch

The second batch (namely A2) will include one graded layer, comprising of a 50% Al_2O_3 /50% Al_2TiO_5 grade which is sandwiched between the Al_2O_3 outer and inner layers (Figure 3-3). The non graded layers are 6mm in thickness. Other than that, the graded layers are 0.1mm in thickness.

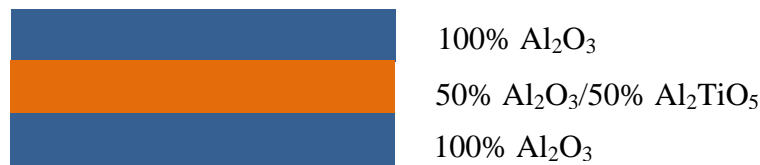


Figure 3.3 Cross section of A2 batch

The third batch (namely A3) will include a 100% Al_2TiO_5 grade which is sandwiched between the Al_2O_3 outer and inner layers (Figure 3-4). Both Al_2O_3 layers are 6mm in thickness. Other than that, the 100% Al_2TiO_5 grade are 0.1mm in thickness.



Figure 3.4 Cross section of A3 batch

3.4 MICROSTRUCTURAL CHARACTERIZATION

Metal Matrix Composite

Samples of the cast MMCs for metallographic examination are prepared by grinding different size of grit papers followed by a polish with 6 μm diamond paste. After that, the samples are etched with Keller's reagent (2.5ml nitric acid, 1.5ml hydrochloric acid, 1.0ml hydrofluoric acid and 95.0ml distilled water). The samples are then examined under optical microscope (Olympus BX60M) to investigate reinforcement particulates' distribution and presence of porosity.

Functionally Graded Material

Samples of fabricated FGM for metallographic examination are prepared by grinding different size of grit papers followed by polishing with 6µm diamond paste. Scanning electron microscopy (JEOL JSM-5610 LV SEM) is performed on samples to investigate the morphology of these materials.

3.5 PROPERTIES TESTING

3.5.1 Density Measurement

Gray Cast Iron, MMC and FGM

Density measurements are carried out on gray cast iron, MMC and FGM specimens. This is carried out in accordance to the Archimedes' principle with the equations listed in Table 3.2. Distilled water is used as the immersion fluid. An electronic balance, Sartorius CP622 with an accuracy of 0.08g is used for all weight measurements.

Table 3.2 Summary of density

	Gray Cast Iron	MMC	FGM
Theoretical density	An estimation of the density has been provided, 7200kg/m ³ (Jang et al., 2004).	$\rho_{th} = (1 - f)\rho_m + f\rho_p$ (McDanel et al., 1960), where f is the volume fraction of reinforcement, ρ_m is the density of matrix and ρ_p is the density of reinforcement.	$\rho_{th} = \frac{\rho_1 + \rho_2 + \rho_3 + \dots + \rho_i}{n_i}$, $\rho_{1,2,3}$ is the density of each layer and n_i is the total number of layers. $\rho_{2,3,4} = g\rho_1 + (1 - g)\rho_2$, g is the weight fraction of ceramic, ρ_1 is the density of alumina and ρ_2 is the density of aluminium titanate.

Experimental density	$\rho = \frac{\rho_w W_a}{W_a - W_w}$, where ρ_w is the density of water*, W_a is the mass of specimen in air, W_w is the mass of specimen submerged in water. *Density of water (at 23°C) is 997.5kg/m ³ (ASTM D792-13, 2014)
Porosity	$Porosity = \frac{\rho_{th} - \rho_e}{\rho_{th} - \rho_a}$, where ρ_{th} is the theoretical density of specimen, ρ_e is the experimental density of specimen and ρ_a is the density of air*. *Density of air is 1.225kg/m ³ (ICAO 7488/2, 2014).

3.5.2 Tensile Test

Gray Cast Iron and MMC

Tensile tests are performed to obtain information on the strength of the material under uniaxial tensile stress. The tensile tests are carried out on a universal testing machine (Lloyd LR10K; accuracy of 0.005%) in accordance to the ASTM test method E8 for tensile testing of metallic materials. The loading rate is 10mm/min. The stress versus strain curves are then plotted. Utilizing the offset method, the 0.2% yield strength of the samples is obtained. The ultimate tensile strength (UTS) is also read from the graphs.

3.5.3 Compression Test

Gray Cast Iron and MMC

The compression tests are carried out on a universal testing machine (Gotech 600kN capacity; accuracy of 5%) in accordance to the ASTM test method E9 for compression testing of metallic materials. The stress versus strain curves are then plotted. Utilizing the offset method, the 0.2% yield strength of the samples is obtained. The compressive strength is also read from the graphs.

FGM

The compression test specimens are fabricated with a diameter of 1.15cm and a height of 2.3cm. The compression tests are carried out on a universal testing machine

(Instron 8801; accuracy of $\pm 0.5\%$) in accordance to the ASTM test method C773 for compression testing of fired whiteware materials. The loading rate is 0.8mm/min. The stress versus strain curves are then plotted. The compressive strength, 0.2% offset yield strength and Young's modulus (E) are calculated from the values read from the graphs.

3.5.4 Hardness Test

Gray Cast Iron and MMC

Hardness tests are performed on a Rockwell hardness tester (Shimadzu HTB; with an accuracy of 0.5%) in accordance to the ASTM test method E18 for Rockwell hardness of metallic materials. According to the Rockwell hardness scale B, a 1/16 inch-diameter steel sphere indenter with total test force of 100kgf is utilized for the metal matrix composite specimens. Three indentations are taken on the matrix for each composite and an average value is calculated. A hardness test is carried out in this way to ensure that the maximum number of indentations fall on the matrix phase which represent the hardness property of the composite.

3.5.5 Estimation of Thermal Properties of MMC and FGM

The thermal conductivity values of MMC are calculated using the Rule of Mixture equation: $k_{th} = (1 - f)k_m + fk_p$ (McDanel et al., 1960), where f is the volume fraction of reinforcement, k_m is the thermal conductivity of matrix and k_p is the thermal conductivity of reinforcement. The specific heat capacity values of MMC are also calculated with the Rule of Mixture equation: $C_{th} = (1 - f)C_m + fC_p$ (McDanel et al., 1960), where f is the volume fraction of reinforcement, C_m is the specific heat capacity of matrix and C_p is the specific heat capacity of reinforcement. The coefficient of thermal expansion values of MMC are computed using the equation:

$$\alpha_{th} = \frac{(1 - f)\alpha_m k_m + f\alpha_p k_p}{(1 - f)k_m + fk_p} \quad (\text{Rohatgi et al., 1986}),$$

where f is the volume fraction of reinforcement, α_m is the CTE of the matrix, k_m is the thermal conductivity of the matrix, α_p is the CTE of the reinforcement and k_p is the thermal conductivity of the reinforcement.

The thermal conductivity values of FGM are calculated using the concept of thermal resistance of a composite wall: $k_T = L_T \div \left(\frac{L_1}{k_1} + \frac{L_2}{k_2} + \frac{L_3}{k_3} + \frac{L_4}{k_4} + \frac{L_5}{k_5} \right)$, where $L_{1,2,3,4,5}$ is the thickness of the respective layer, $k_{1,2,3,4,5}$ is the thermal conductivity of respective layer, L_T is the thickness of the sample and k_T is the thermal conductivity of the sample.

The specific heat capacity values of FGM are computed using thermal energy balance: $C_T = \frac{(m_1C_1 + m_2C_2 + m_3C_3 + m_4C_4 + m_5C_5)}{M}$, where C_T is the specific heat capacity of the sample, $m_{1,2,3,4,5}$ is the mass of respective layer, $C_{1,2,3,4,5}$ is the specific heat capacity of respective layer and M is the mass of the sample.

3.6 FRACTOGRAPHY

Gray Cast Iron, MMC and FGM

Fracture surface characterizations are conducted on the fractured specimens to provide an insight into the various possible fracture mechanisms operative during the fracture. The fracture surfaces are viewed in the JEOL JSM-5610 LV SEM.

3.7 WEAR TEST FOR GRAY CAST IRON AND MMC

Wear Tester and Disc Specimens' Preparation

The wear tests are carried out with a pin on disc tribotester (Ducom TR-20EV-M3) with an accuracy of 1% (Figure 3-6). The wear tests are carried out in accordance to the ASTM test method G99 for wear testing on a pin on disc apparatus. The schematic diagram of the wear and friction monitor is presented in Figure 3-7. The disc specimen (Figure 3-5) has a diameter of 10cm with a thickness of approximately $0.83\text{cm} \pm 0.20\text{cm}$. An electronic balance, Sartorius CP622 with an accuracy of 0.08gm, is used to measure the mass of the disc and pin before and after each run.



Figure 3.5 Disc specimen

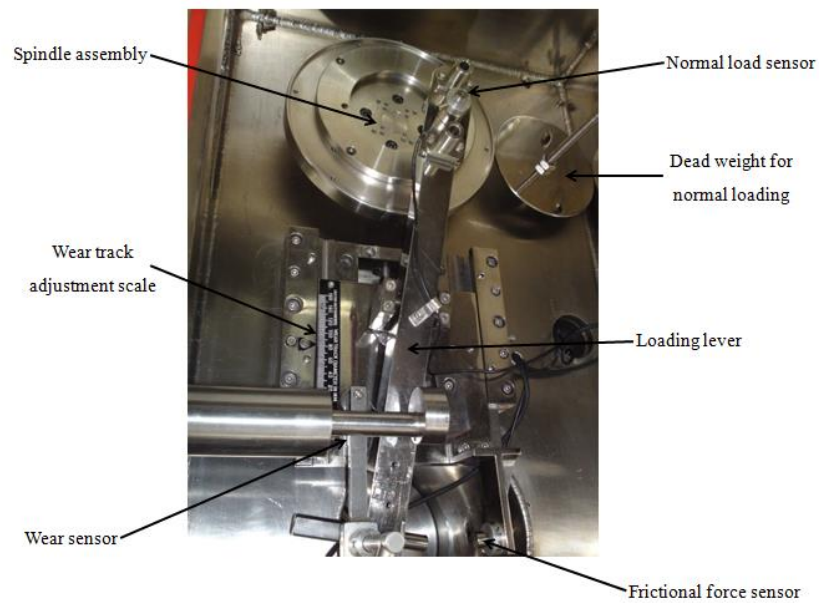


Figure 3.6 Ducom TR-20EV-M3 wear and friction monitor assembly

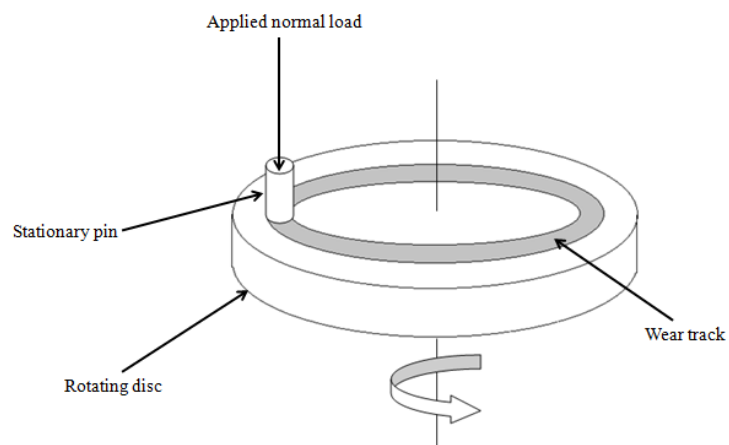


Figure 3.7 Schematic diagram wear and friction monitor (Uyyuru et al., 2006)

Preparation of Pin Specimens

A commercial automotive brake pad is used as pins for the wear test. The brake pads are manufactured by a company, Lapco Auto Parts for local Perodua Kembara cars. A cylindrical grinding machine is used to cut the brake pads into a cylindrical form, with a diameter of $0.8\text{cm} \pm 0.02\text{cm}$ and with a flat surface contact area. Figure 3.8 shows an example of a brake pad pin.



Figure 3.8 Brake pad pin

Density measurements are carried out according to the Archimedes' principle on the pin specimen, using an electronic balance, Sartorius CP622, with an accuracy of 0.08g. Since these commercial brake pads are proprietary items, the exact information on their compositions are not made known. However, it is commonly known that commercial friction material may contain phenolic resin, asbestos fiber, filler materials ($\text{BaSO}_4/\text{CaCO}_3$) and small amount of metal chips (eg. iron) as friction modifier (Daoud and Abou El-khair, 2010; Uyyuru et al., 2007).

Experimental Conditions

It is stated that the contact pressure, contact velocities and contact temperatures should be comparable to those in the real application (Kermc et al., 2005). However, these conditions are generally too high for most conventional tribological testers. In addition, the actual contact pressures are much lower ($< 1\text{MPa}$) for brake applications (Kermc et al., 2005). Moreover, the contact area should be larger than the typically used pin on disc tribotesters. As a result, several researchers (Anoop et al., 2009; Daoud and Abou El-khair, 2010; Gultekin et al., 2010; Natarajan et al., 2006; Uyyuru et al., 2007) have utilized a pin on disc tribotester to study the wear behaviour of aluminium alloy reinforced composites. These researchers studied conditions with nominal contact pressure of $0.01 - 1\text{MPa}$ and sliding speed is in the range of $0.5 - 12\text{m/s}$.

Due to the limitations of the available pin on disc tribotester (Ducom TR-20EV-M3), the wear behaviour of metal matrix composite materials and gray cast iron are

conducted under two different loads (5N and 10N) and sliding speeds (0.42m/s and 1m/s). All wear tests are kept at sliding distance of 2000m as Miyajima and Iwai (2003) noted that the volume loss increases linearly after a certain sliding distance. All wear tests are conducted at the ambient temperature of 26°C and atmospheric pressure of 1bar.

Experimental Procedure

Firstly, the electronic balance is switched on and calibrated to zero. As the disc holder and the spindle assembly are cleaned with acetone to ensure that the clean surface is maintained for all the runs, the radius of the disc is set in accordance to the sliding speeds of 0.42m/s or 1m/s. The disc and pin are cleaned with acetone before measuring and recording their initial weight. After that, dead weights (5N or 10N) are placed onto the pin holder. The wear tester is switched on and the frictional force and displacement of the pin with the disc are calibrated to zero. The experiments are carried out twice to ensure the reliability of the results.

Wear Rate Calculation

Mass loss is calculated based on the mass difference of the disc and pin measured before and after each run. The mass loss is used to determine both the wear rate of the disc and brake pad pin. Daoud and Abou El-khair (2010) and Shivamurthy and Surappa (2011) suggested the following equation to be used to obtain the wear rate for both composite disc and brake pad pin:

$W = \frac{M}{\rho D}$, where W is the wear rate of the material (mm³/m), M denotes mass loss (g) and ρ (g/mm³) and D (m) are the density and sliding distance respectively.

Microscopic Analysis

The worn surface of the discs is examined using scanning electron microscopy (JEOL JSM-5610 LV SEM).

Chapter 4 Results and Discussion

In this chapter, studies are carried out on,

- (i) results of density, tensile properties, compressive strength, fracture of metal matrix composite (MMC),
- (ii) results of density and compressive strength of functionally graded material (FGM),
- (iii) comparison of both MMC and FGM to gray cast iron under the same methodology,
- (iv) theoretical thermal properties of MMC and FGM.

4.1 MICROSTRUCTURAL CHARACTERIZATION

4.1.1 Metal Matrix Composite (MMC)

Figures 4.1 and 4.2 show the optical microscopy images of the cross section of aluminium alloy reinforced with silicon carbide (SiC) MMCs and aluminium alloy reinforced with alumina (Al_2O_3) MMCs. The particles are observed (shown by the white circles) to be dark coloured particles. Due to the bottom pouring method used in this experimental rig, the first drop of slurry occupied the bottom part of the mould, and thus contains fewer particles (Hashim et al., 2001). The settlement of the particles occurs in the middle part of the ingot.

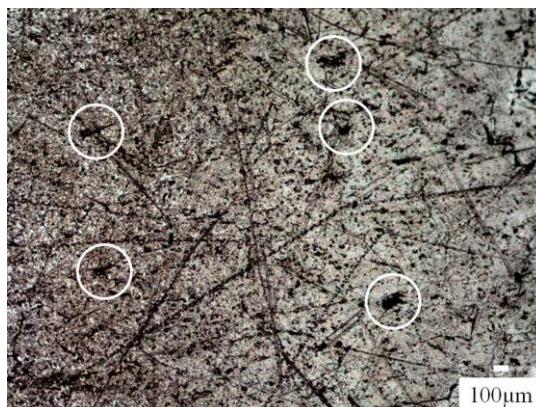


Figure 4.1 Optical microscopy images of the cross section of aluminium alloy MMC with 5wt% of reinforced silicon carbide (SiC)

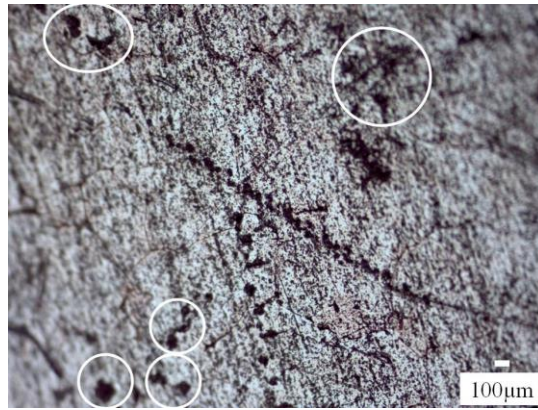


Figure 4.2 Optical microscopy images of the cross section aluminium alloy MMC with 20 wt% of reinforced alumina (Al_2O_3)

4.1.2 Functionally Graded Material (FGM)

Figure 4.3 shows the optical microscopy images of the cross section of FGM and scanning electron microscopy image of the cross section of FGM. Alumina (Al_2O_3) appeared to be grey whereas aluminium titanate (Al_2TiO_5) is of light grey and titania (TiO_2) appeared to be white. Pores were observed as black spots. Figure 4.3a, 4.3b and 4.3c show that alumina and aluminium titanate are uniformly distributed throughout the area with some minor dark spots. Titania, which appeared to be white spots, are observed to be evenly distributed as well. Many grey spots are observed in the second and third batch of FGM. Although MgO as an additive had been added to aluminium titanate, the decomposition of aluminium titanate to alumina and titania is still evident through the observation of white spots of titania and grey colour of alumina. The observation of alumina, aluminium titanate and titania is confirmed in Figure 4.3d.

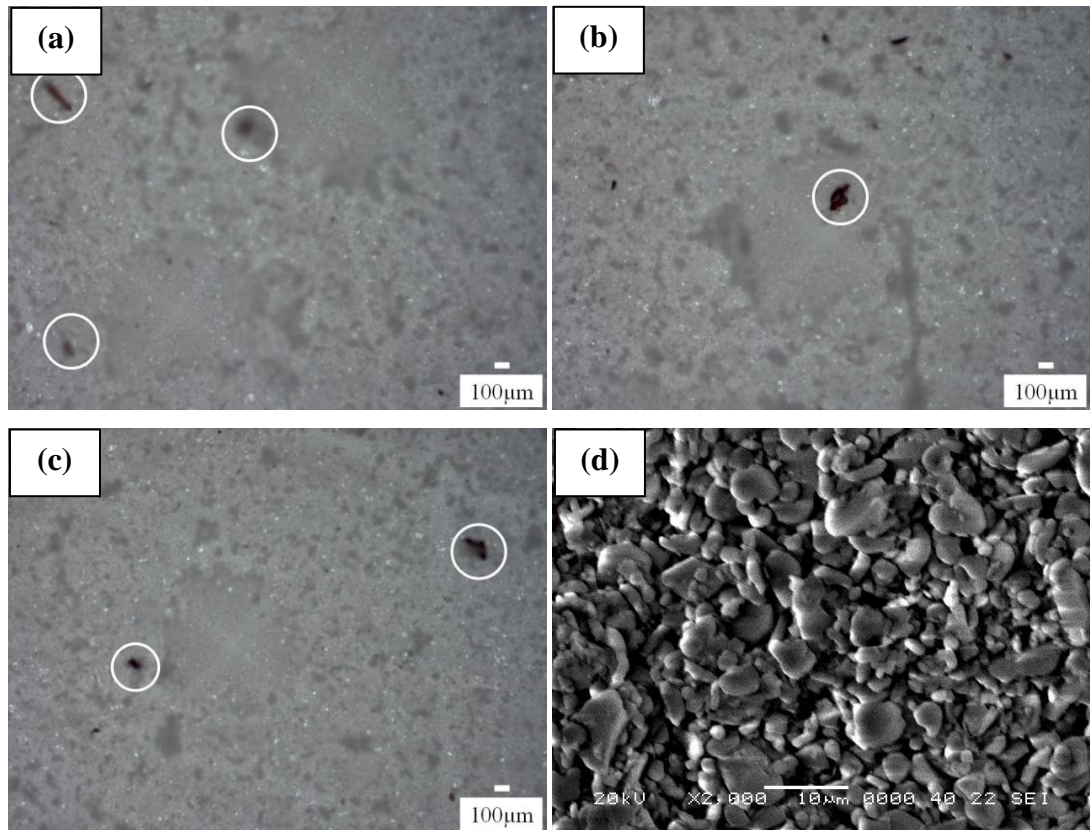


Figure 4.3 Optical microscopy images of the cross section of different batches of FGM (a) A1 batch (b) A2 batch (c) A3 batch, (d) Scanning electron image of cross section of A1 batch

4.2 DENSITY AND POROSITY

Table 4.1 shows the weight and volume percentage of reinforcements for MMC. The results of density measurements are performed according to Archimedes Principle on gray cast iron, MMC and FGM samples are shown in Table 4.2, Table 4.3 and Table 4.4 respectively. The density measurement for each type of specimens is carried out with an average of 3 samples each and errors are the standard deviations.

Table 4.1 Weight and volume percentage of reinforcements for MMC

Material	Weight %	Volume %
Aluminium alloy reinforced with SiC / Al ₂ O ₃ MMC	5	3
	10	7
	15	11
	20	15

It is observed in Table 4.2 that the measured density for gray cast iron is slightly lower than its theoretical density. This could be due to the porosity content as presented in Table 4.3.

Table 4.2 Results of theoretical and experimental density for gray cast iron

Material	Theoretical Density (kg/m³)	Experimental Density (kg/m³)
Gray Cast Iron	7114	6953.69±0.07

Table 4.3 Results of porosity measurements for gray cast iron

Material	Porosity (%)
Gray Cast Iron	3.422±0.994

The theoretical density of aluminium alloy reinforced with SiC increases with the increase of weight percentage of SiC, as shown in Table 4.4. The measured density of aluminium alloy reinforced with SiC shows an increasing trend as well. However, aluminium alloy reinforced with 20 wt% of SiC show a lower density. This is due to the increased amount of porosity (Aqida et al., 2004). Aluminium alloy reinforced with the highest SiC shows the highest percentage of porosity, as shown in Table 4.5. The presence of porosity is attributed to the clustering of particulates which will be confirmed in Section 4.4.1.

Table 4.4 Results of theoretical and experimental density for aluminium alloy reinforced with SiC

Material	Theoretical Density (kg/m³)	Experimental Density (kg/m³)
Aluminium alloy + 5 wt% SiC	2740.92	2643.60±0.02
Aluminium alloy + 10 wt% SiC	2762.16	2683.43±0.01
Aluminium alloy + 15 wt% SiC	2783.74	2715.17±0.02
Aluminium alloy + 20 wt% SiC	2805.66	2626.72±0.11

Table 4.5 Results of porosity measurements for aluminium alloy reinforced with SiC

Material	Porosity (%)
Aluminium alloy + 5 wt% SiC	3.552±0.653
Aluminium alloy + 10 wt% SiC	2.852±0.175
Aluminium alloy + 15 wt% SiC	2.464±0.559
Aluminium alloy + 20 wt% SiC	6.380±3.996

The theoretical density of aluminium alloy reinforced with Al_2O_3 increases with the increase of weight percentage of Al_2O_3 which is shown in Table 4.6. The measured density of aluminium alloy reinforced with Al_2O_3 shows an increasing trend as well. The percentage of porosity in the aluminium alloy reinforced with Al_2O_3 samples is shown in Table 4.7. In comparison with aluminium alloy reinforced with SiC, aluminium alloy reinforced with Al_2O_3 shows lower percentage of porosity.

Table 4.6 Results of theoretical and experimental density for aluminium alloy reinforced with Al_2O_3

Material	Theoretical Density (kg/m^3)	Experimental Density (kg/m^3)
Aluminium alloy + 5 wt% Al_2O_3	2763.75	2716.49±0.02
Aluminium alloy + 10 wt% Al_2O_3	2808.93	2729.11±0.04
Aluminium alloy + 15 wt% Al_2O_3	2855.61	2816.70±0.04
Aluminium alloy + 20 wt% Al_2O_3	2903.86	2849.19±0.01

Table 4.7 Results of porosity measurements for aluminium alloy reinforced with Al_2O_3

Material	Porosity (%)
Aluminium alloy + 5 wt% Al_2O_3	1.711±0.686
Aluminium alloy + 10 wt% Al_2O_3	2.842±1.504
Aluminium alloy + 15 wt% Al_2O_3	1.363±1.416
Aluminium alloy + 20 wt% Al_2O_3	1.883±0.271

Table 4.8 shows the theoretical and measured density for FGM. It is observed that the measured density of FGM is much lower than the theoretical density. This is due to the presence of porosity. It is observed that the presence of porosity is high with the highest percentage of porosity registering at (18.892±1.634)% for FGM – A1. These FGM samples are known to be very porous materials, especially in the presence of aluminium titanate (Figure 4.3d). The presence of porosity can be lowered by sintering at a higher temperature (1600 – 1800°C) but this is not recommended as it might cause residual stress during the cooling phase on top of increasing the tendency for fracture (Roman et al., 2008).

Other composite materials such as carbon/carbon composites (Su et al., 2010), carbon/carbon-silicon carbide composites (Chuan et al., 2008; Fan et al., 2008), carbon/silicon carbide (Fab et al., 2011) contain an unavoidable but reasonable amount of porosity (within 10%). Porosity is to be kept at a minimal percentage and does not encourage the tendency to fracture.

Table 4.8 Results of theoretical and experimental density for FGM

Material	Theoretical Density (kg/m^3)	Experimental Density (kg/m^3)
FGM - A1	3852	3124.50±0.06
FGM - A2	3900	3450.33±0.07
FGM - A3	3840	3454.33±0.08

Table 4.9 Results of porosity measurements for FGM

Material	Porosity (%)
FGM - A1	18.892±1.634
FGM - A2	11.533±1.745
FGM - A3	10.047±2.069

The density for available composite materials in the market is shown in Table 4.10. Both MMC and FGM acquire higher density compared to carbon/carbon composite, C/SiC composite and C/C-SiC composite. Despite that, both MMC and FGM acquire much lower density than that of gray cast iron. This shows that these composite materials are comparatively lighter than gray cast iron.

Table 4.10 Density of available composite materials in the market

Material	Density (kg/m³)
Carbon/carbon composite	1760 (Luo and Li, 2003)
C/SiC composite	2100 (Fan et al., 2007)
C/C-SiC composite	1900 - 2000 (Heidenreich, 2013)

4.3 HARDNESS

Metal Matrix Composite (MMC)

The results of hardness test performed on the gray cast iron and MMC samples are shown in Table 4.11, Table 4.12 and Table 4.13 respectively. The hardness value for each type of specimens is carried out with an average of 3 areas each on a sample and errors are the standard deviations.

Compared to gray cast iron, MMCs have lower hardness values. The presence of hard particles (silicon carbide and alumina) has helped increase the hardness of the MMC but its fluctuating hardness values is attributed to the presence of porosity (Aqida et al., 2004; Hong et al., 2003). Aluminium alloy MMC reinforced with SiC has higher hardness values than aluminium alloy MMC reinforced with Al₂O₃. The hardness property has influence on the tensile properties and wear resistance of MMC (Barmouz et al., 2010). This will be further discussed in the Section 4.4 and Section 4.7.

Table 4.11 Results of hardness tests carried out for gray cast iron

Material	Hardness (HRB)
Gray Cast Iron	86.0±3.7

Table 4.12 Results of hardness tests carried out for aluminium alloy reinforced with SiC

Material	Hardness (HRB)
Aluminium alloy + 5 wt% SiC	51.4±3.3
Aluminium alloy + 10 wt% SiC	65.4±3.1
Aluminium alloy + 15 wt% SiC	57.9±3.2
Aluminium alloy + 20 wt% SiC	73.6±4.7

Table 4.13 Results of hardness tests carried out for aluminium alloy reinforced with Al₂O₃

Material	Hardness (HRB)
Aluminium alloy + 5 wt% Al ₂ O ₃	46.8±1.0
Aluminium alloy + 10 wt% Al ₂ O ₃	53.9±4.8
Aluminium alloy + 15 wt% Al ₂ O ₃	61.3±6.2
Aluminium alloy + 20 wt% Al ₂ O ₃	67.4±2.0

4.4 TENSILE STRENGTH, YIELD STRENGTH AND YOUNG'S MODULUS

The tensile properties of gray cast iron and MMC samples are shown in Table 4.14. The tensile test for each type of specimens was carried out with an average of 3 samples each and errors are the standard deviations. Table 4.15 shows the tensile strength of MMC studied by different researchers.

Table 4.14 Results of tensile properties for gray cast iron and MMC

Material	Tensile Strength (MPa)	Young's Modulus (GPa)
Gray Cast Iron	128.18±0.28	61.43±0.14
Aluminium alloy + 5 wt% SiC	96.93±0.11	3.32±0.18
Aluminium alloy + 10 wt% SiC	104.77±0.62	4.13±0.76

Aluminium alloy + 15 wt% SiC	89.31±0.84	3.37±0.09
Aluminium alloy + 20 wt% SiC	85.09±1.17	4.18±0.59
Aluminium alloy + 5 wt% Al₂O₃	99.33±0.36	5.08±1.31
Aluminium alloy + 10 wt% Al₂O₃	96.56±0.08	3.54±0.20
Aluminium alloy + 15 wt% Al₂O₃	91.78±0.50	3.22±0.32
Aluminium alloy + 20 wt% Al₂O₃	75.03±0.20	2.62±0.02

Table 4.15 Tensile strength of MMC by different researchers

Materials	Tensile Strength (MPa)
Al6061 reinforced with 2, 4, 6wt% of SiC (150µm diameter size)	120 – 170 (Veeresh Kumar et al., 2012)
Aluminium alloy MMC reinforced with 7wt% of Al ₂ O ₃ (20µm diameter size)	145 (Ezatpour et al., 2013)
Aluminium alloy 2024 reinforced with 3, 5, 7, 10 vol% of SiC (10µm diameter size)	264, 320, 374, 308MPa (Hong et al., 2003)
Aluminium alloy 6063 reinforced with 3, 6, 9, 12 vol% of SiC (30µm diameter size)	114.7, 121.4, 150.7, 158.5 (Alaneme and Aluko, 2012)
Aluminium alloy 359 reinforced with 10 vol% of SiC (29.2µm diameter size)	150MPa (Hashim, 2001)

Although gray cast iron acquires lower tensile strength compared to the required strength (150MPa), it is still within its designated SAE J431 G1800 class strength (124MPa).

Table 4.14 shows that aluminium alloy reinforced with 5 wt% of SiC and 10 wt% of SiC MMCs show an increase in tensile strength. Table 4.15 shows that this is in agreement with the findings of Veeresh Kumar et al (2012). When the composite is subject to strain, the hard particles in the aluminium alloy matrix act as a barrier that resists plastic deformation. This explains the increase of tensile strength of the composites. The presence of hard particle in a soft matrix increases the dislocation density. Aluminium alloy reinforced with SiC has higher dislocation density than that of aluminium alloy reinforced with Al₂O₃ (McDanel, 1985).

Aluminium alloy reinforced with Al_2O_3 MMC shows decreasing tensile strength values as the reinforcement particulates increase. This is due to the increase of agglomerations (Kang and Chan, 2004) which is observed in Section 4.4.1.

Aluminium alloy reinforced with 15 wt% of SiC and 20 wt% of SiC MMCs also show a decrease in tensile strength. This is due to the clustering of particulates (Aqida et al., 2004; Hong et al., 2003) which is observed in Section 4.4.1.

Table 4.14 shows that MMC samples acquire lower Young's modulus compared to gray cast iron. The increase of weight fraction will increase the percentage of matrix to constraints, thus it will be unable to deform plastically. Particulates reinforced MMCs' specimen failure arises from the formation and growth of voids at the reinforcement-matrix interface (Aqida et al., 2004). There is further decrease in ductility if microstructural features such as voids are present. Particulates reinforced MMCs' ductility relies on the strain at which damage nucleates and the growth rate to cause failure. It has been predicted that the process of void coalescence is expected to initiate failure. As micropores form during solidification of the reinforced alloys, reinforcement particles appear to have major stress raising effect on the formation of slip bands and cracks. These micropores are favoured nucleation sites for fatigue cracks. During the tensile test, when stress is applied, porosity tends to develop the strain of a particular region in MMC (Aqida et al., 2004).

Figure 4.4 and 4.5 show that the material fractures before it yields. This is due to the presence of hard silicon carbide particles in the MMCs which enhances its hardness as presented in Table 4.12 and Table 4.13 respectively. This results in a brittle fracture.

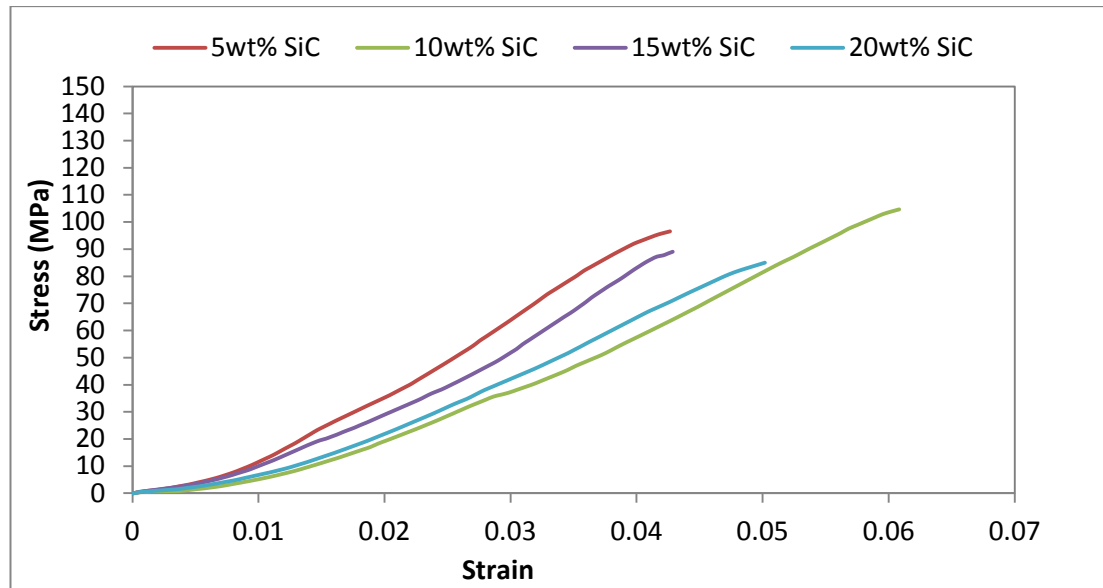


Figure 4.4 Stress versus strain curves for aluminium alloy MMC (reinforced with different weight percentage of SiC)

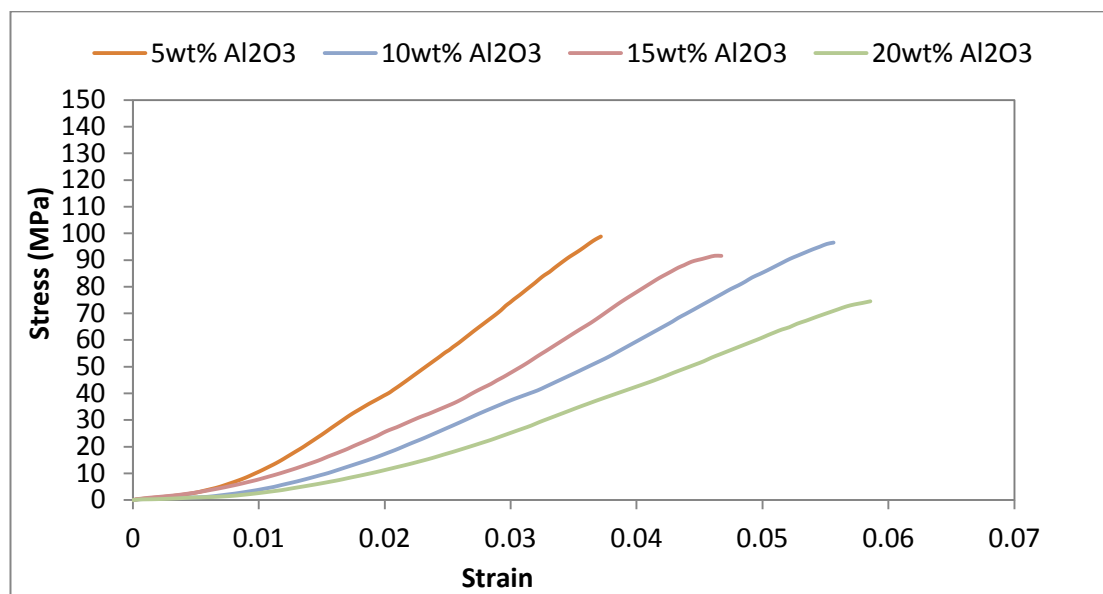


Figure 4.5 Stress versus strain curves for aluminium alloy MMC (reinforced with different weight percentage of Al₂O₃)

Table 4.16 shows Young's modulus of available composite materials in the market. MMC acquired a lower Young's Modulus than that of C/SiC composite and C/C-SiC composite. This shows that the low Young's modulus of MMC helps to promote uniform contact between the disc brake and the brake pads.

Table 4.16 Young's modulus comparison of available materials with MMC

Materials	Young's Modulus (GPa)
Carbon/carbon composite	Not available
C/SiC composite	65 (Fan et al., 2007)
C/C-SiC composite	50 - 70 (Heidenreich, 2013)

Table 4.17 show the available data for tensile strength of composite materials in the market. Although MMC acquire slightly lower tensile strength compared to gray cast iron, it still shows an increase in its tensile strength. The tensile strength and Young's modulus of MMC are promising for the development of a new material for the car brake rotor.

Table 4.17 Tensile strength of available materials in the market

Materials	Tensile Strength (MPa)
Gray Cast Iron (SAE J431 G1800 class)	124MPa
Carbon/carbon composite	Not available
C/SiC composite	145 (Fan et al., 2007)
C/C-SiC composite	80 – 190 (Heidenreich, 2013)

4.4.1 Fracture Analysis

Gray Cast Iron

The microstructure of gray cast iron (with a pearlitic matrix) depends on the amount of carbon because it is able to affect the mechanical properties of the matrix. Figure 4.6 shows a compilation of SEM images of fractured gray cast iron samples. The graphite flakes are observed to be surrounded by ferrite matrix. It can be seen that the fractured path of the sample may follow flake graphite in its longitudinal direction. The tensile fracture surfaces of gray cast iron exhibit the typical cleavage fracture as seen in Figure 4.6c. Cleavage rupture is the dominant fracture under tensile loading and this indicates that there is no significant plastic deformation under loading (Taslicukur et al., 2012). Small amount of visible microvoids or cracks can be seen in Figure 4.6c. These microvoids/cracks are said to be formed by the weak location of

flake graphites (Hsu et al., 2002). These microvoids/cracks may have influence on the crack propagation which leads to the final rupture of the sample.

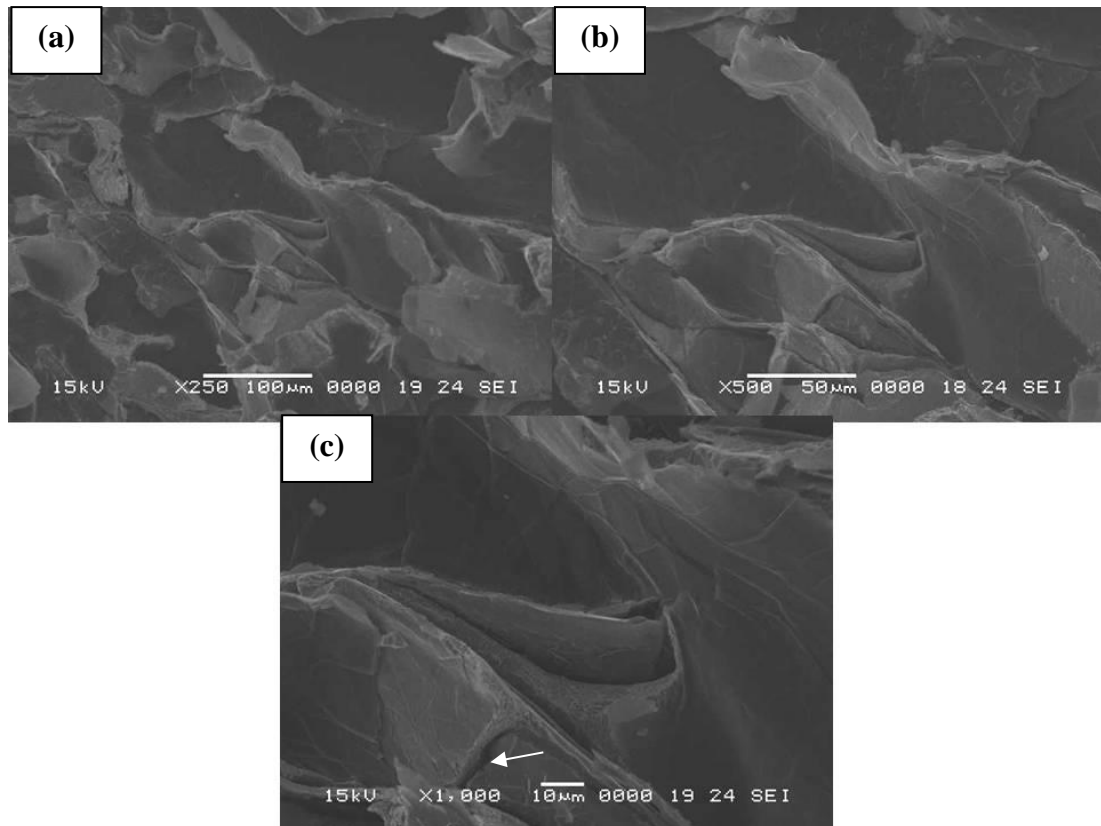


Figure 4.6 Scanning electron images microstructure of tensile fracture surface of gray cast iron

Metal Matrix Composite (MMC)

Cracks are first initiated at the interface between the aluminium alloy matrix and silicon carbide. The second crack initiation is due to cracking of the large size silicon carbide particle. It is observed that particle fracture is the main damage prior to final fracture (Abdullah et al., 2009; Razaghian et al., 1998). It is observed in Figure 4.7 and Figure 4.8 that large particles and regions of clustered particles are prone to damage in the composites (Hashim, 2001). Agglomeration of particles tends to reduce the strong bond between aluminium alloy matrix and silicon carbide particles. Larger particles produce high load transfer from the plastically deforming aluminium alloy matrix and the elastically deforming particle. This can result in cracking. In addition, the presence of porosity also induces cracking.

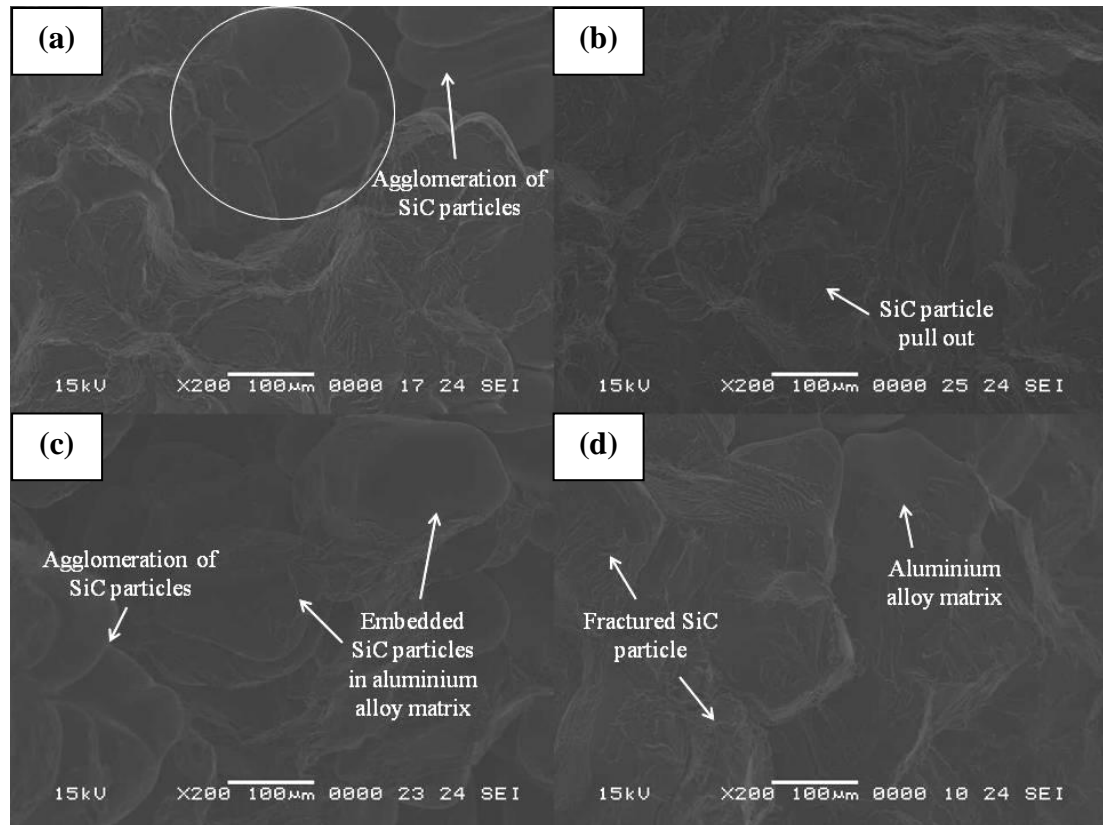


Figure 4.7 Scanning electron images (at 100μm) microstructure of tensile fracture surface of aluminium alloy MMC with different weight percentage of reinforced silicon carbide (SiC) (a) 5 wt% SiC (b) 10 wt% SiC (c) 15 wt% SiC (d) 20 wt% SiC

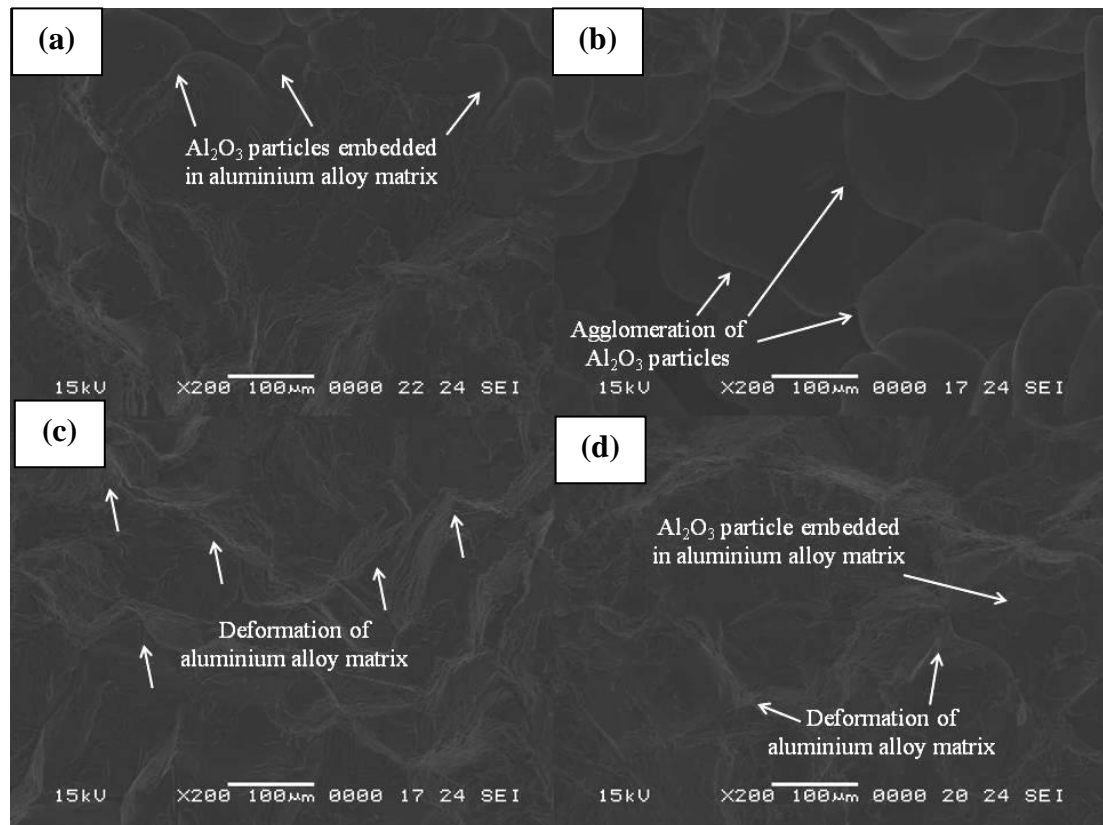


Figure 4.8 Scanning electron images (at 100 μm) microstructure of tensile fracture surface of aluminium alloy MMC with different weight percentage of reinforced alumina (Al_2O_3) (a) 5 wt% Al_2O_3 (b) 10 wt% Al_2O_3 (c) 15 wt% Al_2O_3 (d) 20 wt% Al_2O_3

The arrows in Figure 4.9 and Figure 4.10 illustrate transgranular fracture with flat and cleavage planes. In addition sharp edges are spotted. There is no presence of obvious ductile dimples (Figure 4.14 and Figure 4.15), which is a clear indication of brittle fracture. Hence it can be confirmed that the MMC fracture samples experience brittle fracture.

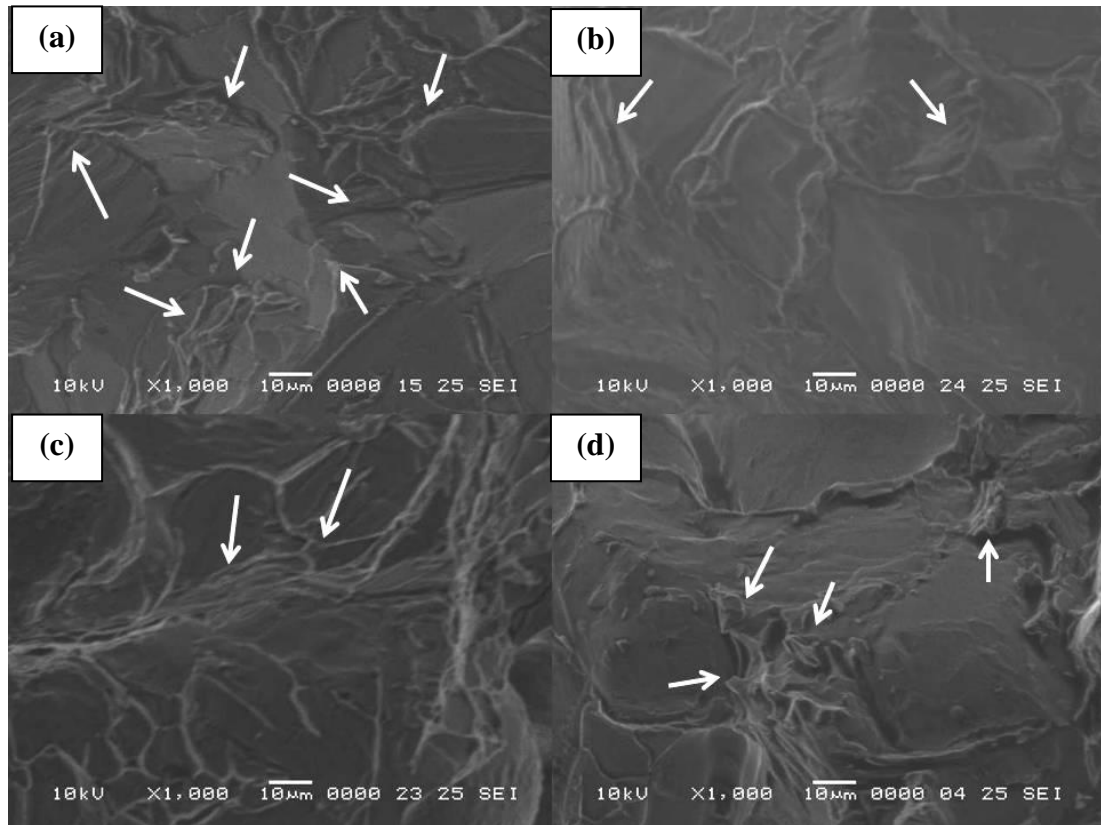


Figure 4.9 Scanning electron images (at 10µm) microstructure of tensile fracture surface of aluminium alloy MMC with different weight percentage of reinforced silicon carbide (SiC) (a) 5 wt% SiC (b) 10 wt% SiC (c) 15 wt% SiC (d) 20 wt% SiC

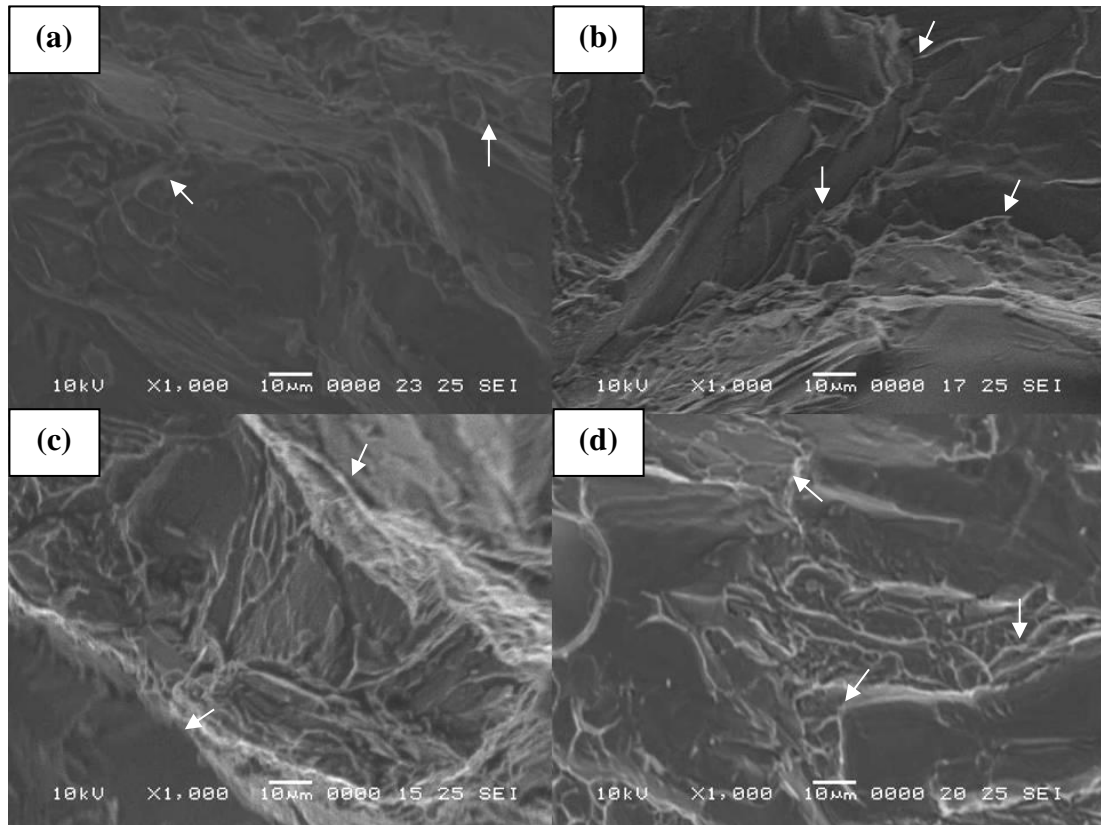


Figure 4.10 Scanning electron images (at 10 μ m) microstructure of tensile fracture surface of aluminium alloy MMC with different weight percentage of reinforced alumina (Al_2O_3) (a) 5 wt% Al_2O_3 (b) 10 wt% Al_2O_3 (c) 15 wt% Al_2O_3 (d) 20 wt% Al_2O_3

4.5 FRACTURE TOUGHNESS

Metal Matrix Composite (MMC)

As the reinforcement particulates content in MMC increases, the fracture toughness reduces as the formation and merge of voids within the matrix tend to cause fracture in MMC. Table 4.18 and Table 4.19 show the fluctuating values of the fracture toughness. This is due to particulates clustering, which is illustrated in Figure 4.12 and Figure 4.13.

ASTM A48 Grade 20/SAE J431 G1800 has provided an estimation of the fracture toughness of gray cast iron, $11\text{MPa}\cdot\text{m}^{1/2}$. The fracture toughness of gray cast iron is comparatively lower than that of MMC. This shows that gray cast iron may be prone to failure.

Aluminium alloy reinforced with 5 wt% silicon carbide, aluminium alloy reinforced with 15 wt% silicon carbide, aluminium alloy reinforced with 10 wt% alumina, aluminium alloy reinforced with 15 wt% alumina and aluminium alloy reinforced with 20 wt% alumina show fracture toughness of more than $15\text{MPa}\cdot\text{m}^{1/2}$ which is in accordance to Ashby (2005).

Table 4.18 Results of fracture toughness for aluminium alloy reinforced with SiC

Material	Fracture toughness ($\text{MPa}\cdot\text{m}^{1/2}$)
Aluminium alloy + 5 wt% SiC	17.45±0.04
Aluminium alloy + 10 wt% SiC	14.94±0.04
Aluminium alloy + 15 wt% SiC	20.45±0.11
Aluminium alloy + 20 wt% SiC	13.97±0.08

Table 4.19 Results of fracture toughness for aluminium alloy reinforced with Al_2O_3

Material	Fracture toughness ($\text{MPa}\cdot\text{m}^{1/2}$)
Aluminium alloy + 5 wt% Al_2O_3	13.43±0.03
Aluminium alloy + 10 wt% Al_2O_3	18.11±0.06
Aluminium alloy + 15 wt% Al_2O_3	16.31±0.14
Aluminium alloy + 20 wt% Al_2O_3	16.72±0.05

4.5.1 Fracture Analysis

Both Figures 4.11 and 4.12 show visible transgranular fracture with flat, cleavage planes and sharp edges are visible. A small amount of ductile dimple is visible in Figure 4.11a, Figure 4.11b, Figure 4.12b and Figure 4.12c. The fracture surface of the MMC samples is still classified as brittle fracture. Figure 4.11b demonstrates a large dimple which is associated with the pullout of silicon carbide particle. As load is applied to the fracture toughness sample, silicon carbide is pulled out from the aluminium alloy matrix.

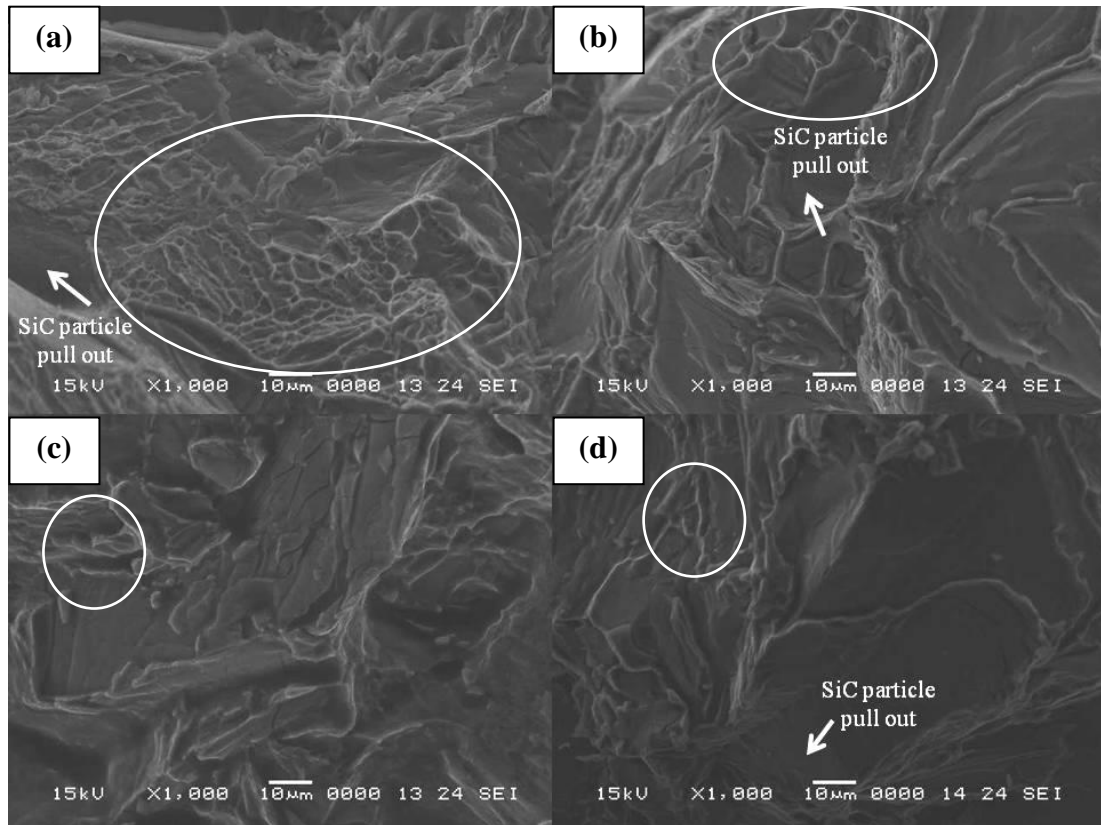


Figure 4.11 Scanning electron images microstructure of fracture toughness' fracture surface of aluminium alloy MMC with different weight percentage of reinforced silicon carbide (SiC) (a) 5 wt% SiC (b) 10 wt% SiC (c) 15 wt% SiC (d) 20 wt% SiC

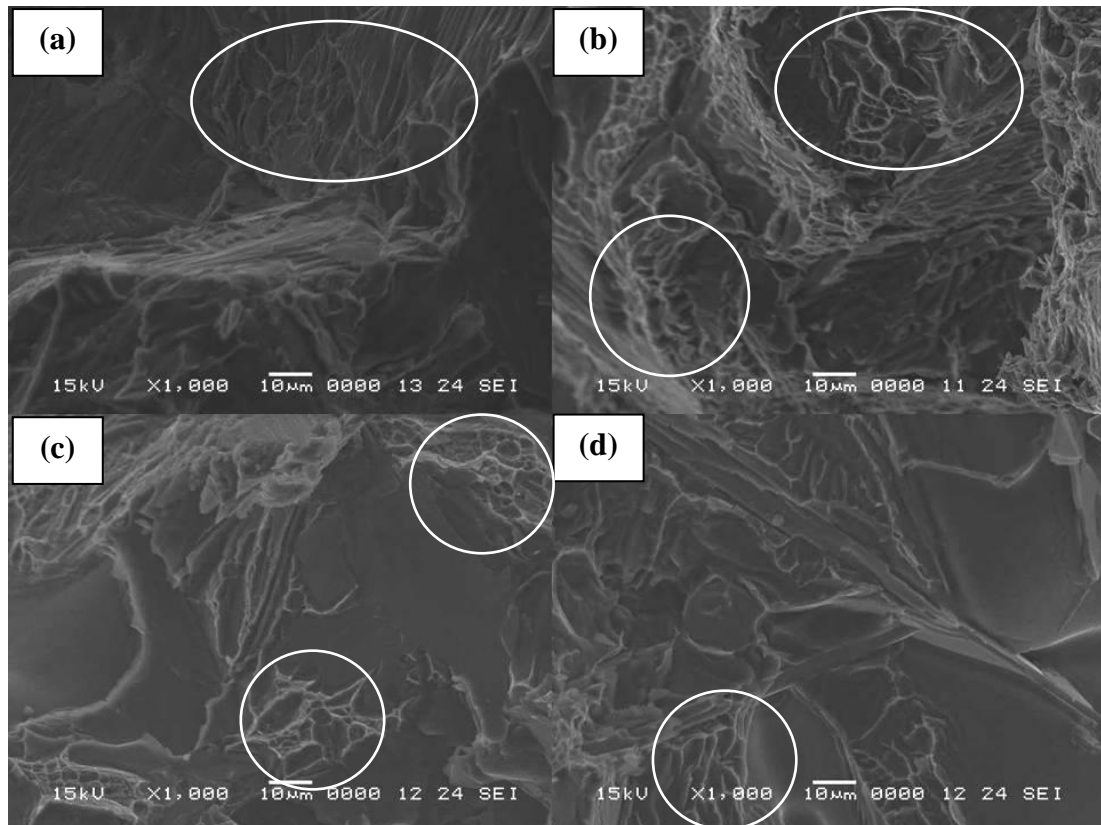


Figure 4.12 Scanning electron images microstructure of fracture toughness' fracture surface of aluminium alloy MMC with different weight percentage of reinforced alumina (Al_2O_3) (a) 5 wt% Al_2O_3 (b) 10 wt% Al_2O_3 (c) 15 wt% Al_2O_3 (d) 20 wt% Al_2O_3

4.6 COMPRESSIVE STRENGTH RESULTS

Compression tests for each type of specimen were carried out with an average of 3 samples each and errors are the standard deviations. The results of the compression tests performed on the gray cast iron and MMC samples are shown in Table 4.20, Table 4.21 and Table 4.22 respectively.

The results of compressive tests of MMC are lower than that of gray cast iron.

It is illustrated in Table 4.21 that aluminium alloy reinforced with 20 wt% of silicon carbide shows the lowest compressive strength and yield strength. Aluminium alloy reinforced with alumina show fluctuating results. This is due to the increased amount of clustering (Hong et al., 2003) which is shown in Figure 4.12 and Figure 4.13.

Table 4.20 Results of compression test for gray cast iron

Material	Compressive Strength (MPa)	Yield Strength (MPa)	Young's Modulus (GPa)
Gray Cast Iron	735.14±0.24	427.81±0.15	22.01±0.04

Table 4.21 Results for compression test for aluminium alloy MMC (with different weight percentage of SiC)

Samples	Compressive Strength (MPa)	Yield Strength (MPa)	Young's Modulus (GPa)
Aluminium alloy + 5 wt% SiC	126.41±0.08	109.38±0.09	2.25±0.05
Aluminium alloy + 10 wt% SiC	147.42±0.15	113.28±0.08	2.54±0.08
Aluminium alloy + 15 wt% SiC	154.30±0.19	125.00±0.15	4.30±0.07
Aluminium alloy + 20 wt% SiC	130.86±0.04	101.56±0.06	3.52±0.08

Table 4.22 Results for compression test for aluminium alloy MMC (with different weight percentage of Al₂O₃)

Samples	Compressive Strength (MPa)	Yield Strength (MPa)	Young's Modulus (GPa)
Aluminium alloy + 5 wt% Al₂O₃	136.72±0.05	113.28±0.08	4.10±0.06
Aluminium alloy + 10 wt% Al₂O₃	126.95±0.04	105.47±0.11	3.32±0.09
Aluminium alloy + 15 wt% Al₂O₃	140.63±0.13	113.28±0.15	4.30±0.06
Aluminium alloy + 20 wt% Al₂O₃	151.41±0.08	125.00±0.09	4.30±0.05

Table 4.23 shows the compressive results for FGM samples. FGM samples show very low compressive strength than that of gray cast iron. The low compressive strength could be due to graded heterogeneous $\text{Al}_2\text{TiO}_5/\text{Al}_2\text{O}_3$ layers which exhibit a relatively ‘soft’ surface. FGM – A1 has the lowest compressive strength due to its high percentage of porosity.

Table 4.23 Results for compressive tests of gray cast iron and FGM samples

Samples	Compressive Strength (MPa)	Yield Strength (MPa)	Young’s Modulus (GPa)
FGM - A1	9.15±0.32	8.97±0.31	0.38±0.04
FGM - A2	11.51±0.26	10.19±0.28	0.90±0.06
FGM - A3	14.34±0.23	10.89±0.26	0.93±0.03

4.6.1 Fracture Analysis

Gray Cast Iron

Figure 4.13 illustrates the compressive fracture surface of gray cast iron. It can be seen that the fractured path of the sample follow flake graphite in its longitudinal direction. Sharp edges and cleavage rupture can be observed as well.

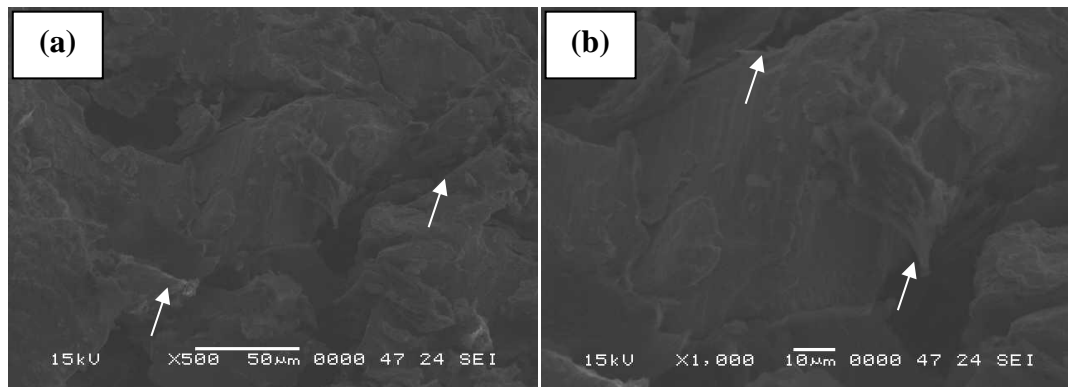


Figure 4.13 Scanning electron images microstructure of compressive fracture surface of gray cast iron

Metal Matrix Composite (MMC)

Figure 4.14 and Figure 4.15 illustrate the compressive fracture surface of MMC. It is observed that transgranular fracture with flat, cleavage planes and sharp edges. Minor amounts of ductile dimple can be observed.

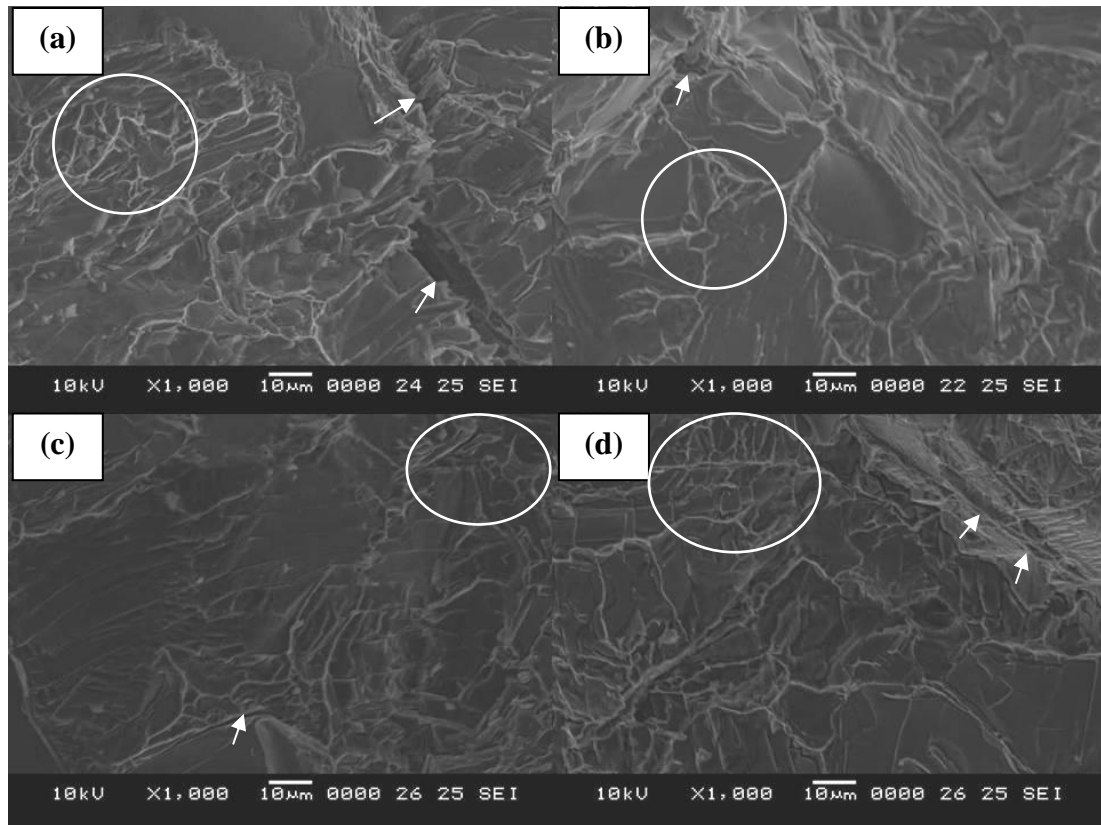


Figure 4.14 Scanning electron images microstructure of compressive fracture surface of aluminium alloy MMC with different weight percentage of reinforced silicon carbide (SiC) (a) 5 wt% SiC (b) 10 wt% SiC (c) 15 wt% SiC (d) 20 wt% SiC

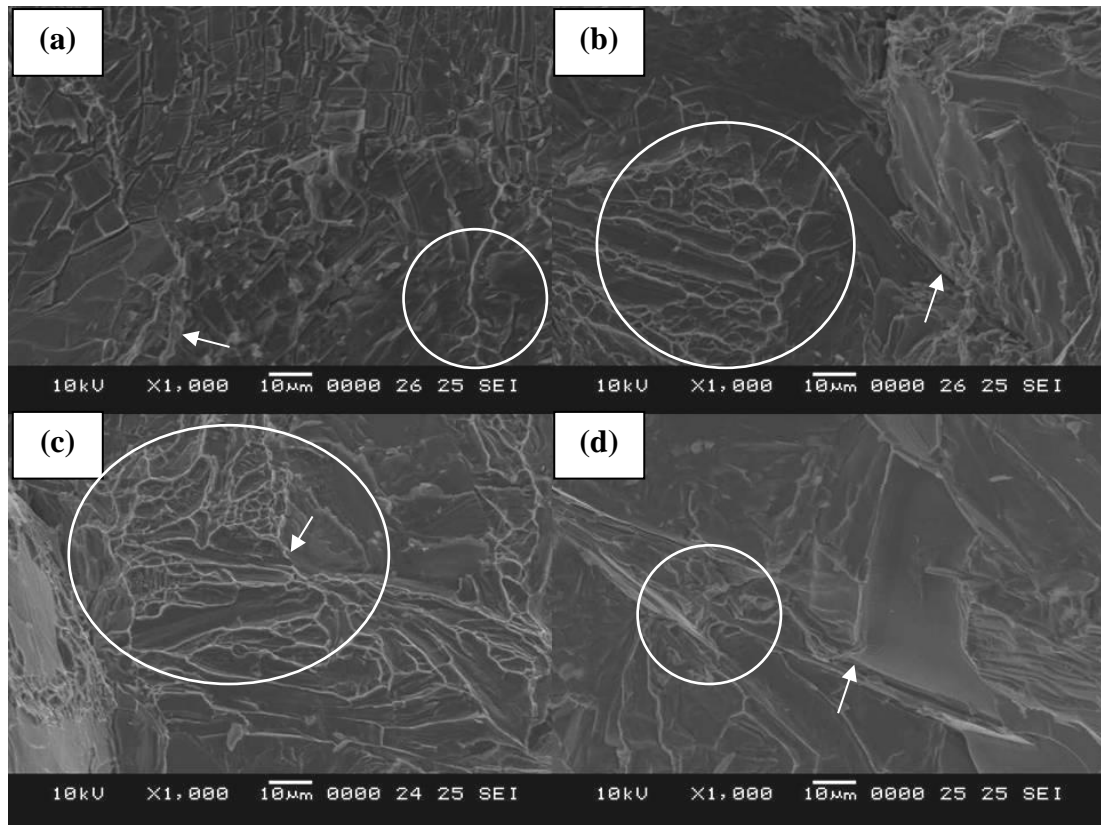


Figure 4.15 Scanning electron images microstructure of compressive fracture surface of aluminium alloy MMC with different weight percentage of reinforced alumina (Al_2O_3) (a) 5 wt% Al_2O_3 (b) 10 wt% Al_2O_3 (c) 15 wt% Al_2O_3 (d) 20 wt% Al_2O_3

Functionally Graded Material (FGM)

Figure 4.16 illustrates the compressive fracture surface of FGM. Figure 4.16a shows the pores as a great amount of black spots. This is parallel to this current study where it is identified that A1 batch contains $(18.892 \pm 1.634)\%$ of porosity.

Figure 4.16a and Figure 4.16b show that there are more white spots which is an indication of the decomposition of aluminium titanate to titania. Grey spots are observed as alumina. It is observed in Figure 4.16c that there are a great amount of sharp edges.

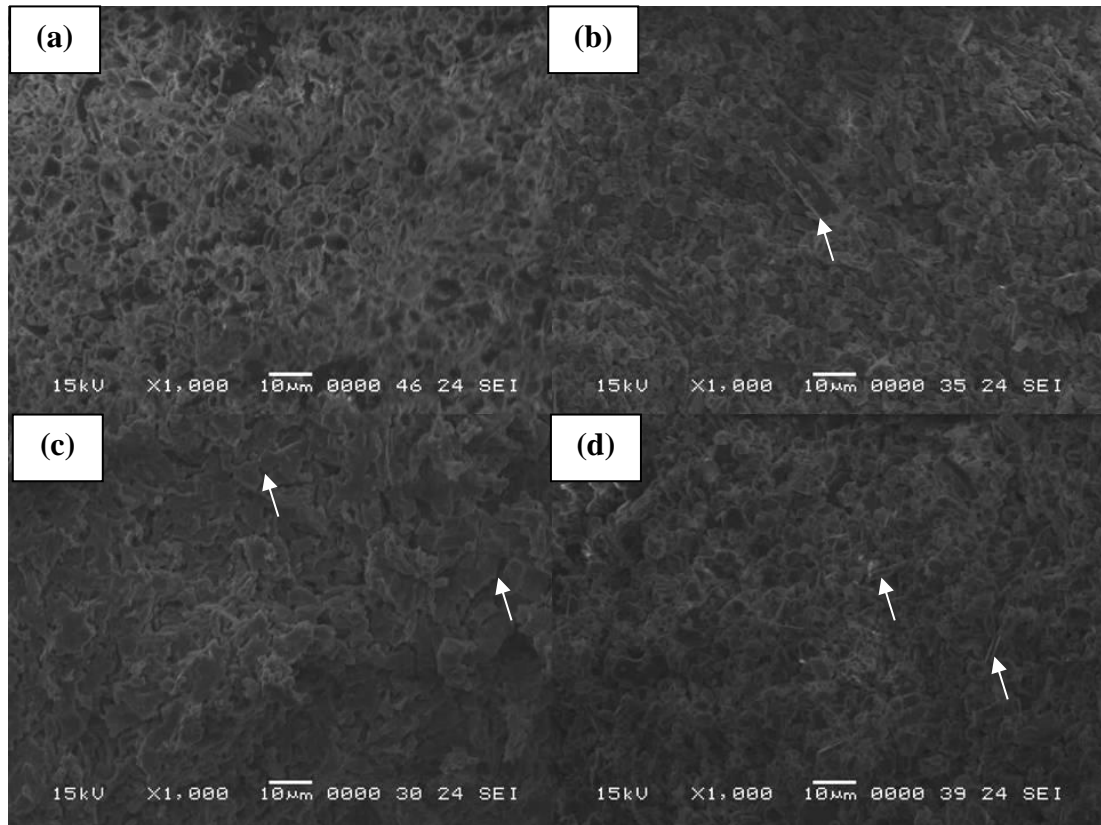


Figure 4.16 Scanning electron images microstructure of compressive fracture surface of FGM (a) A1 batch (b) A2 batch (c) A3 batch (d) Cross section of A1

4.7 WEAR PROPERTIES

To get a better understanding of the tribological characteristics of MMC, it is essential to explore the various parameters that affect their friction and wear performance. There are three principal parameters that are of interest in the present investigation: weight percentage of compositions, contact pressure and sliding speed. Wear data of all the specimens acquired from the wear tests will be presented individually for the two different composites, i.e. Gray cast iron, aluminium alloy reinforced with Al_2O_3 MMC and aluminium alloy reinforced with SiC MMC. Comparison will be made with gray cast iron in the following sections.

4.7.1 Disc Wear Rate

The summary of the disc wear for gray cast iron samples are shown in Figure 4.17. For both contact pressures (0.1MPa and 0.2MPa) under sliding speed of 1m/s, the disc wear rates increases but still remains steadily below $4 \times 10^{-3} \text{ mm}^3/\text{m}$. A similar trend can be observed for sliding speed of 0.42m/s under both contact pressure of

0.1MPa and 0.2MPa. This is consistent to both the findings of Natarajan et al. (2006), Daoud and Abou El-khair (2010). As the contact pressure increased, the disc wear rate increased as well. Despite the high contact pressure (0.3 - 1MPa) utilized for their experiments, its disc wear rate remained below $2 \times 10^{-3} \text{ mm}^3/\text{m}$ (Daoud and Abou El-khair, 2010).

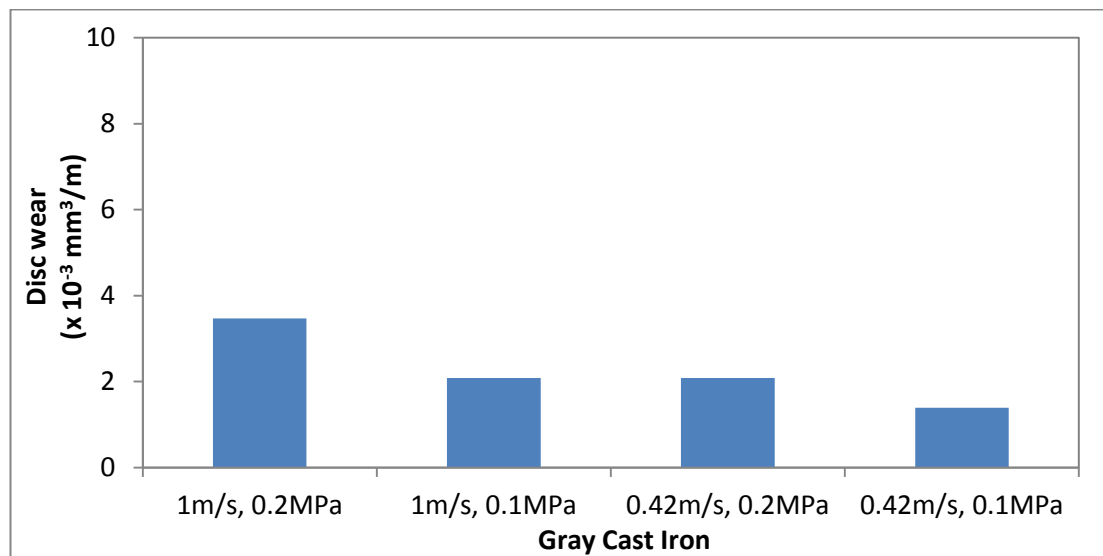


Figure 4.17 Variation of wear rate ($\times 10^{-3} \text{ mm}^3/\text{m}$) for gray cast iron samples

It can be observed in Figure 4.18, that at contact pressure of 0.1MPa under sliding speed of 1m/s, as the weight percentage of silicon carbide increases, the disc wear rate remains constant and below $20 \times 10^{-3} \text{ mm}^3/\text{m}$. The same trend can be observed for the contact pressure of 0.1MPa under sliding speed of 0.42m/s. However, there is an increase in the disc wear at contact pressure of 0.2MPa under sliding speed of 1m/s.

The disc wear rate of aluminium alloy reinforced with SiC MMC ($80 - 220 \times 10^{-3} \text{ mm}^3/\text{m}$) found in this study is higher compared to the MMCs investigated by Natarajan et al (2006), Daoud and Abou El-khair (2010), Zhang and Wang (2007), Uyyuru et al (2007) and Shivamunthy and Surappa (2011), as shown in Table 4.24.

Since a larger silicon carbide particle ($105\mu\text{m}$) is utilized, this could be due to the higher number of particles which contributed in the increase of real contact area (Uyyuru et al., 2007). As the weight percentage of reinforced silicon carbide in the

aluminium alloy increases, the wear rate increases as well. The same case is observed in Figure 4.19 for aluminium alloy reinforced with SiC MMC samples sliding under sliding speed of 0.42m/s and contact pressure of 0.2MPa.

Table 4.24 Summary of disc wear rate of various studies

Authors	Disc material	Contact pressure (MPa)	Sliding speed (m/s)	Wear rate at lowest contact pressure and lowest sliding speed
Natarajan et al (2006)	Aluminium alloy A356 with 25 vol%-SiC MMC	0.25, 0.51, 0.76, 1.02, 1.27	2.5, 3.7, 5, 6.3	$5.0 \times 10^{-5} \text{ mm}^3/\text{m}$ at sliding speed of 2.5m/s and contact pressure of 0.25MPa.
Daoud and Abou El-khair (2010)	Aluminium alloy A359 with 20 vol%-SiC MMC	0.3, 0.5, 1	3, 6, 9, 12	$6.0 \times 10^{-3} \text{ mm}^3/\text{m}$ at sliding speed of 3m/s and contact pressure of 0.3MPa.
Uyyuru et al (2007)	Aluminium MMC with 15 vol%-SiC and 20 vol%-SiC	1, 2, 3, 4	1.5, 2, 3, 4	$1.0 \times 10^{-3} \text{ mm}^3/\text{m}$ at contact pressure of 1MPa.
Shivamurthy and Surappa (2011)	Aluminium alloy A356 with 10 vol%-SiC and 20 vol%-SiC MMC	3	1, 2, 3, 4, 5	$4.3 \times 10^{-4} \text{ mm}^3/\text{m}$ at sliding speed of 1m/s for Aluminium alloy A356 with 10 vol%-SiC. $1.5 \times 10^{-4} \text{ mm}^3/\text{m}$ at sliding speed of 1m/s for Aluminium alloy A356 with 20 vol%-SiC MMC.

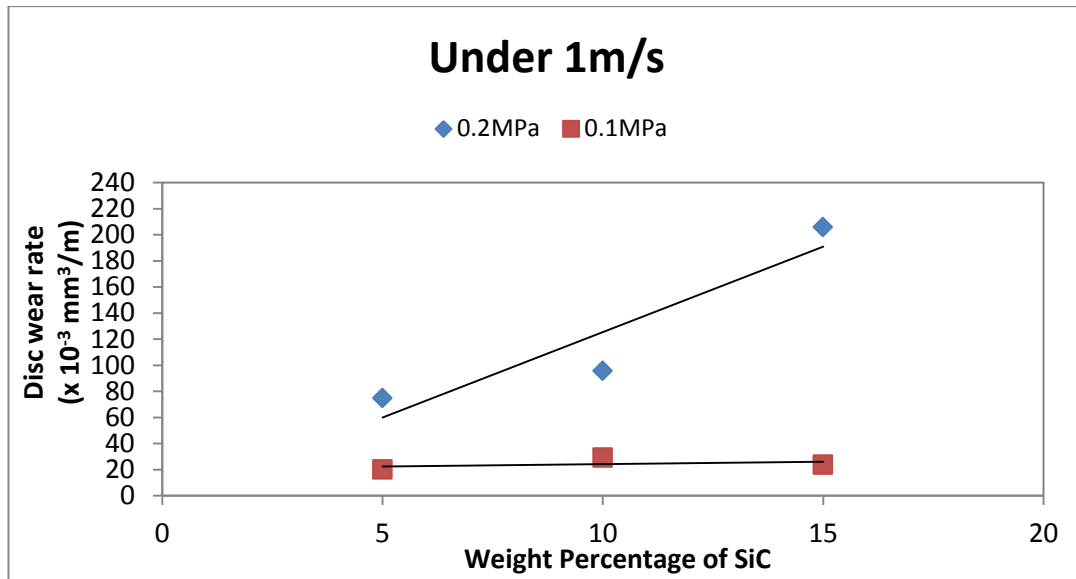


Figure 4.18 Variation of wear rate ($\times 10^{-3} \text{ mm}^3/\text{m}$) with different weight percentage of SiC for aluminium alloy reinforced with SiC MMC samples under 1m/s sliding speed

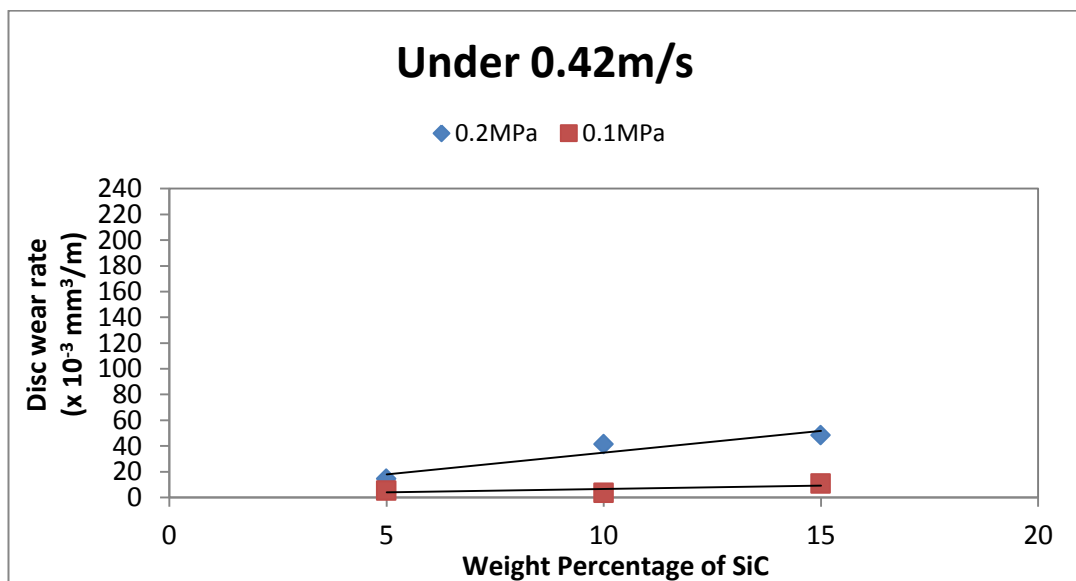


Figure 4.19 Variation of wear rate ($\times 10^{-3} \text{ mm}^3/\text{m}$) with different weight percentage of SiC for aluminium alloy reinforced with SiC MMC samples under 0.42m/s sliding speed

It is observed in Figure 4.20 that at contact pressure of 0.2MPa under sliding speed of 1m/s, as the weight percentage of alumina in the aluminium alloy increases, there is a significant decrease in the disc wear. Figure 4.21 presents a similar trend for the same contact pressure under a low sliding speed of 0.42m/s. For the same contact

pressure of 0.1MPa under sliding speeds of 0.42m/s and 1m/s, as the weight percentage of alumina in the aluminium alloy increases, there is a minor decrease in the disc wear. It can be observed that the wear rate of the disc decreases at higher weight percentage of alumina particles in the aluminium alloy.

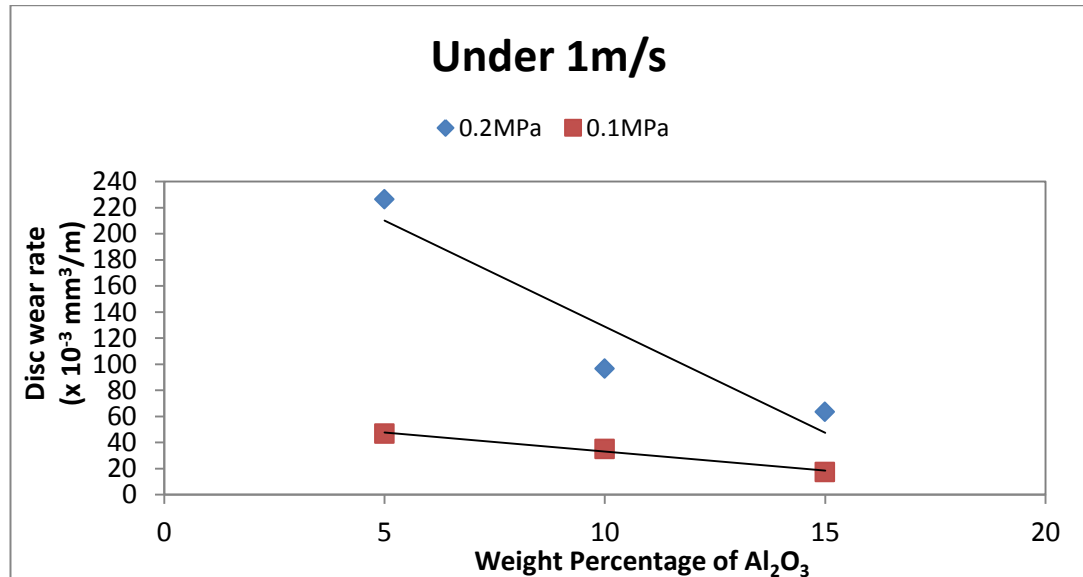


Figure 4.20 Variation of wear rate ($\times 10^{-3} \text{ mm}^3/\text{m}$) with different weight percentage of Al₂O₃ for aluminium alloy reinforced with Al₂O₃ MMC samples under 1m/s sliding speed

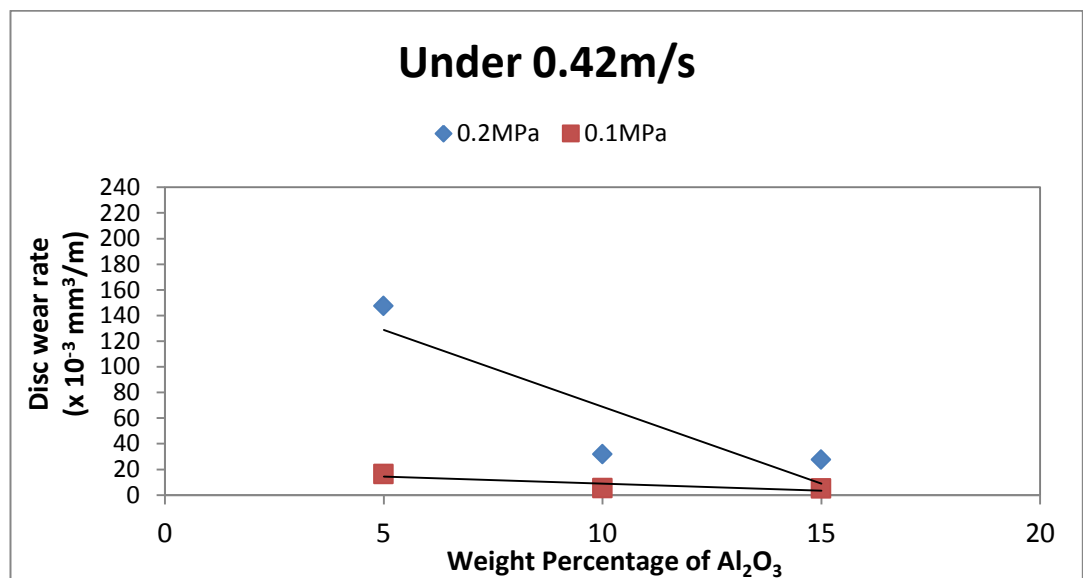


Figure 4.21 Variation of wear rate ($\times 10^{-3} \text{ mm}^3/\text{m}$) with different weight percentage of Al₂O₃ for aluminium alloy reinforced with Al₂O₃ MMC samples under 0.42m/s sliding speed

At the highest weight percentage (15%) of alumina in the aluminium alloy, lower wear rate is acquired at high contact pressure (0.2MPa) for both sliding speeds; whereas lowest weight percentage (5%) of silicon carbide in the aluminium alloy performs better at high contact pressure (0.2MPa) for both sliding speeds. However, in comparison to gray cast iron, both aluminium alloy reinforced with SiC MMC and aluminium alloy reinforced with Al₂O₃ MMC still attain higher wear rate. This is in agreement with what Anoop et al (2009) have found, where at higher contact pressure, the wear rate of the disc increases.

4.7.2 Coefficient of Friction (COF)

Figure 4.22 shows the summary of the coefficient of friction (COF) for gray cast iron samples is shown in Figure 4.22. Under sliding speed of 1m/s and both contact pressure of 0.1MPa and 0.2MPa, the COF remains within the range of 0.2 to 0.3. However, under sliding speed of 0.42m/s and both contact pressures of 0.1MPa and 0.2MPa, lower COF values in the range of 0.1 to 0.2 are acquired. In this study, gray cast iron has performed unsatisfactorily under all conditions, with COF registering below 0.3. This is consistent to the findings of Daoud and Abou El-khair (2010). As the contact pressure (0.3 – 1MPa) increased, the COF decreases and goes below 0.3 as well. However, Natarajan et al (2006) found that as the contact pressure increased (0.25 – 1.27MPa), the COF decreased and stays within the range of 0.25 to 0.45.

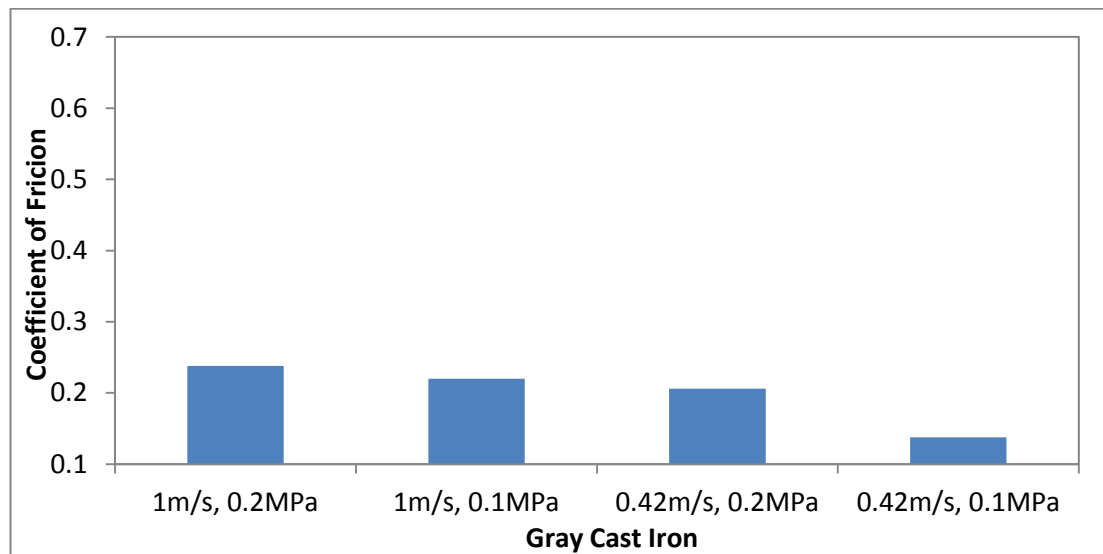


Figure 4.22 Variation of coefficient of friction for gray cast iron samples

It is shown in Figure 4.23 that for both contact pressures of 0.1MPa and 0.2MPa under sliding speed of 1m/s, the weight percentage of silicon carbide in the aluminium alloy increases; the best trend line shows that the COF increase but remain in the range of 0.3 to 0.6. Friction coefficient for all aluminium alloy reinforced with SiC is observed to be within range for automotive vehicles. Aluminium alloy reinforced with SiC MMC achieves better COF than that of gray cast iron. This is in agreement with the findings of Natarajan et al (2006) where the COF tends to be much higher than gray cast iron. However, Figure 4.24 shows that at contact pressure of 0.1MPa under sliding speed of 0.42m/s, as the weight percentage of silicon carbide in the aluminium alloy increases, the COF remains in the range of 0.1 to 0.2. The same case is observed for gray cast iron under the same condition. While for contact pressure of 0.2MPa under sliding speed of 0.42m/s, Aluminium alloy reinforced with SiC MMC achieves COF in the range of 0.2 to 0.4 whereas gray cast iron registering at around 0.2. Both aluminium alloy reinforced with SiC MMC and gray cast iron acquire lower friction coefficient at the same condition.

Table 4.25 shows the COF ranges based on various research. Natarajan et al (2006) found that at lowest contact pressure (0.25MPa) and sliding speed (2.5m/s), the COF is still quite high at 0.6. Daoud and Abou El-khair's obtained similar findings where at lowest contact pressure (0.30MPa) and sliding speed (3m/s), COF is 0.46. The experimental condition of Shorowordi et al (2004) is close to this study. They have observed that at lowest speed of 1.62m/s and 3MPa of contact pressure, COF is 0.45. All of these researchers' findings are consistent with what is observed in this study.

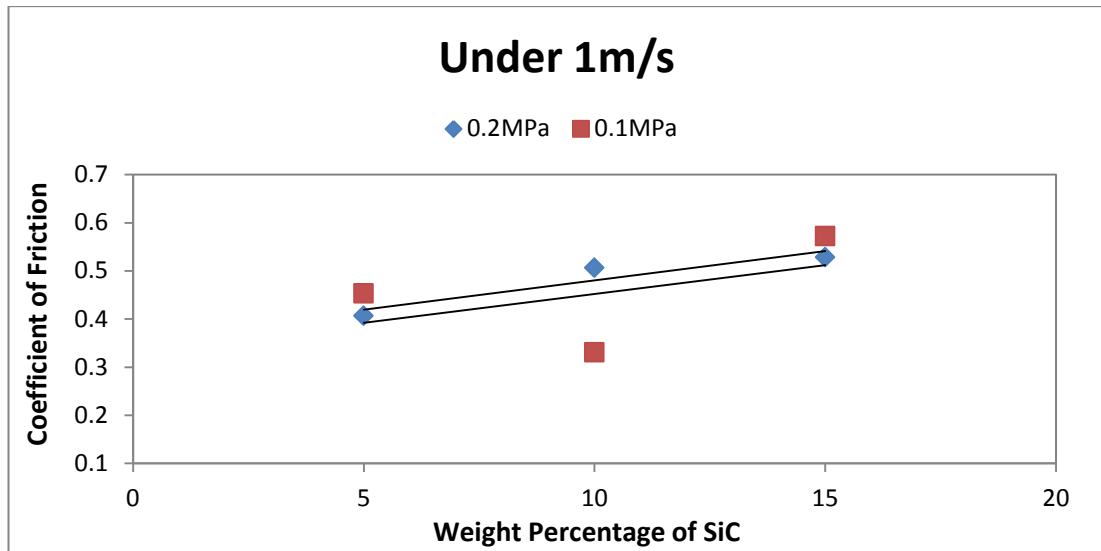


Figure 4.23 Variation of coefficient of friction with different weight percentage of SiC for aluminium alloy reinforced with SiC MMC samples under 1m/s sliding speed

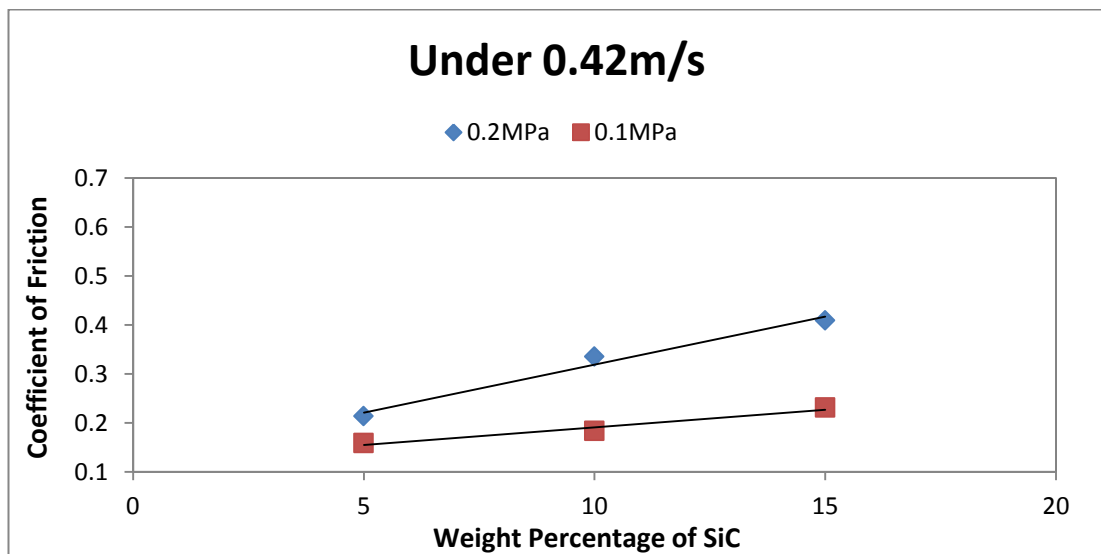


Figure 4.24 Variation of coefficient of friction with different weight percentage of SiC for aluminium alloy reinforced with SiC MMC samples under 0.42m/s sliding speed

Table 4.25 Summary of range of COF of various studies

Authors	Materials		Applied pressure (MPa)	Sliding speed (m/s)	Range of COF
	Disc	Pin			
Natarajan et al (2006)	Aluminium alloy A356 with 25 vol%-SiC MMC and cast iron	Brake shoe lining of a commercial passenger car	0.25, 0.51, 0.76, 1.02, 1.27	2.5, 3.7, 5, 6.3	0.5 – 0.7
Daoud and Abou El-khair (2010)	Aluminium alloy A359 with 20 vol%-SiC MMC and cast iron	Commercial automotive brake material	0.3, 0.5, 1	3, 6, 9, 12	0.2 – 0.55
Shorowordi et al (2004)	Aluminium with 13 vol%-SiC MMC	Commercial phenolic brake pad	0.75	1.62, 4.17	0.3 – 0.45
Uyyuru et al (2007)	Aluminium MMC with 15 vol%-SiC and 20 vol%-SiC	Brake pad material	1, 2, 3, 4	1.5, 2, 3, 4	0.2 – 0.35
Shivamurthy and Surappa (2011)	Aluminium alloy A356 with 10 vol%-SiC and 20 vol%-SiC MMC	Commercial polymer based brake pad	3	1, 2, 3, 4, 5	0.3 – 0.4

Figure 4.25 shows that at contact pressure of 0.1MPa under 1m/s, it can be observed that as the weight percentage of alumina in the aluminium alloy increases, there is a significant decrease in the COF but it remains in the range of 0.3 to 0.5. The same trend is observed for contact pressure of 0.2MPa, where the COF remains in the range of 0.3 to 0.7. It can be observed in Figure 4.26 that at contact pressure of 0.1MPa under sliding speed of 0.42m/s, as the weight percentage of alumina in the aluminium alloy increases, the COF remains in the range of 0.1 to 0.2. At contact pressure of 0.2MPa under sliding speed of 0.42m/s, the COF remains in the range of 0.3 to 0.5.

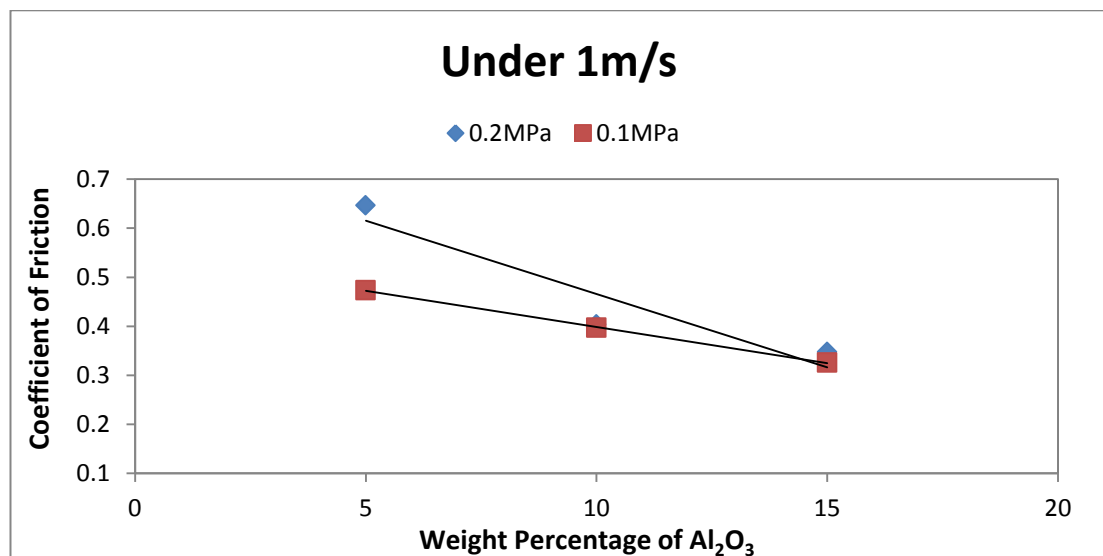


Figure 4.25 Variation of coefficient of friction with different weight percentage of Al_2O_3 for aluminium alloy reinforced with Al_2O_3 MMC samples under 1m/s sliding speed

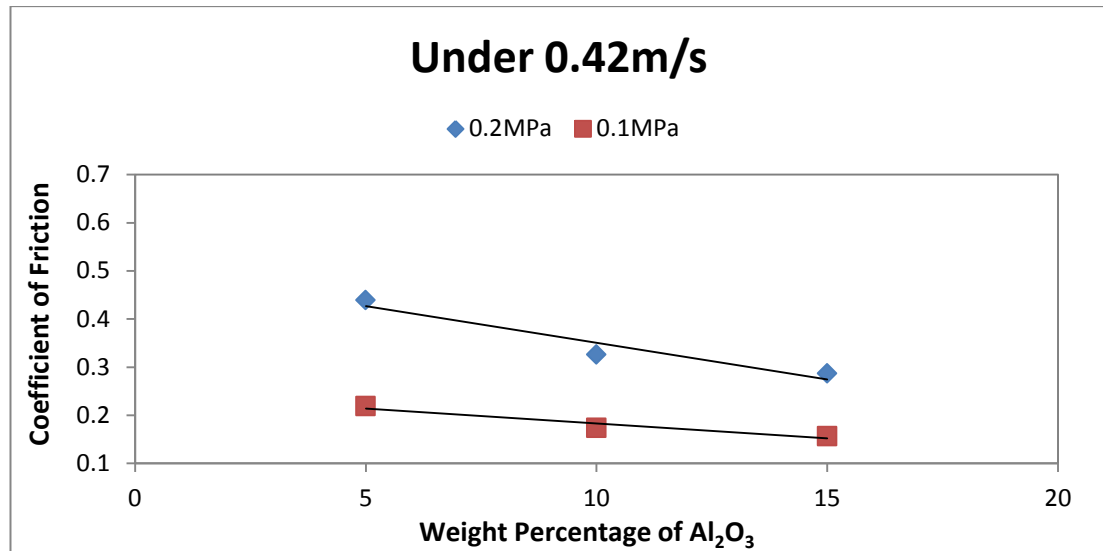


Figure 4.26 Variation of coefficient of friction with different weight percentage of Al₂O₃ for aluminium alloy reinforced with Al₂O₃ MMC samples under 0.42m/s sliding speed

Both aluminium alloy reinforced with SiC MMC and aluminium alloy reinforced with Al₂O₃ MMC (except 5 wt% alumina) perform much better at high contact pressure (0.2MPa) for both sliding speeds. Gray cast iron, aluminium alloy reinforced with SiC MMC and aluminium alloy reinforced with Al₂O₃ MMC perform relatively worse at low contact pressure (0.1MPa) and low sliding speed (0.42m/s). It has been reported that as the contact pressure decreases, the real area of contact at the sliding interface decreases as well (Daoud and Abou El-khair, 2010). In addition, the softening of lubricating agents from the friction material pin may have contributed to the lower coefficient of friction (Rohatgi et al., 1992; Lasa and Rodriguez, 2003).

4.7.3 Pin Wear Rate

Figure 4.27 shows the summary of the wear rate of brake pad pins sliding against gray cast iron is shown in Figure 4.27. At high contact pressure of 0.2MPa under both sliding speeds, the wear rate of brake pins registers in the range of 6 to 8 x 10⁻³mm³/m. However at contact pressure of 0.1MPa under both sliding speeds, the wear rate of brake pins is 2 times lower, registering in the range of 2 to 4 x 10⁻³mm³/m. Daoud and Abou El-khair (2010) and Natarajan et al (2006) have found that as the contact pressure increased, the wear rate of brake pad pins increased as well.

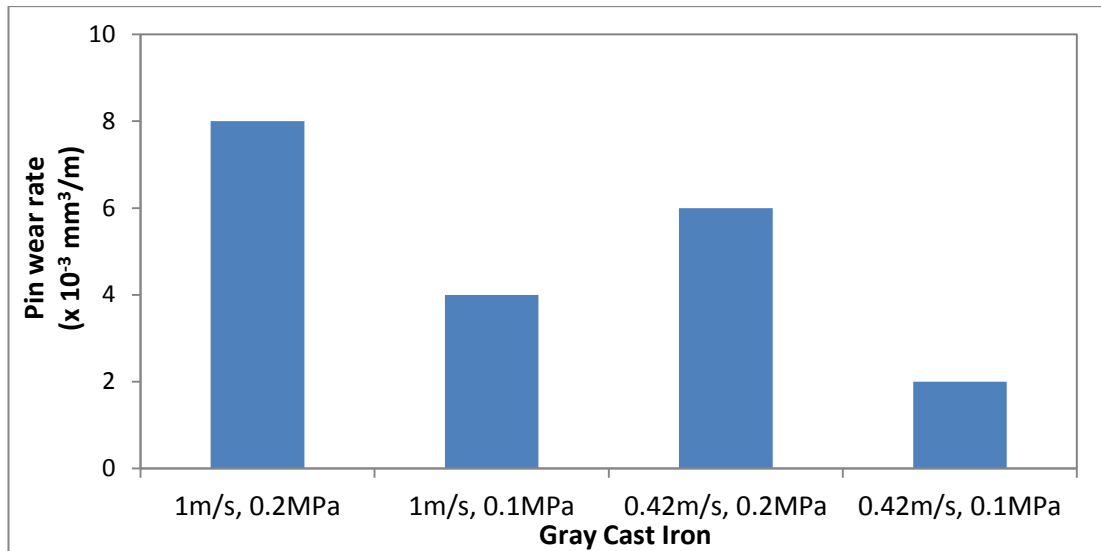


Figure 4.27 Variation of pin wear rate ($\times 10^{-3} \text{ mm}^3/\text{m}$) for gray cast iron samples

Figure 4.28 shows that at contact pressure of 0.2MPa under both sliding speeds, the pin wear rate increases with the increase of weight percentage of silicon carbide. The highest weight percentage (15 wt%) of silicon carbide in aluminium alloy acquires the highest wear rate at high contact pressure (0.2MPa) for sliding speed of 1m/s. At contact pressure of 0.1MPa under both sliding speeds, the wear of brake pad pin remains below $10 \times 10^{-3} \text{ mm}^3/\text{m}$.

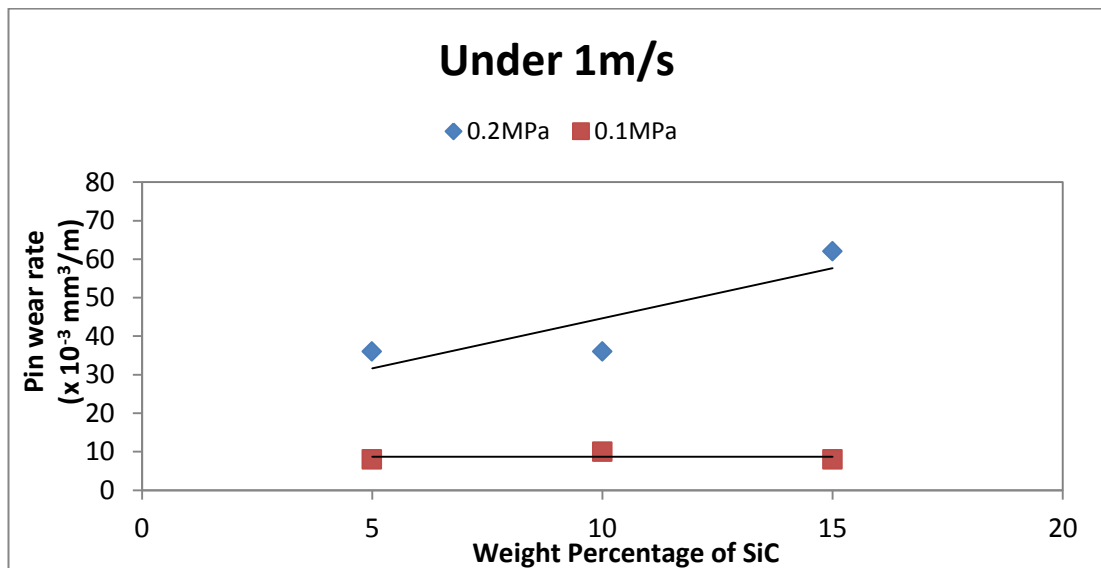


Figure 4.28 Variation of pin wear rate ($\times 10^{-3} \text{ mm}^3/\text{m}$) with different weight percentage of SiC for aluminium alloy reinforced with SiC MMC samples under 1m/s sliding speed

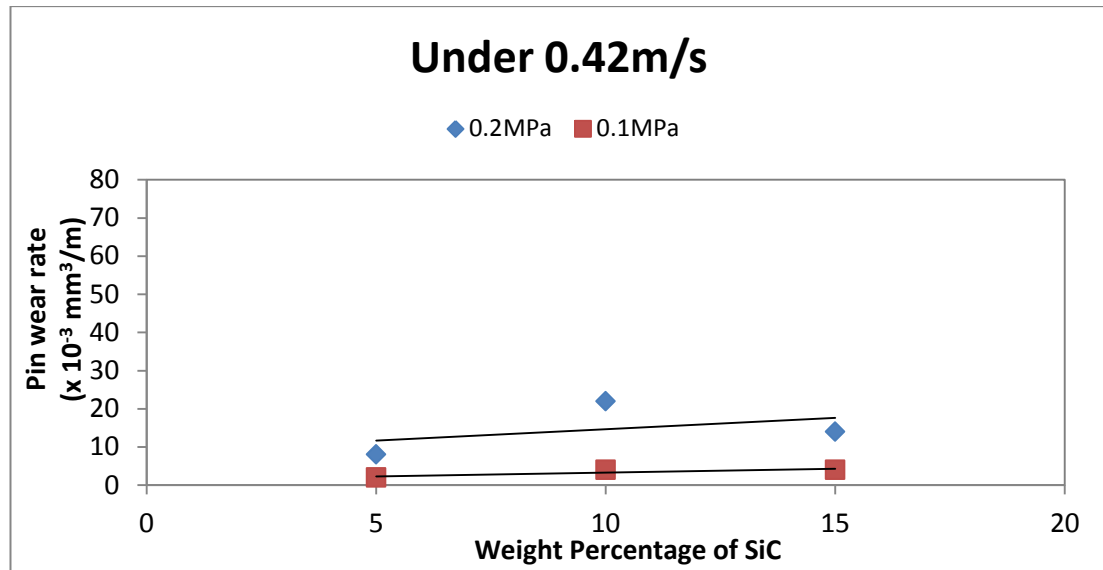


Figure 4.29 Variation of pin wear rate ($\times 10^{-3} \text{mm}^3/\text{m}$) with different weight percentage of SiC for aluminium alloy reinforced with SiC MMC samples under 0.42m/s sliding speed

Table 4.26 summarizes the wear rate of brake pad pins based on various research. Daoud and Abou El-khair (2010) have found that at the lowest contact pressure (0.30MPa) and sliding speed (3m/s), the wear rate of brake pad pins is only $4 \times 10^{-3} \text{mm}^3/\text{m}$. All of these researchers' findings contrast what is observed in this study. It is observed in Figure 4.28 that the wear rate of brake pad pins is high in the range of 8 to $62 \times 10^{-3} \text{mm}^3/\text{m}$.

Table 4.26 Summary of brake pad pin wear rate of various studies

Authors	Pin's material	Applied pressure (MPa)	Sliding speed (m/s)	Wear rate at lowest contact pressure and lowest sliding speed
Natarajan et al (2006)	Brake shoe lining of a commercial passenger car	0.25, 0.51, 0.76, 1.02, 1.27	2.5, 3.7, 5, 6.3	5×10^{-4} mm ³ /m
Daoud and Abou El-khair (2010)	Commercial automotive brake material	0.3, 0.5, 1	3, 6, 9, 12	4×10^{-3} mm ³ /m
Shivamurthy and Surappa (2011)	Commercial polymer based brake pad	3	1, 2, 3, 4, 5	2.25×10^{-3} mm ³ /m

Figure 4.30 and Figure 4.31 show that at contact pressure of 0.2MPa under both sliding speeds, the pin wear rate decreases with the increase of weight percentage of alumina. However, at contact pressure of 0.1MPa under both sliding speeds, the wear of brake pad pin remains low (below 10×10^{-3} mm³/m). A higher content of alumina particles is favourable in reducing the wear of brake pad.

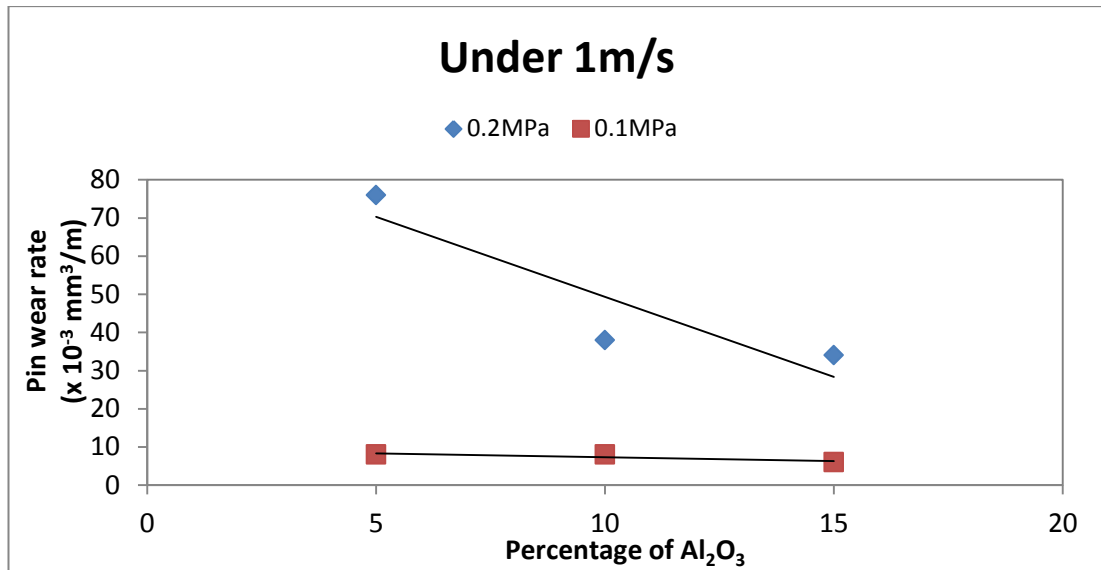


Figure 4.30 Variation of pin wear rate ($\times 10^{-3} \text{ mm}^3/\text{m}$) with different weight percentage of Al₂O₃ for aluminium alloy reinforced with Al₂O₃ MMC samples under 1m/s sliding speed

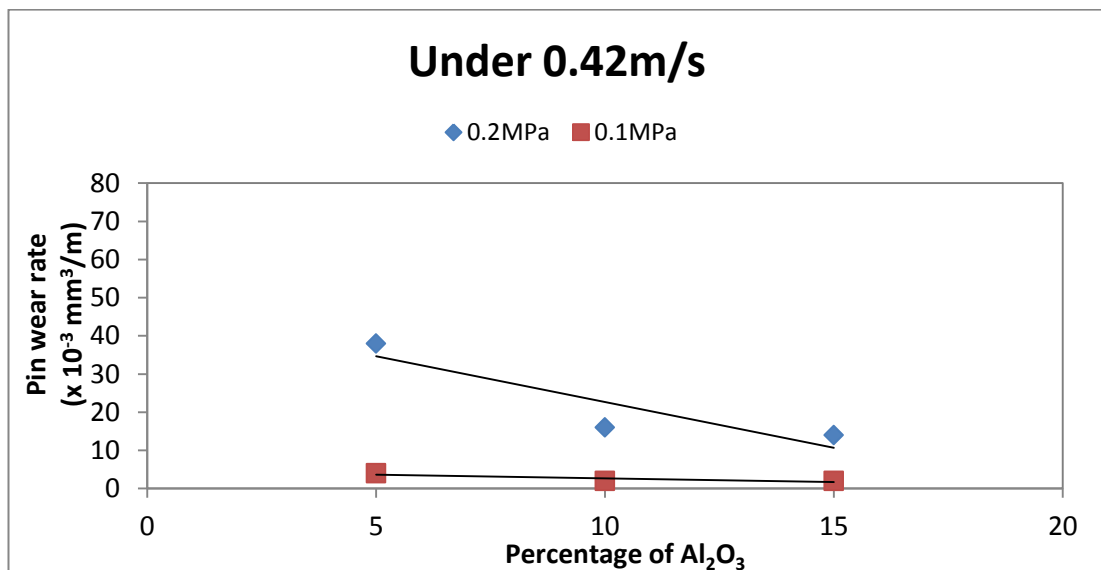


Figure 4.31 Variation of pin wear rate ($\times 10^{-3} \text{ mm}^3/\text{m}$) with different weight percentage of Al₂O₃ for aluminium alloy reinforced with Al₂O₃ MMC samples under 0.42m/s sliding speed

Several researchers have dictated that the wear rate of brake pad pin sliding against aluminium alloy reinforced with SiC MMC is much higher than that of the brake pad pin sliding against cast iron (Daoud and Abou El-khair, 2010; Natarajan et al., 2006). This is in agreement with the current study. For all test conditions of aluminium alloy

reinforced with SiC MMC and aluminium alloy reinforced with Al_2O_3 MMC, the wear of brake pins sliding against MMC is much higher than that of brake pad pins sliding against gray cast iron.

4.7.4 Wear Analysis

This section contains identification of wear mechanisms and also the scanning electron micrographs of the wear tracks.

Gray Cast Iron

There is more wear debris and they can be identified with the arrows labeled (unless specified) in Figure 4.32. Figure 4.32a shows that at high contact pressure (0.2MPa) and high speed (1m/s), worn tracks of gray cast iron show surface cutting.

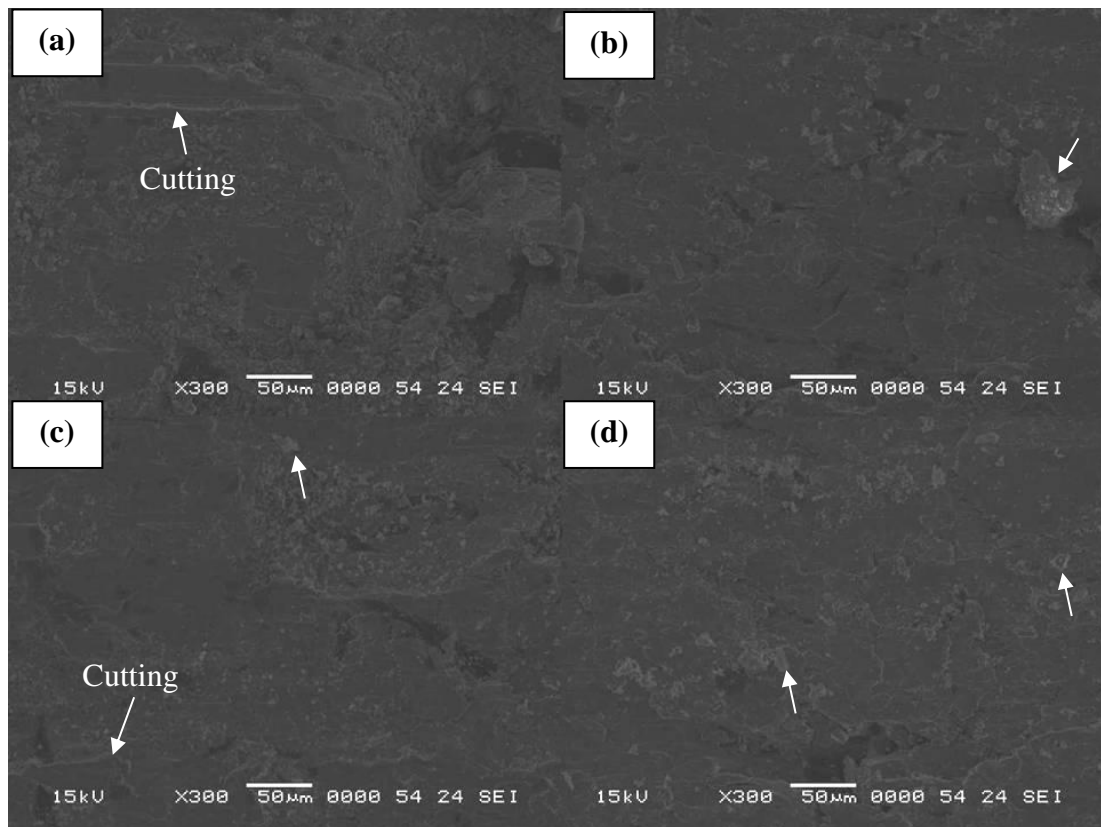


Figure 4.32 Scanning electron images microstructure of worn surface of gray cast iron samples (a) 0.2MPa, 1m/s (b) 0.1MPa, 1m/s (c) 0.2MPa, 0.42m/s (d) 0.1MPa, 0.42m/s

Metal Matrix Composite (MMC)

Aluminium Alloy reinforced with SiC MMC

Figure 4.33a shows that there is a deep ploughing. This can be due to the uneven polished surface of the brake pad pin. In addition, the heavy removal of aluminium matrix can be due to the hard transfer particles from the brake pad pin and silicon carbide particles (Anoop et al., 2009). A combination of micro cutting and grooves can be seen.

It is observed in Figure 4.33b that there are numerous grooves (indicated by the arrow). Fractured silicon carbide particle and numerous micro cutting can also be seen. There is visible ploughing (indicated by the arrow in Figure 4.33a) formed by abrasive actions of debris. Abrasive wear is observed, which is caused by material being removed from the pin surface by hard particles on the counterface, forcing against and cutting or ploughing into the surface.

It can be observed in Figure 4.33c that at highest weight percentage of silicon carbide in the aluminium alloy, the composite materials show numerous delamination of the aluminium matrix. Since a larger silicon carbide particle (105 μ m) was utilized, the higher number of particles could have contributed to the increase of real contact area (Uyyuru et al., 2007).

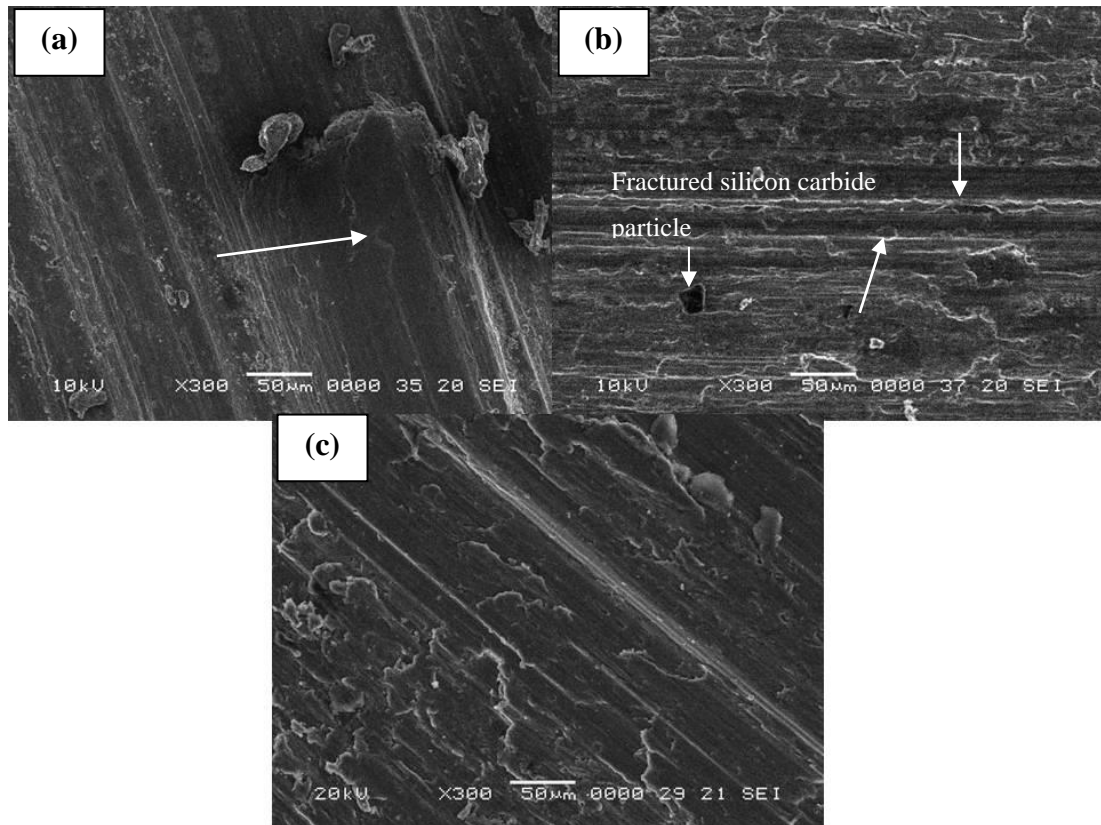


Figure 4.33 Scanning electron images microstructure of worn surface of aluminium alloy MMC with different weight percentage of reinforced silicon carbide (SiC) (a) 5 wt% SiC (b) 10 wt% SiC (c) 15 wt% SiC

It is observed in Figure 4.34a that at low contact pressure (0.1MPa) under a high sliding speed (1m/s), there is a combination of micro cutting and grooves as indicated by the arrows. A copious amount of wear debris (as indicated by the circles) can be seen as well.

Figure 4.34b shows that numerous grooves (formed by abrasive action of debris), Fractured silicon carbide particle and micro cutting can be seen as well.

It can be observed in Figure 4.34c that the composite materials show numerous delamination of the aluminium matrix. The heavy removal of matrix material can be due to the hard transfer particles from the brake pad pin and silicon carbide particles. Fractured and protruding silicon carbide particles can be seen as well.

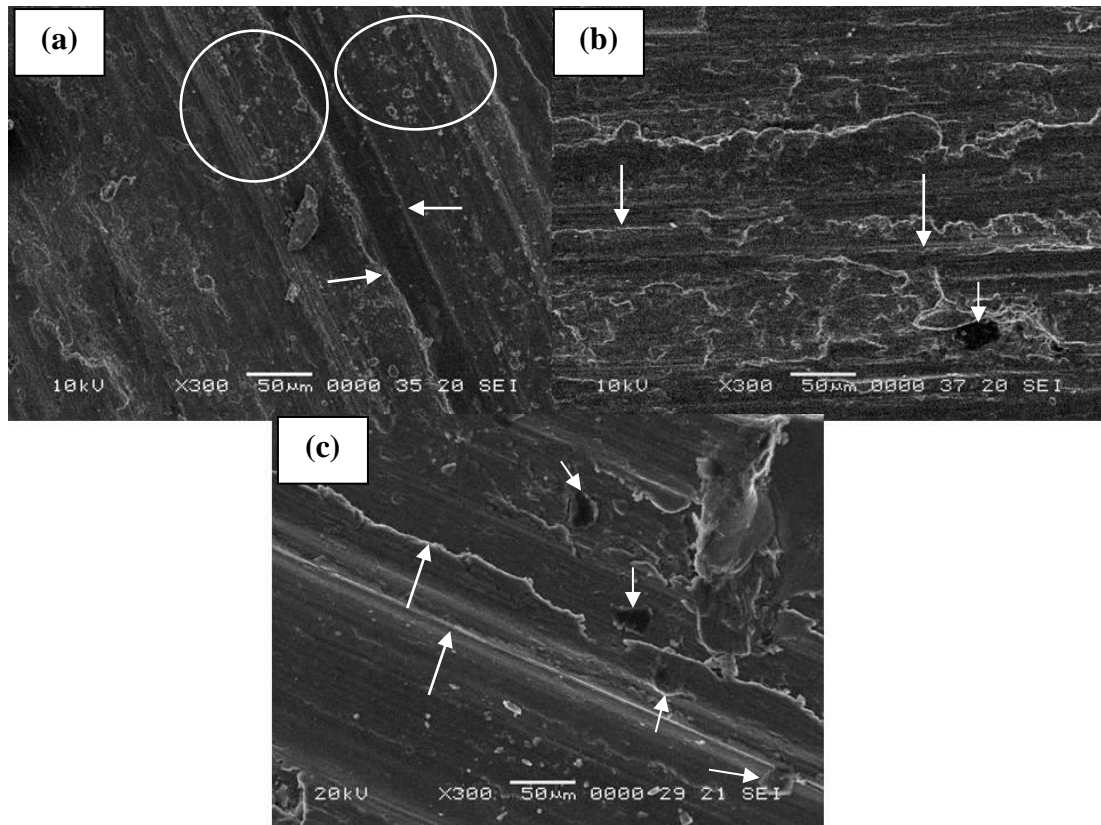


Figure 4.34 Scanning electron images microstructure of worn surface of aluminium alloy MMC with different weight percentage of reinforced silicon carbide (SiC) (a) 5 wt% SiC (b) 10 wt% SiC (c) 15 wt% SiC

It is observed in Figure 4.35a that at high contact pressure (0.2MPa) under a low sliding speed (0.42m/s), there is a combination of micro cutting and grooves. Wear debris can be seen as well.

Figure 4.35b shows numerous grooves (formed by abrasive action of debris) and micro cutting.

It can be observed in Figure 4.35c that the composite materials show numerous delamination of the aluminium matrix. The heavy removal of matrix material can be due to the hard transfer particles from the brake pad pin and silicon carbide particles. Fractured and protruding silicon carbide particles together with wear debris can be seen as well.

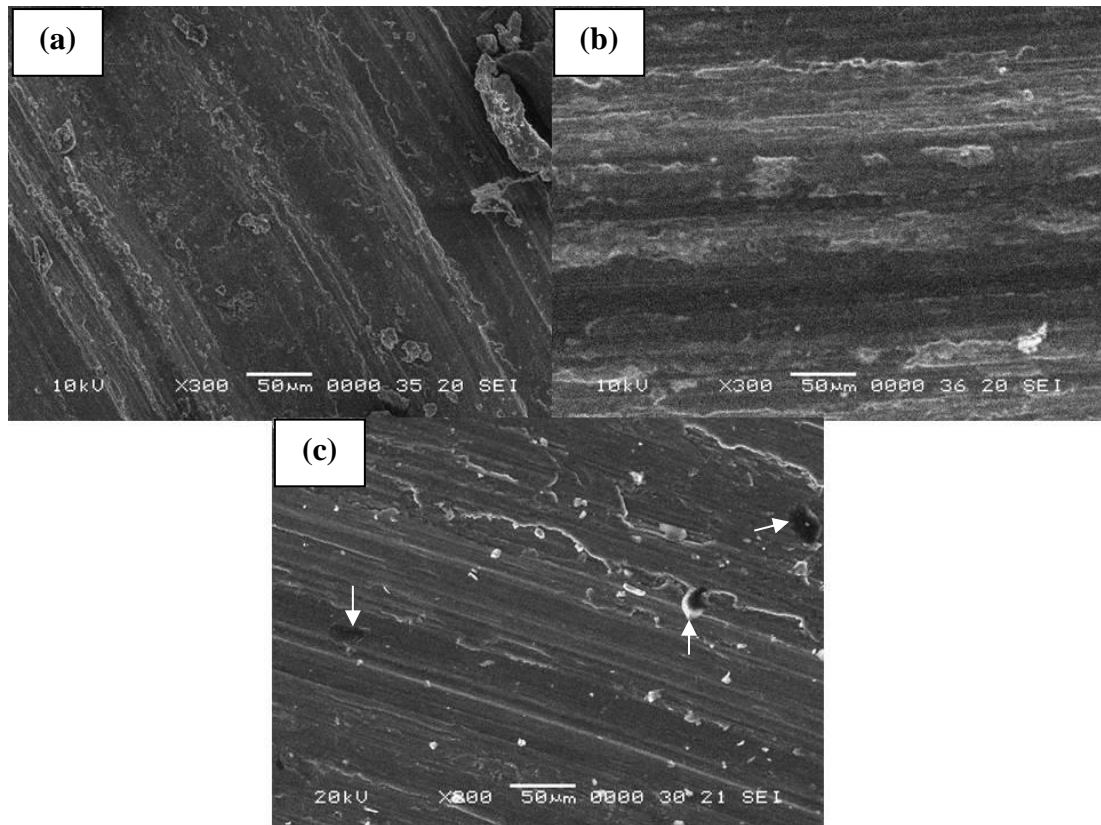


Figure 4.35 Scanning electron images microstructure of worn surface of aluminium alloy MMC with different weight percentage of reinforced silicon carbide (SiC) (a) 5 wt% SiC (b) 10 wt% SiC (c) 15 wt% SiC

It is observed in Figure 4.36a that at low contact pressure (0.1MPa) under a low sliding speed (0.42m/s), less grooves are visible. Micro cutting and wear debris can be seen as well.

Figure 4.36b shows numerous grooves (formed by abrasive action of debris) and micro cutting.

It can be observed in Figure 4.36c that the composite materials show numerous grooves. Fractured and protruding silicon carbide particles, together with wear debris can be seen as well.

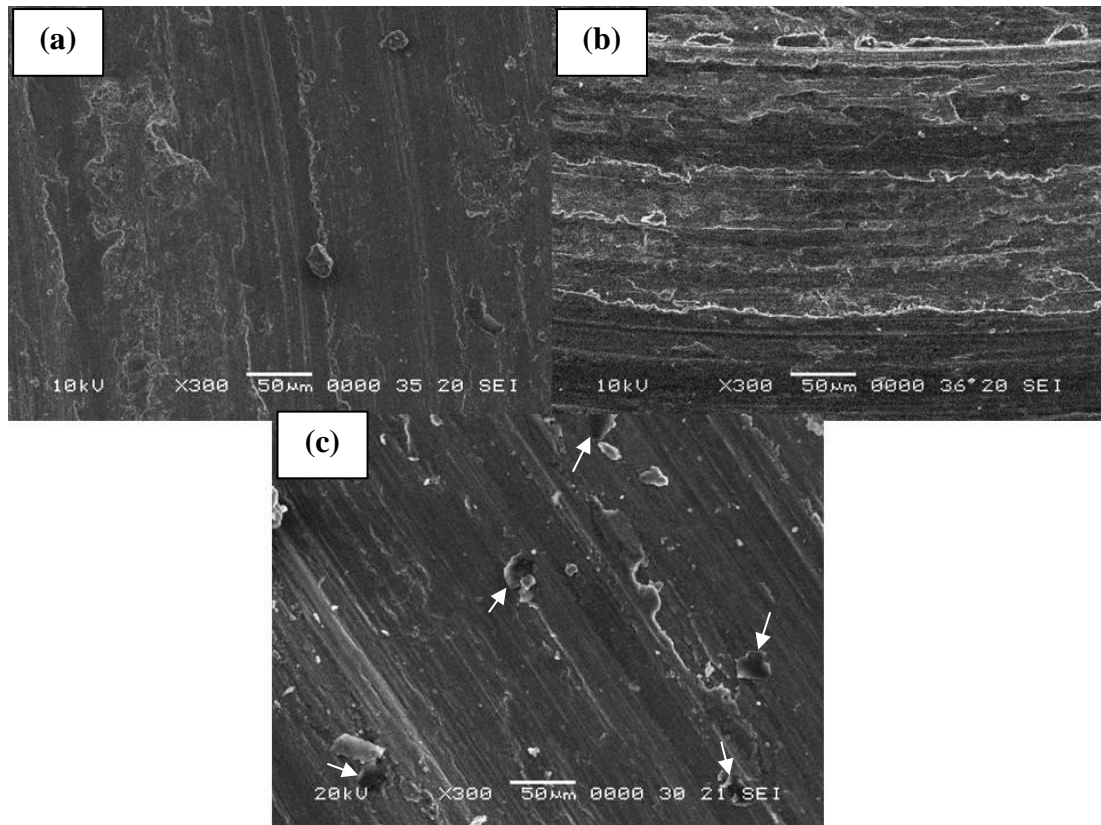


Figure 4.36 Scanning electron images microstructure of worn surface of aluminium alloy MMC with different weight percentage of reinforced silicon carbide (SiC) (a) 5 wt% SiC (b) 10 wt% SiC (c) 15 wt% SiC

Aluminium Alloy reinforced with Al_2O_3 MMC

It is observed in Figure 4.37a that there is severe delamination of the aluminium matrix. There is less amount of alumina particles that are able to carry the load. This leads to cracking of the aluminium matrix followed by delamination of surface layer.

Figure 4.37b shows numerous grooves (formed by abrasive action of debris) and micro cutting. Fractured and protruding alumina particles can be seen as well.

It can be observed in Figure 4.37c that the composite materials show numerous grooves and micro cutting.

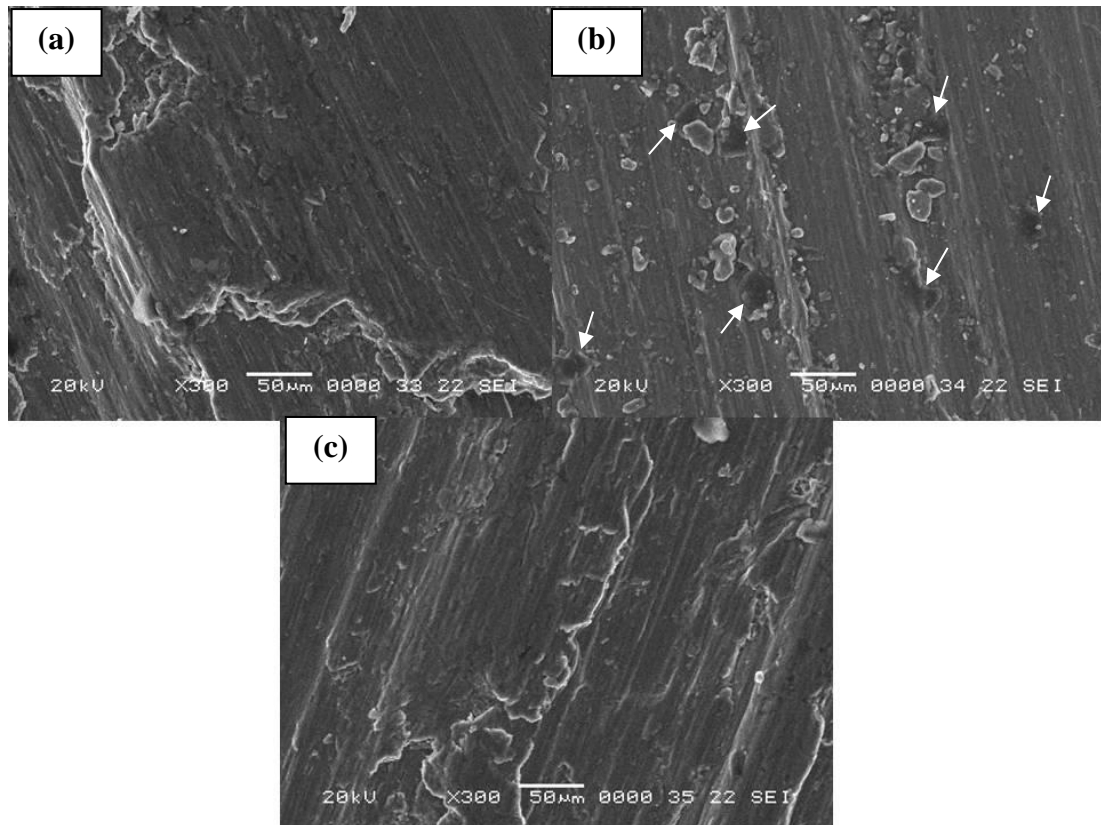


Figure 4.37 Scanning electron images microstructure of compressive fracture surface of aluminium alloy MMC with different weight percentage of reinforced alumina (Al_2O_3) (a) 5 wt% Al_2O_3 (b) 10 wt% Al_2O_3 (c) 15 wt% Al_2O_3

Figure 4.38a shows severe delamination of the aluminium matrix. There is less amount of alumina particles that are able to carry the load. This leads to cracking of the aluminium matrix followed by delamination of surface layer. A fractured alumina particle (labeled with an arrow) can be seen.

Figure 4.38b shows that less grooves, and micro cutting can be seen. Fractured and protruding alumina particles can be seen as well.

It can be observed in Figure 4.38c that the composite materials show numerous micro cutting.

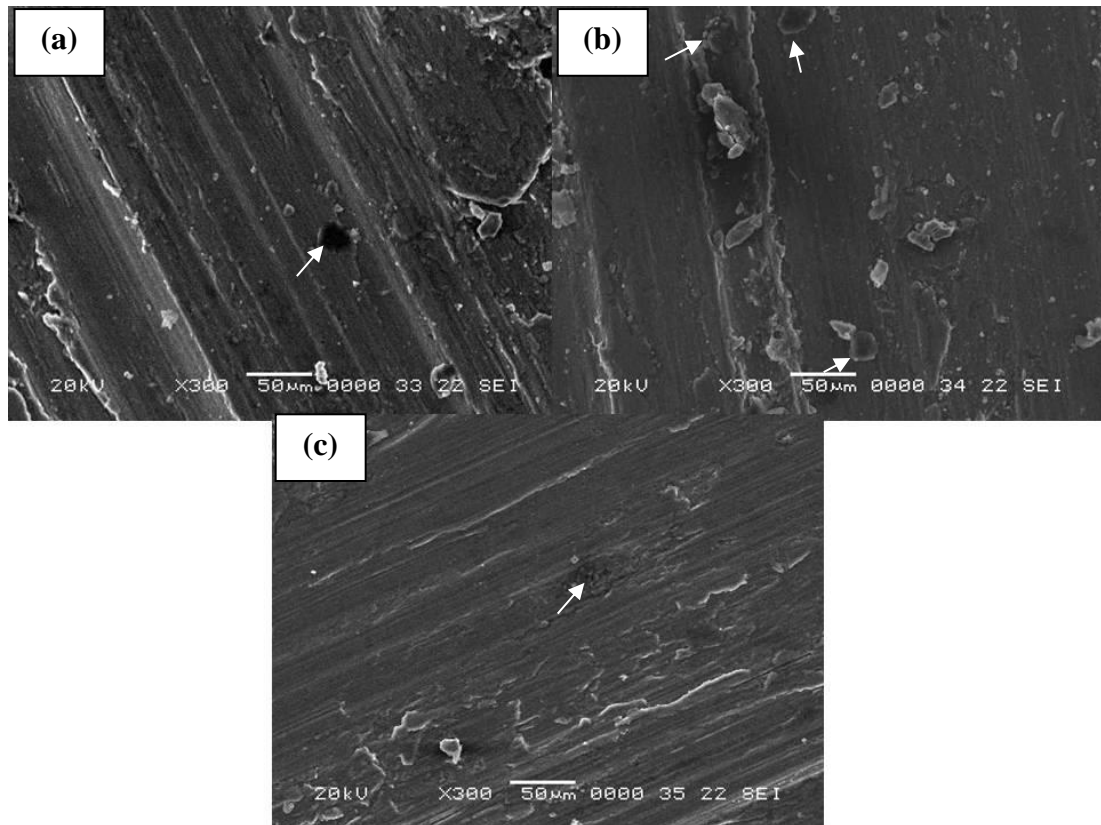


Figure 4.38 Scanning electron images microstructure of compressive fracture surface of aluminium alloy MMC with different weight percentage of reinforced alumina (Al_2O_3) (a) 5 wt% Al_2O_3 (b) 10 wt% Al_2O_3 (c) 15 wt% Al_2O_3

Figure 4.39a shows numerous grooves and micro cutting.

Figure 4.39b shows less grooves, and micro cutting can be seen. Fractured and protruding alumina particles can be seen as well.

It can be observed in Figure 4.39c that the composite materials show numerous micro cutting and less grooves.

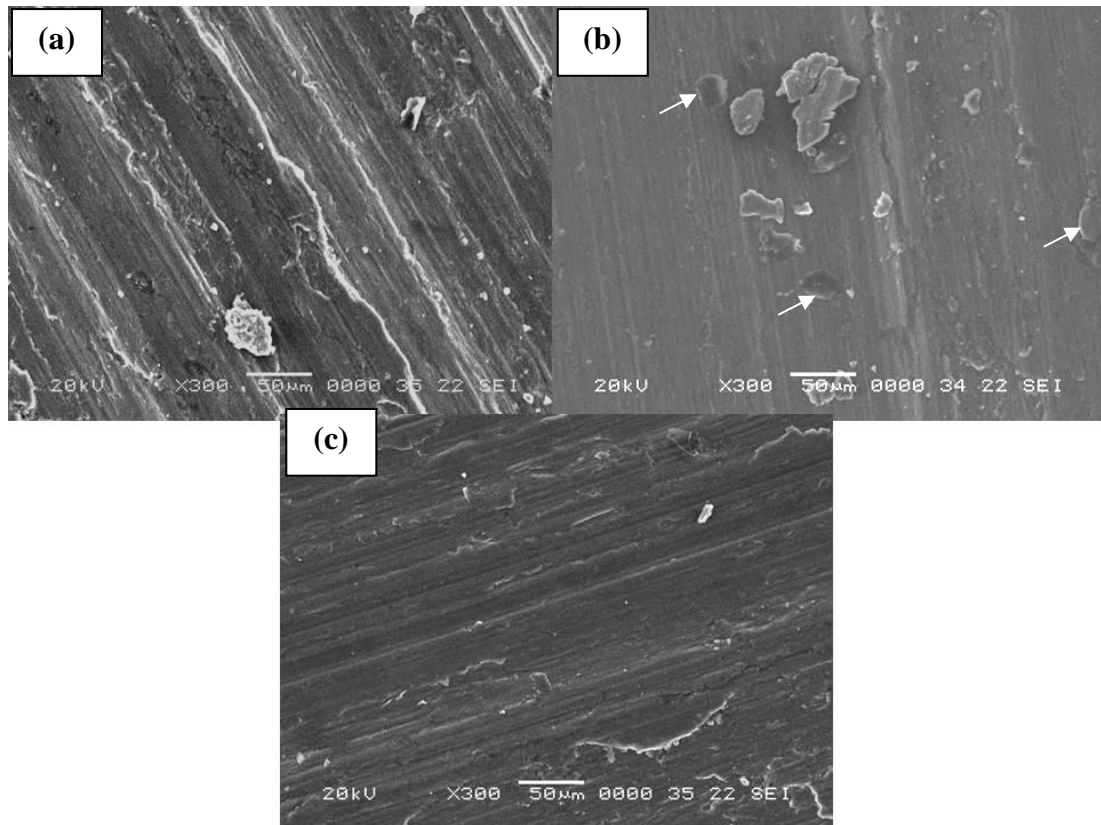


Figure 4.39 Scanning electron images microstructure of compressive fracture surface of aluminium alloy MMC with different weight percentage of reinforced alumina (Al_2O_3) (a) 5 wt% Al_2O_3 (b) 10 wt% Al_2O_3 (c) 15 wt% Al_2O_3

Figure 4.40a shows numerous grooves and micro cutting. Wear debris can be seen as well.

Figure 4.40b shows less grooves, and micro cutting can be seen. Fractured alumina particles can be seen as well.

It can be observed in Figure 4.40c that the composite materials show numerous micro cutting and less grooves.

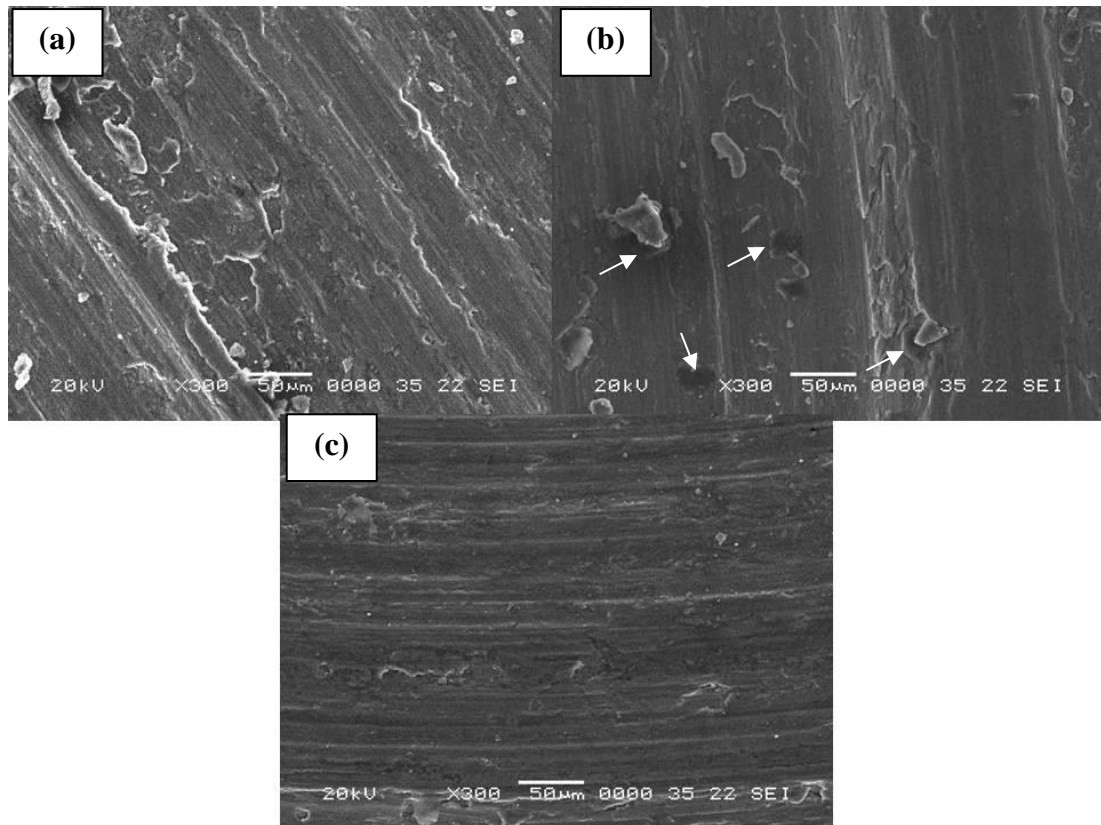


Figure 4.40 Scanning electron images microstructure of compressive fracture surface of aluminium alloy MMC with different weight percentage of reinforced alumina (Al_2O_3) (a) 5 wt% Al_2O_3 (b) 10 wt% Al_2O_3 (c) 15 wt% Al_2O_3

4.8 THERMAL PROPERTIES

Metal Matrix Composite (MMC)

The thermal properties of gray cast iron are summarised in Table 4.27. Table 4.28 shows the typical thermal properties of aluminium, silicon carbide and alumina based ceramic. These properties are used to estimate the thermal properties of MMC as shown in Table 4.29 and Table 4.30. It is observed that of aluminium alloy reinforced with Al_2O_3 acquires higher specific heat capacity and thermal conductivity compared to aluminium alloy reinforced with SiC. Both aluminium alloy reinforced with Al_2O_3 and aluminium alloy reinforced with SiC acquire higher specific heat capacity and thermal conductivity than that of gray cast iron. However, both aluminium alloy reinforced with Al_2O_3 and aluminium alloy reinforced with SiC acquire higher thermal expansion coefficient compared to gray cast iron.

Table 4.27 Thermal properties of gray cast iron (Dunaevsky, 1997; Ihm, 2013).

Samples	Specific heat capacity (J/kg.K)	Thermal expansion coefficient ($\times 10^{-6} 1/K$)	Thermal conductivity (W/m.K)
Gray Cast Iron	498	12.6	47.3

Table 4.28 Typical thermal properties of aluminium, silicon carbide and alumina based ceramic (Callister, 2001)

Material	Specific heat capacity (J/kg.K)	Thermal expansion coefficient ($\times 10^{-6} 1/K$)	Thermal conductivity (W/m.K)
Aluminium	896	23.6	205
Silicon Carbide	590	4.1	71
Alumina based ceramic	775	8.4	35.6

Table 4.29 Estimated thermal properties of aluminium alloy reinforced with SiC

Material	Specific heat capacity (J/kg.K)	Thermal expansion coefficient ($\times 10^{-6} 1/K$)	Thermal conductivity (W/m.K)
Aluminium alloy + 5 wt% SiC	882.9	23.3	199.3
Aluminium alloy + 10 wt% SiC	869.7	23.0	193.5
Aluminium alloy + 15 wt% SiC	856.2	22.6	187.6
Aluminium alloy + 20 wt% SiC	842.5	22.3	181.6

Table 4.30 Estimated thermal properties of aluminium alloy reinforced with Al₂O₃

Material	Specific heat capacity (J/kg.K)	Thermal expansion coefficient ($\times 10^{-6}$ 1/K)	Thermal conductivity (W/m.K)
Aluminium alloy + 5 wt% Al ₂ O ₃	892.1	23.6	199.1
Aluminium alloy + 10 wt% Al ₂ O ₃	888.2	23.7	193.0
Aluminium alloy + 15 wt% Al ₂ O ₃	884.1	23.7	186.8
Aluminium alloy + 20 wt% Al ₂ O ₃	879.8	23.8	180.3

Functionally Graded Material (FGM)

Table 4.31 shows the typical thermal properties of alumina and aluminium titanate based ceramic. These properties are used to estimate the thermal properties of FGM as shown in Table 4.32. FGM possesses higher specific heat capacity than that of gray cast iron.

The thermal conductivity values of FGM differ from one another, with FGM – A3 showing the lowest thermal conductivity value of 3.31W/m.K while both FGM – A1 and FGM – A2 show slightly lower thermal conductivity values compared to that of gray cast iron.

Table 4.31 Typical data for thermal properties of alumina and aluminium titanate based ceramics (Auerkari, 1996; Azom, 2014; Callister, 2001)

Samples	Specific heat capacity (J/kg.K)	Thermal conductivity (W/m.K)
Alumina based ceramic	775	35.6
Aluminium titanate based ceramic	800	1.5

Table 4.32 Theoretical data for thermal properties of FGM samples

Samples	Specific heat capacity (J/kg.K)	Thermal conductivity (W/m.K)
FGM - A1	876.54	31.94
FGM - A2	872.30	30.07
FGM - A3	847.58	3.31

The peak temperature of the brake depends mainly on the disc material's thermal conductivity during long and low intensity brakings. MMC acquires much higher thermal conductivity compared to gray cast iron. FGM possesses slightly lower thermal conductivity compared to gray cast iron.

All three thermal properties, specific heat capacity, thermal expansion coefficient and thermal conductivity, play a different role in affecting the durability of the disc brake. During short and high speed stops, specific heat capacity is a crucial thermal property. Hence, a high specific heat capacity is very much needed for a disc brake. Both MMC and FGM show advantage in this area.

4.9 SUMMARY

In this chapter, the mechanical properties of gray cast iron (GCI), metal matrix composite (MMC) and functionally graded material (FGM) are studied; the wear behaviour of gray cast iron (GCI) and metal matrix composite (MMC) is investigated and; the theoretical thermal behaviour of both MMC and FGM are evaluated.

The density measurement is performed according to the Archimedes Principle on the gray cast iron, MMC and FGM samples. The theoretical density of aluminium alloy reinforced with SiC increases with the increase of weight percentage of SiC in the aluminium alloy. The measured density of aluminium alloy reinforced with SiC shows an increasing trend as well. However, aluminium alloy reinforced with 20 wt% of SiC show a lower density. This is due to the increased amount of porosity (Aqida et al., 2004). The measured density of aluminium alloy reinforced with Al₂O₃ shows an increasing trend as well. In comparison with aluminium alloy reinforced with SiC, aluminium alloy reinforced with Al₂O₃ shows lower percentage of porosity. The presence of porosity in the MMC samples is attributed to the clustering of particulates.

It is observed that the measured density of FGM is much lower than its theoretical density. This is due to the presence of porosity. It is observed that the porosity is high for FGM – A1, at (18.892±1.634)%. These FGM samples are known to be very porous materials, especially in the presence of aluminium titanate.

The presence of hard particles (silicon carbide and alumina) results in the increase of hardness of the MMCs. Aluminium alloy MMC reinforced with silicon carbide has higher hardness values than aluminium alloy MMC reinforced with alumina. Hardness values of MMCs are lower than that of gray cast iron. The tensile property and wear resistance of MMC are related to the hardness property. Although MMC acquire slightly lower tensile strength as compared to gray cast iron, it still shows an increase in its tensile strength with the increase of particulate contents. MMC acquires a lower Young's Modulus than that of gray cast iron, C/SiC composite and C/C-SiC composite. This shows that low Young's modulus of MMC helps to promote uniform contact between the disc brake and the brake pads. The tensile

strength and Young's modulus of MMC are promising for the use of the car brake rotor.

Aluminium alloy reinforced with 5 wt% silicon carbide, aluminium alloy reinforced with 15 wt% silicon carbide, aluminium alloy reinforced with 10 wt% alumina, aluminium alloy reinforced with 15 wt% alumina and aluminium alloy reinforced with 20 wt% alumina show fracture toughness of more than $15\text{MPa}\cdot\text{m}^{1/2}$ which is in accordance to the recommended values found in Ashby (2005). The fracture toughness of gray cast iron is comparatively lower than that of MMC.

Compression tests were performed on gray cast iron, MMC and FGM samples. It is revealed that MMC and FGM have a lower compressive strength compared to gray cast iron. This is due to the increase amount of clustering in MMC whereas the low compressive strength of FGM is due to the graded heterogeneous $\text{Al}_2\text{TiO}_5/\text{Al}_2\text{O}_3$ layers which exhibit a relatively 'soft' surface.

In comparison to gray cast iron, both aluminium alloy reinforced with SiC MMC and aluminium alloy reinforced with Al_2O_3 MMC still attain a higher wear rate. For both sliding speeds (0.42m/s and 1m/s) and high contact pressure (0.2MPa), the highest weight percentage (15 wt%) of alumina in the aluminium alloy acquires a lower wear rate whereas the highest weight percentage (15%) of silicon carbide in aluminium alloy attains the highest wear rate. The disc wear rate of aluminium alloy reinforced with SiC MMC ($80 - 220 \times 10^{-3} \text{mm}^3/\text{m}$) found in this study is higher compared to MMCs investigated by Natarajan et al (2006), Daoud and Abou El-khair (2010), Zhang and Wang (2007), Uyyuru et al (2007) and Shivamunthy and Surappa (2011). This could be due to the larger size and higher number of particles which contributed in the increase of real contact area (Uyyuru et al., 2007).

In terms of coefficient of friction, both aluminium alloy reinforced with SiC MMC and aluminium alloy reinforced with Al_2O_3 MMC (except 5 wt% alumina) have friction coefficient within the range for automotive vehicles at high contact pressure (0.2MPa) for both sliding speeds (0.42m/s and 1m/s). For both contact pressures (0.1MPa and 0.2MPa) under 1m/s sliding speed, friction coefficient for all aluminium alloy reinforced with SiC is observed to be within range for automotive

vehicles. Gray cast iron, aluminium alloy reinforced with SiC MMC and aluminium alloy reinforced with Al₂O₃ MMC show low COF at low contact pressure (0.1MPa) and low sliding speed (0.42m/s). The experimental condition of Shorowordi et al (2004) is close to this study. They have observed that at lowest speed of 1.62m/s and contact pressure of 0.75MPa, MMC's COF is 0.45. In addition, Natarajan et al (2006) found that at lowest contact pressure (0.25MPa) and sliding speed (2.5m/s), the COF is still quite high at 0.6. The same can be observed in Daoud and Abou El-khair's (2010) findings where at lowest contact pressure (0.3MPa) and sliding speed (3m/s), the COF is 0.46. All of these researchers' findings are consistent with what is observed in this study. As the contact pressure decreases, the real area of contact at the sliding interface decreases as well (Daoud and Abou El-khair, 2010). Hence this results in a low coefficient of friction. In addition, the softening of lubricating agents from the friction material pin may have contributed to the lower coefficient of friction (Rohatgi et al., 1992; Lasa and Rodriguez, 2003).

For all test conditions of aluminium alloy reinforced with SiC MMC and aluminium alloy reinforced with Al₂O₃ MMC, the wear of brake pins sliding against MMC is higher than that of brake pad pins sliding against gray cast iron. Despite that the wear rate of brake pad pin sliding against aluminium alloy reinforced with SiC MMC and aluminium alloy reinforced with Al₂O₃ MMC is higher than the conclusions made by the other researchers (Daoud and Abou El-khair, 2010; Natarajan et al., 2006; Shivamurthy and Surappa, 2011). A few researchers (Daoud and Abou El-khair, 2010; Natarajan et al., 2006) have concluded that the wear rate of brake pad pin sliding against aluminium alloy reinforced with SiC MMC is higher than that of the brake pad pin sliding against cast iron.

The thermal properties of MMC and FGM samples are estimated. Both aluminium alloy reinforced with Al₂O₃ and aluminium alloy reinforced with SiC acquire higher specific heat capacity and thermal conductivity than that of gray cast iron. They also attain higher thermal expansion coefficient compared to gray cast iron. FGM possesses higher a specific heat capacity than that of gray cast iron. The thermal conductivity values of FGM – A3 shows the lowest thermal conductivity value of 3.31W/m.K. Both FGM – A1 and FGM – A2 show slightly lower thermal conductivity values compared to that of gray cast iron. During short and high speed

stops, specific heat capacity is a crucial thermal property. Consequently, a high specific heat capacity is very much needed for a disc brake. Both MMC and FGM show advantage in this area.

Chapter 5 Conclusions and Recommendations

5.1 Conclusions

There are two types of brakes used in today's automotive world; drum brakes and disc brakes. The front brakes are usually of the disc type and the rear brakes are of the drum type (Kapoor et al., 2001). Gray cast iron is the commonly used material for mass produced family vehicles (Macnaughtan and Krosnar, 1998).

As braking system efficiency improved, cars could go faster hence causing the disc operating temperatures to increase as well. Due to the temperature gradients generated from braking, the friction surface of the disc brake undergoes compressive yield followed by plastic deformation. When the disc brake subsequently cools down, it suffers from residual tensile stress generated in these spots (Yamabe et al., 2003). Repetition of these actions will cause cracks to appear on the friction surface. This may also lead to a variety of performance related problems such as distortion and heat cracking. Subsequently, this led to the development of other advanced materials for disc brakes, namely carbon/carbon composite, carbon/silicon carbide composite and carbon/carbon-silicon carbide composite. Despite the attractive qualities of composite disc brakes, they are only utilized for high-end performance vehicles and luxury vehicles.

These advanced composite materials are far from ideal. Each of these composite materials has its own shortcomings. Carbon/carbon (C/C) composite disc brakes exhibit a low coefficient of friction (0.25) below 450°C and also a high wear rate for the brake pads. The fabrication process for carbon/silicon carbide (C/SiC) composites, poses a high risk of toxicity to the handlers. The preforms involved are also expensive. Carbon/carbon-silicon carbide (C/C-SiC) composite disc brakes share similar fabrication methods with carbon/silicon carbide (C/SiC), hence both composite materials share the same problems. Therefore it is of great interest to explore other composite materials which have the potential to be integrated into commercial vehicles.

In this study, aluminium alloy 6082 is selected to be reinforced with two different ceramic particulates, namely silicon carbide and alumina. The resultant material is metal matrix composite (MMC). Stir casting technique is used to fabricate MMC as it is the most commercial and relatively low cost liquid processing method.

Alumina and aluminium titanate based ceramics are selected for this study due to their high specific heat capacity and low thermal expansion coefficient. Its benefit is the combination of the attractive properties of alumina and aluminium titanate based ceramics which will produce functionally graded material (FGM). The powder stacking method is used to fabricate FGM, where two or more different powders are mixed at the desired compositional ratio before the mixture is gradually changed in a die.

The density measurement is performed according to Archimedes Principle on the gray cast iron, MMC and FGM samples. Both MMC and FGM acquire higher density as compared to carbon/carbon composite, C/SiC composite and C/C-SiC composite. They attain lower density than that of gray cast iron. The porosity for the MMC and FGM samples is computed from experimentally determined density values. The porosity of MMC samples is less than 5% whereas the porosity for FGM – A1 sample is as high as $(18.892 \pm 1.634)\%$. The presence of porosity in the MMC samples is attributed to the clustering of particulates. FGM samples are known to be very porous materials, especially in the presence of aluminium titanate.

The presence of hard particles (silicon carbide and alumina) results in the increase of hardness of the MMCs. Aluminium alloy MMC reinforced with silicon carbide has slightly higher hardness value compared to aluminium alloy MMC reinforced with alumina. Hardness values of MMCs are slightly lower than that of gray cast iron. The tensile property and wear resistance of MMC are related to the hardness property. Although MMC attains a slightly lower tensile strength compared to gray cast iron, it still shows an increase in its tensile strength with the increase of particulate content. MMC possesses a lower Young's Modulus than that of gray cast iron, C/SiC composite and C/C-SiC composite. This shows that a low Young's modulus of MMC is able to promote uniform contact between the disc brake and the brake pads.

The values of tensile strength and Young's modulus of MMC make the material promising for the use of car brakes.

Aluminium alloy reinforced with 5 wt% silicon carbide and 15 wt% silicon carbide, aluminium alloy reinforced with 10 wt% alumina, 15 wt% alumina and 20 wt% alumina show fracture toughness of more than $15\text{MPa}\cdot\text{m}^{1/2}$ which is in accordance to the recommended values (Ashby, 2005). It is worth noting as well ASTM A48 Grade 20/SAE J431 G1800 has provided an estimation of the fracture toughness of gray cast iron, $11\text{MPa}\cdot\text{m}^{1/2}$. The fracture toughness of gray cast iron is comparatively lower than that of MMC, as it is estimated in ASTM A48 Grade 20/SAE J431 G1800.

Compression tests were performed on gray cast iron, MMC and FGM samples. It is revealed that MMC and FGM samples have lower compressive strength compared to gray cast iron. This is due to the increased amount of clustering in MMC whereas the low compressive strength of FGM is due to inherited brittleness and the graded heterogeneous $\text{Al}_2\text{TiO}_5/\text{Al}_2\text{O}_3$ layers which exhibit a relatively 'soft' surface.

The wear resistance of MMC is attributed to the hardness property. It is observed that the increased number presence of hard particles (silicon carbide) results in the increase of real contact area. Consequently, at a higher content of silicon carbide, the wear becomes higher. In comparison to gray cast iron, both aluminium alloy reinforced with SiC MMC and aluminium alloy reinforced with Al_2O_3 MMC attain higher wear rate. For both sliding speeds (0.42m/s and 1m/s) and high contact pressure (0.2MPa), at 15 weight percentage of alumina in aluminium alloy, it acquires lower wear rate whereas at 15 weight percentage of silicon carbide in aluminium alloy it attains the highest wear rate. It is observed that alumina particulates have helped to reduce the wear of the disc.

Both aluminium alloy reinforced with SiC MMC and aluminium alloy reinforced with Al_2O_3 MMC (except 5 wt% of alumina in aluminium alloy) attain friction coefficient within the range that is characteristic for automotive vehicle at high contact pressure (0.2MPa) for both sliding speeds (0.42m/s and 1m/s). For both contact pressures (0.1MPa and 0.2MPa) under 1m/s sliding speed, friction coefficient

for aluminium alloy reinforced with SiC is observed to be within range for automotive vehicles. Gray cast iron, aluminium alloy reinforced with SiC MMC and aluminium alloy reinforced with Al₂O₃ MMC acquire low COF at low contact pressure (0.1MPa) and low sliding speed (0.42m/s). These findings are consistent with what is observed from other types of MMCs reported in literature. As the contact pressure decreases, the real area of contact at the sliding interface decreases as well. This results in low coefficient of friction. In addition, the softening of lubricating agents from the friction material pin may have contributed to the lower coefficient of friction.

For all test conditions of aluminium alloy reinforced with SiC MMC and aluminium alloy reinforced with Al₂O₃ MMC, the wear of brake pins sliding against MMC is higher than that of brake pad pins sliding against gray cast iron. Despite that, the wear rate of brake pad pin sliding against aluminium alloy reinforced with SiC MMC and aluminium alloy reinforced with Al₂O₃ MMC is higher than other types of MMCs reported in literature. The wear rate of brake pad pin sliding against aluminium alloy reinforced with SiC MMC is also higher than that of the brake pad pin sliding against cast iron.

The thermal properties of MMC and FGM samples were estimated. Both aluminium alloy reinforced with Al₂O₃ and aluminium alloy reinforced with SiC acquire higher specific heat capacity, coefficient of thermal expansion and thermal conductivity than that of gray cast iron. FGM possesses higher specific heat capacity than that of gray cast iron. Both FGM – A1 and FGM – A2 show slightly lower thermal conductivity values compared to that of gray cast iron. Specific heat capacity, thermal expansion coefficient and thermal conductivity, play a diverse role in affecting the durability of the disc brake. During short and high speed stops, specific heat capacity is a crucial thermal property. Hence, a high specific heat capacity is very much needed for a disc brake. Both MMC and FGM show benefit in this area.

From the results of this experimental study it follows, such properties including density, tensile strength, Young's modulus, fracture toughness, estimated values for thermal conductivity and specific heat capacity for both aluminium alloy reinforced with silicon carbide and alumina, while density and estimated values for specific heat

capacity for FGM, show promising results for the use of these materials for car brake rotors.

5.2 Recommendations

The tensile behaviour of MMC can be improved by reducing the number of silicon carbide particulates to lower increment content, for e.g. 1.5%. In addition, the particulate size of silicon carbide can be reduced to less than $100\mu\text{m}$ but beyond $13\mu\text{m}$ (Jokinen et al., 1990). However it should be made aware that the wear resistance of the MMC is attributed to the ceramic particulate's size and how well the particulates are bonded within the aluminium alloy matrix. The optimum ceramic particulate size needs to be explored to ensure that MMC has the adequate tensile and wear behaviour.

The stir casting method is recommended to be modified for better bonding between the particulates and aluminium matrix. The bottom pouring method can be improved by sealing the passageway from the outlet of the crucible into the mould (Figure 5-1). Re-stirring is also needed before pouring it into the mould. It is thought to help disperse the silicon carbide particles to a more uniform distribution.

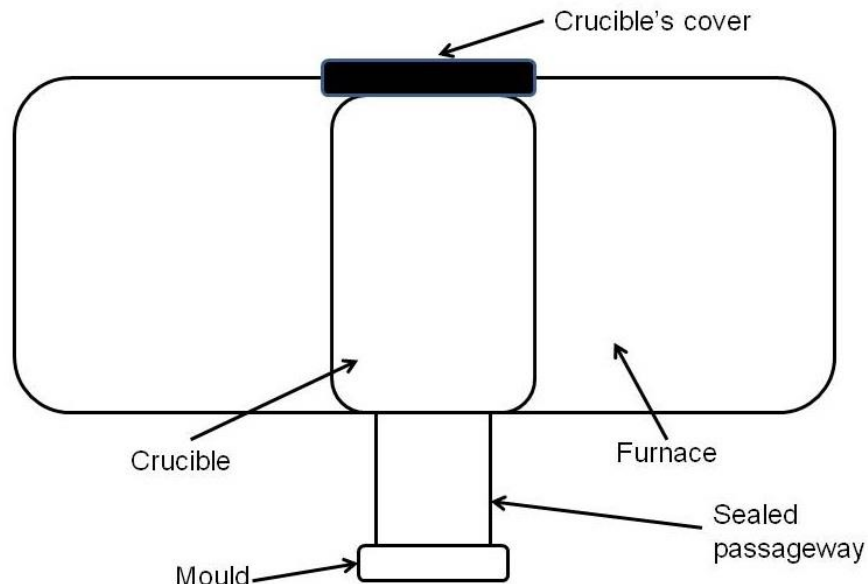


Figure 5.1 Modified stir casting equipment

Other fabrication methods for FGM such reaction sintering can be suitable to help reduce the porosity of the materials. Aluminium titanate with different additives (MgO, Fe₂O₃ or SiO₂) fabricated by reaction sintering method had less than 5% of porosity (Jiang et al., 2011). Besides that, further studies need to be conducted on the physical and mechanical properties of FGM.

Friction power, friction work, friction surface temperature, material of friction partners, wear, geometry of the friction partners, environmental influences and local mechanism are essential parameters to evaluate brake material. An accurate balance of physical and mechanical properties is essential for a tribo component (Rehman et al., 2012). In order for these materials to be suitable for the commercial market, a full inertial dynamometer and actual vehicle testing with a full evaluation of in-use performance need to be utilized (Blau, 2001).

References

- Adamowicz, A. & Piotr, G. 2011. Analysis of Disc Brake Temperature Distribution During Single Braking under Non-Axisymmetric Load. *Applied Thermal Engineering* 31 (6-7): 1003-1012.
- Adamowicz, A. & Piotr, G. 2011. Influence of Convective Cooling on a Disc Brake Temperature Distribution During Repetitive Braking. *Applied Thermal Engineering* 31 (14-15): 2177-2185.
- Adebisi, A. A., Maleque M. A. & Shah Q. H. 2011. Surface Temperature Distribution in a Composite Brake Rotor. *International Journal of Mechanical and Materials Engineering* 6 (3): 356-361.
- Alaneme, K. K. & Aluko, A. O. 2012. Fracture Toughness (K_{IC}) and Tensile Properties of as-Cast and Age-Hardened Aluminium (6063)–Silicon Carbide Particulate Composites. *Scientia Iranica* 19 (4): 992-996.
- Aluminium Titanate*. 2014. Azom.
<http://www.azom.com/article.aspx?ArticleID=1223> (Accessed on 03/03/2014)
- Amirkhanlou, S. & Behzad, N. 2011. Effects of Reinforcement Distribution on Low and High Temperature Tensile Properties of Al356/SiCp Cast Composites Produced by a Novel Reinforcement Dispersion Technique. *Materials Science and Engineering: A* 528 (24): 7186-7195.
- Anderson, A. E. 1992. Friction and wear of automotive brakes. *ASM Handbook* 18: 569-577.

-
- Anoop, S., Natarajan, S. & Babu, S. P. K. 2009. Analysis of Factors Influencing Dry Sliding Wear Behaviour of Al/SiCp–Brake Pad Tribosystem. *Materials & Design* 30 (9): 3831-3838.
- Aqida, S. N., Ghazali, M. I. & Hashim, J. 2004. Effects of Porosity on Mechanical Properties of Metal Matrix Composite: An Overview. *Jurnal Teknologi* 40 (A): 17-32.
- Aqida, S. N. & Ghazali, M. I. 2003. The Effects of Stirring Speed and Reinforcement Particles on Porosity Formation in Cast MMC. *Jurnal Mekanikal* 16: 22-30.
- Ashby, Michael F. 2005. *Materials Selection in Mechanical Design*: Elsevier.
- Auerkari, P. 1996. Mechanical and physical properties of engineering alumina ceramics. *Technical Research Centre of Finland, Research Notes* 1792: 26.
- Behera, R., Das, S., Chatterjee, D. & Sutradhar, G. 2011. Forgeability and Machinability of Stir Cast Aluminium Alloy Metal Matrix Composites. *Journal of Minerals and Materials Characterization and Engineering* 10 (10): 923-939.
- Bergman, F., Eriksson, M. & Jacobson, S. 2000. The effect of reduced contact area on the occurrence of disc brake squeals for an automotive brake pad. *Proceedings of the Institution of Mechanical Engineers D* 214 (D5): 561-568.
- Blanco, C., Bermejo, J., Marsh, H. & Menendez, R. 1997. Chemical and Physical Properties of Carbon as Related to Brake Performance. *Wear* 213: 1-12.
- Blau, P. J. 2001. Compositions, Functions, and Testing of Friction Brake Materials and Their Additives. *Metals and Ceramics Division*, www.ornl.gov/~webworks/cppr/y2001/rpt/112956.pdf. (Accessed on 02/01/2012)

- Blau, P. J., Jolly, B. C., Qu, J., Peter, W. H. & Blue, C. A. 2007. Tribological Investigation of Titanium-Based Materials for Brakes. *Wear* 263 (7-12): 1202-1211.
- Bueno, S., Micele, L., Melandri, C., Baudin, C. & De Portu, G. 2011. Improved Wear Behaviour of Alumina–Aluminium Titanate Laminates with Low Residual Stresses and Large Grained Interfaces. *Journal of the European Ceramic Society* 31 (4): 475-483.
- Bueno, S., Rodrigo, M. & Baudín, C. 2005. Design and Processing of Al_2O_3 – Al_2TiO_5 Layered Structures. *Journal of the European Ceramic Society* 25 (6): 847-856.
- Buscaglia, V. & Nanni, P. 1998. Decomposition of Al_2TiO_5 and $\text{Al}_{2(1-x)}\text{Mg}_x\text{Ti}_{(1+x)}\text{O}_5$ ceramics. *Journal of American Ceramic Society* 81: 2645-2653.
- Bruno, G., Efremov A., Wheaton, B.R. & Webb, J. E. 2010. Microcrack Orientation in Porous Aluminum Titanate. *Acta Materialia* 58 (20): 6649-6655.
- Callister, William D. Jr. *Material Science And Engineering An Introduction*. John Wiley & Sons, Inc., 2003.
- Chan, W. 2007. Analysis of heat dissipation on Mechanical Braking Systems. *MAE 221A – Heat Transfer*.
- Chatterley, T. C. & Macnaughtan, M. P. 1999. Cast Iron Brake Discs - Current Position, Performance and Future Trends in Europe. 1-10, papers.sae.org. (Accessed on 01/03/2012)
- Chen, C. H. & Awaji, H. 2007. Temperature Dependence of Mechanical Properties of Aluminum Titanate Ceramics. *Journal of the European Ceramic Society* 27 (1): 13-18.

-
- Cueva, G., Sinatora A., Guesser, W. L. & Tschiptschin, A. P. 2003. Wear Resistance of Cast Irons Used in Brake Disc Rotors. *Wear* 255 (7-12): 1256-1260.
- Daoud, A. & Abou El-khair, M. T. 2010. Wear and Friction Behavior of Sand Cast Brake Rotor Made of A359-20vol% SiC Particle Composites Sliding against Automobile Friction Material. *Tribology International* 43 (3): 544-553.
- Day, A. J. & Newcomb, T. P. 1988. The dissipation of frictional energy from the interface of an annular disc brake. *Proceedings of the Institution of Mechanical Engineers, Part D: Transport Engineering* 198: 201-209.
- Deng, H. L., Li, K. Z., Li, H. J., Wang, P. Y., Xie, J. & Zhang, L. L. 2010. Effect of Brake Pressure and Brake Speed on the Tribological Properties of Carbon/Carbon Composites with Different Pyrocarbon Textures. *Wear* 270 (1-2): 95-103.
- Devi G. R. & Rao, K. R. Carbon-Carbon Composites – an Overview. *Defence Science Journal* 43 (4): 369-383.
- Downes, T. J. & King, J. E. 1992. The Effect of Microstructure on the Fracture Toughness of a Metal-Matrix Composite. *Composites* 24 (3): 276-281.
- Dunaevsky, V. V. 1991. Prediction of Railroad Friction Braking Temperatures: Prediction of Average Bulk and Average Surface Temperatures of Railroad Wheels and Brake Discs. *Tribology Transactions* 34 (3): 343-352.
- Eriksson, M., Bergman, F. & Jacobson, S. 2002. On the Nature of Tribological Contact in Automotive Brakes. *Wear* 252: 26-36.
- Eriksson, M. & Jacobson, S. 2000. Tribological Surfaces of Organic Brake Pads. *Tribology International* 22: 817-827

-
- Ezatpour, H. R., Torabi-Parizi, M. & Sajjadi, S. A. 2013. Microstructure and Mechanical Properties of Extruded Al/Al₂O₃ Composites Fabricated by Stir-Casting Process. *Transactions of Nonferrous Metals Society of China* 23 (5): 1262-1268.
- Fan, S.W., Zhang, L.T., Cheng, L. F. & Yang, S. J. 2011. Microstructure and Frictional Properties of C/SiC Brake Materials with Sandwich Structure. *Ceramics International* 37 (7): 2829-2835.
- Fan, S.W., Zhang, L.T., Cheng, L. F., Zhang, J. X., Yang, S. J. & Liu, H. Y. 2011. Wear Mechanisms of the C/SiC Brake Materials. *Tribology International* 44 (1): 25-28.
- Fan, S.W., Zhang, L.T., Xu, Y. D., Cheng, L. F., Lou, J. J., Zhang, J. Z. & Yu, L. 2007. Microstructure and Properties of 3d Needle-Punched Carbon/Silicon Carbide Brake Materials. *Composites Science and Technology* 67 (11-12): 2390-2398.
- Fan, S., Zhang, L., Xu, Y., Cheng, L., Tian, G., Ke, S., Xu, F. & Liu, H. 2008. Microstructure and Tribological Properties of Advanced Carbon/Silicon Carbide Aircraft Brake Materials. *Composites Science and Technology* 68 (14): 3002-3009.
- Gao, C. H. 2007. Stress analysis of thermal fatigue fracture of brake disks based on thermomechanical coupling. *Journal of Tribology*, 129 (3): 536-543.
- Grieve, D. G., Barton, D. C., Crolla, D. A. & Buckingham, J. T. 1998. Design of a lightweight automotive brake disc using finite element and Taguchi techniques. *Proc. Instn Mech Engrs, Part D: J. Automobile Engineering* 212: 245-254.
- Harper, G. A. 1998. Brakes and friction materials: the history and development of the technologies. Mechanical Engineering Publications Limited, London, England.

-
- Hashim, J. 2001. The Production of Cast Metal Matrix Composite by a Modified Stir Casting Method. *Jurnal Teknologi* 35 (A): 9-20.
- Hashim, J., Looney, L. & Hashmi, M. S. J. 2001. The Wettability of SiC Particles by Molten Aluminium Alloy. *Journal of Materials Processing Technology* 119: 324-328.
- Heidenreich, B. 2013. *Carbon Fibre Reinforced Sic Materials Based on Melt Infiltration*.
http://elib.dlr.de/52517/1/Paper_Heidenreich_C_fibre_reinforced_SiC_mat_based_on_MI-HTCMC6.pdf. (Accessed on 01/03/2012)
- Heine, M. & Gruber, U. 2000. Silicon carbide particles reinforced with short graphite fibers. *U. S. Pat.* 6030913.
- Hong, S. J., Kim, H. M., Huh, D., Suryanarayana C. & Chun B. S. 2003. Effect of Clustering on the Mechanical Properties of SiC Particulate-Reinforced Aluminum Alloy 2024 Metal Matrix Composites. *Materials Science and Engineering A347*: 198-204.
- Howell, G. J. & Ball, A. 1995. Dry Sliding Wear of Particulate-Reinforced Aluminium Alloys against Automobile Friction Materials. *Wear* 181-183: 379-390.
- Hung, N. P., Zhou, W., Peh, E. T. & Chan, C. S. 1995. Fracture Toughness and Low Cycle Fatigue of 6061/Al₂O₃ Composites. *Composites Engineering* 5 (5): 509-517.
- Ihm, Mark. 2013. Introduction to Gray Cast Iron Brake Rotor Metallurgy.
www.sae.org/events/bce/tutorial-ihm.pdf (Accessed on 01/03/2012)
- Jacobsson, H. 2003. Aspects of Disc Brake Judder. *Proceedings of the Institution of Mechanical Engineers Part D* 217: 419-430.

- Jang, H., Ko, K., Kim, S. J., Basch, R. H. & Fash, J. W. 2004. The Effect of Metal Fibers on the Friction Performance of Automotive Brake Friction Materials. *Wear* 256 (3-4): 406-414.
- Jayasankar, M., Hima, K. P., Ananthakumar, S., Mukundan, P., Pillai, P. K. & Warriar, K. G. K. 2010. Role of Particle Size of Alumina on the Formation of Aluminium Titanate as Well as on Sintering and Microstructure Development in Sol–Gel Alumina–Aluminium Titanate Composites. *Materials Chemistry and Physics* 124 (1): 92-96.
- Jokinen, A. & Anderson, P. 1990. Tribological properties of PM aluminium alloy matrix composites. *Annual Powder Metallurgy Conference Proceedings, American Powder Metallurgy Institute, Princeton, NJ*, 517-530.
- Kainer, K. U. 2006. Basics of Metal Matrix Composites. Wiley-VCH Verlag GmbH & Co. KGaA, Weinheim.
- Kao, T., Richmond, J. & Douarre, A. 2000. Brake disc hot spotting and thermal judder: an experimental and finite element study. *International Journal of Vehicle Design*, 23 (3): 276-296.
- Kapranos, P., Kirkwood, D. H., Atkinson, H. V., Rheinlander, J. T., Bentzen, J. J., Toft, P. T., Debel, C. P., Laslaz, G., Maenner, L., Blais, S., Rodriguez-Ibabe, J. M., Lasa, G., Chiarmettaand, P. G. & Giese, A. 2003. Thixoforming of an automotive part in A390 hypereutectic Al–Si alloy. *Journal of Materials Processing Technology*, 20: 271–7.
- Kapoor, A., Tung, S.C., Schwartz, S. E., Priest, M. & Dwyer-Joyce, R.S. 2001. 32. Automotive Tribology. *Modern Tribology Handbook*, Two Volume Set, 32: 1209-1211,
- Kermc, M., Kalin, M. & Vižintin, J. 2005. Development and Use of an Apparatus for Tribological Evaluation of Ceramic-Based Brake Materials. *Wear* 259 (7-12): 1079-1087.

-
- Kinkaid, N. M., O'Reilly, O. M. & Papadopoulos, P. 2003. Automotive Disc Brake Squeal. *Journal of Sound and Vibration* 267 (1): 105-166.
- Korim, T. 2009. Effect of Mg²⁺-and Fe³⁺-Ions on Formation Mechanism of Aluminium Titanate. *Ceramics International* 35 (4): 1671-1675.
- Krenkel, W. & Berndt, F. 2005. C/C-SiC composites for space applications and advanced friction systems. *Material Science Engineering A* 412: 177-81.
- Krosnar, John. 2013. *The Benefits of High carbon brake disc materials*, http://www.euracgroup.com/hres/technical%20briefing%20_%20high%20carbon.pdf. (Accessed on 01/03/2012)
- Kwok, J. K. M. & Lim, S. C. 1999. High-Speed Tribological Properties of Some Al/SiCp Composites: I. Frictional and Wear-Rate Characteristics. *Composites Science and Technology* 59: 55-63.
- Lim, D. W., Kim, T. H., Choi, J. H., Kweon, J. H. & Park, H. S. 2008. A Study of the Strength of Carbon–Carbon Brake Disks for Automotive Applications. *Composite Structures* 86 (1-3): 101-106.
- Limpert, R. 1999. Brake Design and Engineering *Fundamentals*. Society of Automotive Engineers Inc, Warrendale, PA.
- Lindroos, V. K., Hellman, J. T., Lou, D., Nowak, R., Pagounis, E., Liu X. W. & Penttinen, I. M. 2004. Designing with metal matrix composites. Marcel Dekker, Inc.
- Low, I. M. 1998. Synthesis and Properties of in Situ Layered and Graded Aluminium Titanate/Alumina Composites. *Materials Research Bulletin* 33 (10): 1475-1482.
- Low, I. M. & Oo, Z. 2008. Reformation of Phase Composition in Decomposed Aluminium Titanate. *Materials Chemistry and Physics* 111 (1): 9-12.

- Low, I. M., Oo, Z. & O'Connor, B. H. 2006. Effect of Atmospheres on the Thermal Stability of Aluminium Titanate. *Physica B: Condensed Matter* 385-386: 502-504.
- Luo, R. Y. & Li, Q. 2004. Brake Characteristics of 2d Carbon/Carbon Composites Prepared by Rapid Direction Diffused Cvi Technology. *Materials Science and Engineering: A* 379 (1-2): 33-38.
- Macnaughtan, M. P. 1998. Cast Iron Brake Discs - a Brief History of Their Development and Metallurgy. 321-324, http://www.eurac-group.com/hres/cast%20iron%20brake%20discs%20_%20a%20brief%20history%20of%20their%20development%20and%20metallurgy.pdf. (Accessed on 01/03/2012)
- Macnaughtan, M. P. & Krosnar, J. G. 1998. Cast Iron - a Brake Disc Material for the Future? In *2nd International Seminar on Automotive Braking - Recent Developments and Future Trends, University of Leeds, Weetwood Hall, Leeds, UK*. http://www.eurac-group.com/hres/cast%20iron%20_%20a%20brake%20disc%20material%20for%20the%20future.pdf. (Accessed on 01/03/2012)
- Maluf, O., Angeloni, M., Milan, M. T., Spinelli, D. & Filho, W. W. B. 2013. Development of Materials for Automotive Disc Brakes. *Minerva* 4 (2): 149-158.
- Manocha, Lalit M. 2003. "High Performance Carbon–Carbon Composites." *Sadhana* 28 (Parts 1 & 2): 349-358.
- Manocha, L. M. 2013. Carbon–Carbon Composites. *Sadhana* 28: 349 - 358.
- Manurung, P., Low, I. M., O'Connor, B. H. & Kennedy, S. 2005. Effect of B-Spodumene on the Phase Development in an Alumina/Aluminium-Titanate System. *Materials Research Bulletin* 40 (12): 2047-2055.

-
- Miracle, D. B. 2005. Metal matrix composites – from science to technological significance. *Composites Science and Technology* 65: 2526-2540.
- Miyajima, T. & Iwai, Y. 2003. Effects of Reinforcements on Sliding Wear Behavior of Aluminum Matrix Composites. *Wear* 255 (1-6): 606-616.
- Mohsen, M., Blau, P. J. & Dumitrescu, D. 2004. Characteristics and Morphology of Wear Particles from Laboratory Testing of Disk Brake Materials. *Wear* 256 (11-12): 1128-1134.
- Naher, S., Brabazon, D. & Looney, L. 2007. Computational and Experimental Analysis of Particulate Distribution During Al–SiC MMC Fabrication. *Composites Part A: Applied Science and Manufacturing* 38 (3): 719-729.
- Natarajan, N., Vijayarangan, S. & Rajendran, I. 2006. Wear Behaviour of A356/25SiCp Aluminium Matrix Composites Sliding against Automobile Friction Material. *Wear* 261 (7-8): 812-822.
- Nayiroh, N., & Pratapa, S. n.d.. Phase-composition analysis of Al₂TiO₅-based functionally-graded materials with MgAl₂O₄ additive produced by multiple infiltration technique. *Powder Diffraction*, 2–6.
- Newcomb, T. P. & Spurr, R. T. 1989. *A Technical History of the Motor Car*. Adam Hilger, New York.
- Nicholson, G. 1995. *Facts about Friction*. P&W Price Enterprise, Inc, Croydon, PA.
- Nikhilesh, C. & Shen, Y. L. 2001. Mechanical Behavior of Particle Reinforced Metal Matrix Composites. *Advanced Engineering Materials* 3 (6): 357-370.
- Perera, F. H., Pajares, A., & Meléndez, J. J. 2011. Strength of aluminium titanate/mullite composites containing thermal stabilizers. *Journal of the European Ceramic Society*, 31(9), 1695–1701.

- Rao, R. N. & Das, S. 2011. Effect of SiC Content and Sliding Speed on the Wear Behaviour of Aluminium Matrix Composites. *Materials & Design* 32 (2): 1066-1071.
- Rehman, A., Das, S. & Dixit, G. 2012. Analysis of Stir Die Cast Al–SiC Composite Brake Drums Based on Coefficient of Friction. *Tribology International* 51: 36-41.
- Rohatgi, P. K., Liu, Y. & Lim, S. C. 1993. Wear mapping for metal and ceramic matrix composites. *Advanced in Composites Tribology, Composite Materials Series* (8): 291-309.
- Savage, G. 2009. Sub-Critical Crack Growth in Highly Stressed Formula 1 Race Car Composite Suspension Components. *Engineering Failure Analysis* 16 (2): 608-617.
- Shivamurthy, R. C. & Surappa, M. K. 2011. Tribological Characteristics of A356 Al Alloy–SiCp Composite Discs. *Wear* 271 (9-10): 1946-1950.
- Shorowordi, K. M., Haseeb, A. S. M. A. & Celis, J. P. 2004. Velocity Effects on the Wear, Friction and Tribochemistry of Aluminum MMC Sliding against Phenolic Brake Pad. *Wear* 256 (11-12): 1176-1181.
- Skala, R. D., Manurung, P. & Low, I. M. 2006. Microstructural Design, Characterisation and Indentation Responses of Layer-Graded Alumina/Aluminium–Titanate Composites. *Composites Part B: Engineering* 37 (6): 466-480.
- Skala, R. D., Li, D. & Low, I. M. 2009. Diffraction, Structure and Phase Stability Studies on Aluminium Titanate. *Journal of the European Ceramic Society* 29 (1): 67-75.
- Surappa, M. K. (2003). Aluminium matrix composites: Challenges and opportunities. *Sadhana*, 28(1-2), 319–334.

- Su, J. M., Xiao, Z. C., Liu, Y. Q., Meng, F. C., Peng, Z. G., Gu, L. M., Li, G. F. & Xing, R. P. 2010. Preparation and Characterization of Carbon/Carbon Aircraft Brake Materials with Long Service Life and Good Frictional Properties. *New Carbon Materials* 25 (5): 329-334.
- Suresha, S. & Sridhara, B. K. 2010. Wear Characteristics of Hybrid Aluminium Matrix Composites Reinforced with Graphite and Silicon Carbide Particulates. *Composites Science and Technology* 70 (11): 1652-1659.
- Stadler, Z., Krnel, K. & Kosmac, T. 2007. Friction Behavior of Sintered Metallic Brake Pads on a C/C–SiC Composite Brake Disc. *Journal of the European Ceramic Society* 27 (2-3): 1411-1417.
- Stadler, Z., Krnel, K. & Kosmac, T. 2008. Friction and Wear of Sintered Metallic Brake Linings on a C/C–SiC Composite Brake Disc. *Wear* 265 (3-4): 278-285.
- Tatar, C. & Özdemir, N. 2010. Investigation of Thermal Conductivity and Microstructure of the A–Al₂O₃ Particulate Reinforced Aluminum Composites (Al/Al₂O₃-MMC) by Powder Metallurgy Method. *Physica B: Condensed Matter* 405 (3): 896-899.
- Uyyuru, R. K., M. K. Surappa, and S. Brusethaug. 2006. "Effect of Reinforcement Volume Fraction and Size Distribution on the Tribological Behavior of Al-Composite/Brake Pad Tribo-Couple." *Wear* 260 (11-12): 1248-1255.
- Uyyuru, R. K., Surappa, M. K. & Brusethaug, S. 2007. Tribological Behavior of Al–Si–SiCp Composites/Automobile Brake Pad System under Dry Sliding Conditions. *Tribology International* 40 (2): 365-373.
- Veeresh, G. B. K., Rao, C. S. P. & Selvaraj, N. 2012. Studies on Mechanical and Dry Sliding Wear of Al6061–SiC Composites. *Composites Part B: Engineering* 43 (3): 1185-1191.

-
- Vukcevic, M. & Delijic, K. 2002. Some New Directions in Aluminum-Based Pm Materials for Automotive Applications. *Materiali In Tehnologije* 36 (3-4): 101-105.
- Wang, H. M., Li, G. R., Zhao, Y. T. & Chen, G. 2010. In Situ Fabrication and Microstructure of Al₂O₃ Particles Reinforced Aluminum Matrix Composites. *Materials Science and Engineering: A* 527 (12): 2881-2885.
- Wang, W. X., Takao, Y. & Matsubara, T. 2008. Tensile Strength and Fracture Toughness of C/C and Metal Infiltrated Composites Si-C/C and Cu-C/C. *Composites Part A: Applied Science and Manufacturing* 39 (2): 231-242.
- Wang, Y., Yang, Y., Zhao, Y., Tian, W., Bian, H. M. & He, J. Q. 2009. Sliding Wear Behaviors of in Situ Alumina/Aluminum Titanate Ceramic Composites. *Wear* 266 (11-12): 1051-1057.
- Wang, R. M., Surappa, M.K., Tao, C. H., Li, C. Z. & Yan, M. G. 1998. Microstructure and Interface Structure Studies of SiCp-Reinforced Al (6061) Metal-Matrix Composites. *Materials Science and Engineering A*254: 219-226.
- Xiao, P., Li, Z., & Xiong, X. 2010. Microstructure and tribological properties of 3D needle-punched C/C-SiC brake composites. *Solid State Sciences*, 12(4): 617-623.
- Zhuan, L. I., Peng, X., Xiang, X., & Su-hua, Z. H. U. 2008. Tribological characteristics of C / C-SiC braking composites under dry and wet conditions. *Transactions of Nonferrous Metals Society of China*, 18(5): 1071-1075.